

**PERFORMANCE INVESTIGATION OF
APPLICABLE WIRELESS
COMMUNICATION PROTOCOLS FOR
VEHICLE-TO-GRID (V2G) IN SMART GRID
ENVIRONMENT**

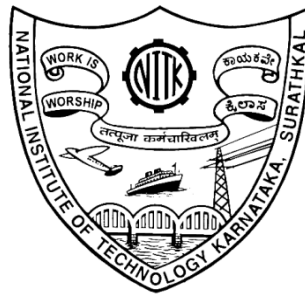
Thesis

submitted in partial fulfillment of the requirements for the degree of

DOCTOR OF PHILOSOPHY

by

SANTOSHKUMAR



DEPARTMENT OF ELECTRICAL AND ELECTRONICS ENGINEERING
NATIONAL INSTITUTE OF TECHNOLOGY KARNATAKA
SURATHKAL, MANGALORE - 575 025

JUNE, 2016

DECLARATION

by the Ph.D. Research Scholar

I hereby *declare* that the Research Thesis entitled **Performance Investigation of Applicable Wireless Communication Protocols for Vehicle-to-Grid (V2G) in Smart Grid Environment** which is being submitted to the **National Institute of Technology Karnataka, Surathkal** in partial fulfilment of the requirements for the award of the Degree of **Doctor of Philosophy** in department of Electrical and Electronics Engineering is a *bonafide report of the research work carried out by me*. The material contained in this Research Thesis has not been submitted to any University or Institution for the award of any degree.

SANTOSHKUMAR

(123042EE12F07)

(Register Number, Name & signature of the Research Scholar)

Department of Electrical and Electronics Engineering

Place: NITK-Surathkal

Date:

C E R T I F I C A T E

This is to certify that the Research Thesis entitled **Performance Investigation of Applicable Wireless Communication Protocols for Vehicle-to-Grid (V2G) in Smart Grid Environment** submitted by **SANTOSHKUMAR** (Register Number, 123042EE12F07) as the record of the research work carried out by him, is *accepted as the Research Thesis submission* in partial fulfilment of the requirements for the award of degree of **Doctor of Philosophy**.

(Prof. Udaykumar R. Y.)

Research Guide

(Name and Signature with Date and Seal)

Chairman-DRPC

(Signature with Date and Seal)

ACKNOWLEDGEMENTS

It gives me immense pleasure and great sense of satisfaction to express my heartfelt gratitude to those who made this dissertation possible.

I take this opportunity to sincerely thank my research supervisor Prof. Udaykumar R.Y. for all his invaluable guidance, patience, encouragement, timely advice and support. He has been a constant source of inspiration throughout this journey. I feel proud to have worked under his guidance.

I thank National Institute of Technology Karnataka for giving me an opportunity for doing research and Ministry of Human Resource Department(MHRD)-Government of India for awarding research scholarship.

I wish to thank my research progress assessment committee (RPAC) members Dr. A. Karthikeyan and Dr. Basavaraj Manu, for their constructive feedback and guidance from research problem definition stage to thesis submission stage. Without their help the thesis would not have taken this shape.

I would like to thank Prof. K.P.Vittal, former HOD for providing the necessary resources in the department to carry out my research. Also, I would like to thank HOD, Mr. Jora M. Gonda for encouragement and providing valuable suggestions.

I take this opportunity to thank all teaching and non-teaching staff of EEE Department, NITK Surathkal.

I express my gratitude and thanks to the Management, Principal and HOD of SDMCET, Dharwad for deputing me to pursue Doctoral studies at NITK Surathkal.

My stay at NITK Surathkal was a sweet and memorable in the company of my fellow researchers who never let me know that I am away from home. Big thanks to all the research scholars.

Finally, I would like to thank my Guru, Family members for their patience, care and love which drew me with inspiration to carry out my research.

SANTOSHKUMAR

ABSTRACT

The restructuring policy has motivated the private players to participate in power generation and thereby distributed energy resources (DER) such as photovoltaics (PV), wind turbines, micro turbine, fuel cell and internal combustion engine are integrated to the grid. As the sources (PV, wind) and load demand are intermittent in nature, the concept of storage devices aroused. Electrical Vehicles (EV) are one among the storage devices which can serve as a connected load or distributed resource (DR) being a transportation tool.

EVs will gradually replace other contemporary vehicles due to serious environmental concerns and growing oil demand. Vehicles are usually parked for 90-95% of the time in parking stations, residential apartments and office buildings. These EVs can be connected to the grid for power transaction in order to meet the time varying load demand. A single EV can only consume power and may not be appealing but the group of EVs can make a large difference and support the grid requirements.

EV connected to home is Vehicle-to-Home (V2H), EV connected to EV is Vehicle-to-Vehicle (V2V) and group of EVs connected to the grid is Vehicle-to-Grid (V2G). V2G can be used for peak shaving, valley filling, load leveling and supplying reactive power to the grid. In comparison to the other existing methods for peak shaving and valley filling, V2G is more efficient and effective. V2G has become a reality with the developments in Power grid and advancement in Vehicle technology.

Grid control center (GCC), aggregator and EV are the three key elements in V2G communication. GCC will have the information about the power requirements based on the energy market and it sends this information to the aggregator. Aggregator acts as an interface between GCC and EV and in turn sends the information received by GCC to EVs. Aggregator facilitates EVs to get connected to the grid by providing parking lot and charging slots. EV owner will decide to participate in power transaction with grid based on the State-of-Charge (SOC) of EV battery.

The development of wireless communication infrastructure for V2G communication is essential in order to support the V2G operation. The wireless communication link is proposed for GCC to Aggregator communication, Aggregator to EV communication, EV to EV communication and Smart Meter to EV communication. The applicable wireless communication protocols are considered for these links. The end-to-end downlink physical layers of the applicable protocols are modeled using MATLAB/SIMULINK and their performances are investigated using bit error rate and signal-to-noise ratio curves (BER v/s SNR). The suitable channel models (path loss) are analyzed and compared for the applicable protocols considered for V2G communication. The path loss is estimated and suitable path loss models are suggested for V2G communication.

Markov chain based queuing model (M/M/m) is developed for EVs connected to the charging slots for power transaction with the grid. The simulation is carried out for the developed model and the idle probability, EVs waiting in system, queue in hours are plotted. A Stochastic model based on Markov chain is developed for EVPL occupancy and the simulation is carried out to estimate the charging slots in EVPL and the time required for EV to charge or discharge. The communication links established will support the in time operation and functioning of V2G and increase its performance and efficiency. This study will help in facilitating the V2G operation in Smart grid environment.

TABLE OF CONTENTS

LIST OF FIGURES	V
LIST OF TABLES	IX
ABBREVIATIONS	X
CHAPTER 1	1
INTRODUCTION.....	1
1.1 VEHICLE-to-GRID (V2G)	1
1.2 WIRELESS COMMUNICATION	5
1.2.1 Path Loss	5
1.2.2 Shadowing.....	5
1.2.3 Small Scale Fading.....	6
1.3 LITERATURE REVIEW	6
1.4 RESEARCH OBJECTIVES	9
1.5 THESIS ORGANISATION.....	10
1.6 CONTRIBUTIONS OF THE THESIS WORK.....	11
CHAPTER 2.....	13
MODELING OF V2G INTEGRATORS.....	13
2.1 INTRODUCTION	13
2.2 MODELING OF V2G INTEGRATOR	14
2.2.1 Grid-to-Vehicle (G2V) mode of operation	16
2.2.2 Three level bidirectional DC-AC converter control	17
2.2.2.1 Bidirectional DC-DC converter control	21
2.2.3 Vehicle-to-Grid (V2G) mode of operation	22
2.3 SIMULATION RESULTS	22
2.4 CONCLUSION	27

CHAPTER 3.....	29
WIRELESS ACCESS SUPPORT FOR V2G COMMUNICATION.....	29
3.1 GENERAL STRUCTURE OF PHYSICAL LAYER COMMUNICATION SYSTEM.....	30
3.1.1 Digital Modulation:	31
3.2 GCC TO AGGREGATOR COMMUNICATION	33
3.2.1 Fixed WiMAX Protocol for GCC to Aggregator Communication	34
3.2.1.1 Physical Layer for WiMAX	35
3.2.1.1.1 WiMAX Transmitter:.....	35
3.2.1.1.1.1 Randomisation:.....	35
3.2.1.1.1.2 Error Correction Code:	36
3.2.1.1.1.3 Reed Solomon (RS) Encoding:.....	36
3.2.1.1.1.4 Convolution Encoding (RS Code)	37
3.2.1.1.1.5 Interleaving:.....	39
3.2.1.1.1.6 Modulation	40
3.2.1.1.2 Channel:	43
3.2.1.1.3 WiMAX Receiver Model:.....	43
3.2.1.2 Path Loss Models	43
3.2.1.2.1 Free Space Path Loss Model	44
3.2.1.2.2 COST 231 Hata Model	44
3.2.1.2.3 Stanford University Interim (SUI) Model	45
3.2.1.2.4 Hata Okumara extended model or ECC 33 Model.....	45
3.2.1.2.5 COST 231 Walfish-Ikegami Model (W-I) Model.....	45
3.2.1.2.6 ERICSSON Model	46
3.2.2 3GPP LTE PROTOCOL FOR GCC TO AGGREGATOR COMMUNICATION	46
3.2.2.1 LTE Physical Layer	47
3.2.2.2 Implementation.....	48
3.2.3 Results and Discussion	50
3.2.3.1 Fixed WiMAX.....	50
3.2.3.1.1 Path Loss Results	51
3.2.3.2 3GPP LTE	54
3.3 AGGREGATOR TO EV COMMUNICATION	56
3.3.1 Mobile WiMAX Protocol for Aggregator to EV Communication	56
3.3.2 Wireless Fading Channels for Aggregator to EV Communication	57
3.3.2.1 Path Loss Models	59
3.3.2.2 Shadowing	59
3.3.2.2.1 IEEE 802.16d Models:.....	60

3.3.2.3 Small Scale Fading.....	62
3.3.2.3.1 Spreading in Time:	63
3.3.2.3.2 Spreading in Frequency:	63
3.3.2.3.3 Models of Fading Channel:.....	64
3.3.3 Results and Discussion	65
3.3.3.1 Mobile WiMAX.....	65
3.3.3.2 Channel Fading	66
3.3.3.2.1 Large scale fading: (Outdoor –to- Outdoor scenario).....	66
3.3.3.2.2 Shadowing: Hilly regions	67
3.3.3.2.3 Small Scale Fading	70
3.3.3.2.3.1 Flat Fading.....	70
3.3.3.2.3.2 Frequency Selective Fading	71
3.4 EV TO EV COMMUNICATION.....	73
3.4.1 Path Loss Models for LTE	75
3.4.1.1 3GPP Model:.....	75
3.4.1.2 WINNER B5f Model:	75
3.4.1.3 COST 231 Hata model:.....	75
3.4.1.4 Standard university interim (SUI) model:	76
3.4.1.5 Lee model.....	76
3.4.1.6 Vehicular Test Environment:	76
3.4.2 LTE Protocol for EV to EV Communication	77
3.4.2.1 LTE Physical Layer	77
3.4.3 Results and Discussion	79
3.4.3.1 Path Loss Models	79
3.4.3.2 Shadowing.....	82
3.4.3.3 LTE Physical layer.....	83
3.5. EV TO SMART METER COMMUNICATION	85
3.5.1 Indoor Wireless Communication Channels	85
3.5.2 EV to Smart Meter Communication	87
3.5.2.1 WI-FI protocol for EV to Smart Meter Communication.....	87
3.5.2.2 WiMAX protocol for EV to Smart Meter Communication.....	89
3.5.3 RESULTS AND DISCUSSION.....	89
3.5.3.1 Indoor Wireless Fading Channels	89
3.5.3.2 Wi-Fi Protocol for EV to Smart Meter Communication	96
3.5.3.3 WiMAX Protocol for EV to Smart Meter Communication	97
3.6 CONCLUSION	98

CHAPTER 4.....	98
STOCHASTIC MODELING OF EV PARKING LOT OCCUPANCY AND QUEUING	99
4.1 STOCHASTIC MODELING OF EVPL OCCUPANCY	100
4.1.1 Transition Probabilities:.....	101
4.2 QUEUING MODEL OF V2G	102
4.3 RESULTS AND DISCUSSION.....	106
4.3.1 Stochastic modeling of EVPL Occupancy.....	106
4.3.2. Queuing Model Simulation.....	109
4.4 CONCLUSION.....	112
CHAPTER 5.....	113
CONCLUSION AND FUTURE SCOPE	113
REFERENCES.....	117
LIST OF PUBLICATIONS	125
CURRICULUM VITAE.....	129

LIST OF FIGURES

Figure 1. 1 Conceptual framework of V2G.	2
Figure 1. 2 EV action based on SOC of a battery.	3
Figure 1. 3 Communication Model of V2G.	4
Figure 2. 1 Off-board and On-board integrator.	14
Figure 2. 2 Configuration of the system under study.	15
Figure 2. 3 Bode diagram of LCL filter.	18
Figure 2. 4 Block diagram of LCL filter.	18
Figure 2. 5 Bode diagram of uncompensated and compensated current control loop.	20
Figure 2. 6 Control block diagram of the bidirectional DC-AC & DC-DC converter.	21
Figure 2. 7 Operating waveforms during V2G operation (a) DC link voltage (b) Battery voltage (c) Battery current (d) Grid voltage and current (e) Active and reactive power (f) Harmonic spectrum of grid current (1.83% THD).	24
Figure 2. 8 Operating waveforms during G2V operation (a) DC link voltage (b) Battery voltage (c) Battery current (d) Grid voltage and current (e) Active and reactive power (f) Harmonic spectrum of grid current (2% THD).	27
Figure 3. 1 Overview of physical layer communication system.	30
Figure 3. 2 Steps involved in physical layer communication system.	31
Figure 3. 3 BPSK and 4-QAM Modulation.	32
Figure 3. 4 16-QAM Modulation.	32
Figure 3. 5 Wireless Infrastructure Framework for V2G.	34
Figure 3. 6 Block diagram of Physical Layer Fixed WiMAX.	35
Figure 3. 7 Block Diagram of Randomizer Chain.	36
Figure 3. 8 RS coding.	37
Figure 3. 9 FEC Convolution and Puncturing.	38
Figure 3. 10 Subblock interleaving.	39
Figure 3. 11 OFDM Symbol.	41
Figure 3. 12 Guard band, pilot carriers and DC carrier.	41
Figure 3. 13 Frequency selective fading.	42

Figure 3. 14 OFDM Symbol.	42
Figure 3.15 LTE Frame structure.	48
Figure 3. 16 Block diagram of LTE Physical Layer.	49
Figure 3. 17 BER v/s SNR for GCC to Aggregator Link.	51
Figure 3. 18 Path loss for the Suburban environment with 6m receiver antenna height.	52
Figure 3. 19 Path loss for Suburban environment with 10m receiver antenna height.	53
Figure 3. 20 Path loss for the Urban environment with 6m receiver antenna height.	53
Figure 3. 21 Path loss for the Urban environment with 10m receiver antenna height.	54
Figure 3. 22 BER v/s SNR for 16QAM different channel models.	55
Figure 3. 23 BER v/s SNR for different Bandwidths.	55
Figure 3. 24 Category of Fading Channels.	58
Figure 3. 25 Variations in the transmitted signal due to path loss, shadowing and multipath.	58
Figure 3. 26 Shadowing.	59
Figure 3. 27 Multipath.	62
Figure 3. 28 Time Spreading.	63
Figure 3. 29 Spreading Frequency.	63
Figure 3. 30 Rayleigh distribution.	64
Figure 3. 31 Rician distribution.	65
Figure 3. 32 Simulated graph for the Aggregator to EV Communication.	66
Figure 3. 33 Path Loss for Urban environment at 10m receiver antenna height. ...	68
Figure 3. 34 Path Loss for Suburban environment at 6m receiver antenna height. ...	68
Figure 3. 35 Path Loss for Urban/Suburban Environment with IEEE 802.16d Model.	69
Figure 3. 36 Path Loss for Terrain Regions with IEEE 802.16d Model.	69
Figure 3. 37 Flat Fading Received Power Spectrum.	70
Figure 3. 38 Frequency Selective Fading.	71
Figure 3. 39 NLOS Rayleigh Fading (QAM).	72

Figure 3. 40 NLOS Rayleigh Fading (QPSK).	72
Figure 3. 41 LOS Rician QPSK.	73
Figure 3. 42 Communication Model of V2G.	74
Figure 3. 43 Block diagram of LTE Physical Layer.	78
Figure 3. 44 Path loss for Urban Environment.	80
Figure 3. 45 Path loss for Suburban Environment.	81
Figure 3. 46 Lognormal distribution of a signal.	81
Figure 3. 47 Received envelope (Rayleigh).	82
Figure 3. 48 Received envelope (Rician).	83
Figure 3. 49 BER v/s SNR for EV to EV Communication Link.	84
Figure 3. 50 BER v/s SNR for EV to EV Communication Link.	84
Figure 3. 51 EV to Smart Meter Communication in Charging Station.	88
Figure 3. 52 Block diagram of Wi-Fi (SISO) physical layer.	88
Figure 3. 53 Doppler spectrum estimate.	90
Figure 3. 54 Doppler spectrum estimate.	90
Figure 3. 55 Path1 Fading Envelopes for Tx1-Rx1 and Tx2-Rx2 links.	91
Figure 3. 56 Path1 Fading Envelopes for Tx1-Rx2 and Tx2-Rx2 links.	91
Figure 3. 57 Path1 Fading Envelopes for Tx1-Rx1 and Tx1-Rx2 links.	92
Figure 3. 58 Path1 Fading Envelopes for Tx2-Rx1 and Tx2-Rx2 links.	92
Figure 3. 59 Doppler spectrum estimate.	93
Figure 3. 60 Doppler spectrum estimate.	93
Figure 3. 61 Path1 Fading Envelopes for Tx1-Rx1 and Tx2-Rx1 links.	94
Figure 3. 62 Path1 Fading Envelopes for Tx1-Rx2 and Tx2-Rx2 links.	94
Figure 3. 63 Path1 Fading Envelopes for Tx1-Rx1 and Tx1-Rx2 links.	95
Figure 3. 64 Fading Envelopes for the links Tx2-Rx1 and Tx2-Rx2 for path 1. ...	95
Figure 3. 65 BER v/s SNR for EV to Smart Meter Communication link.	97
Figure 3. 66 BER v/s SNR for for EV to Smart Meter Communication link.	97
Figure 4. 1 EV arrivals and departures in the EVPL.	99
Figure 4. 2 Markov Model for Electrical Vehicle Parking Lot Occupancy.	101
Figure 4. 3 Queuing Model of EVs Connected to the Charging Station.	103
Figure 4. 4 State transition diagram for M/M/s queue.	104
Figure 4. 5 EVPL Utilisation.	106

Figure 4. 6 Average waiting time in EVPL.....	107
Figure 4. 7 Number of Backlogs v/s Probability of EV arrivals.	107
Figure 4. 8 Queue Size v/s Time in Hours for 20 EV arrivals.	108
Figure 4. 9 Queue Size v/s Time in Hours for 50 EV arrivals.	108
Figure 4. 10 Queue Size v/s Time in Hours for 100 EV arrivals.	109
Figure 4. 11 PDF of EVs in System.	109
Figure 4. 12 Idle Probability for different Chargers.	110
Figure 4. 13 EVs in Queue.	110
Figure 4. 14 EVs in System.....	111
Figure 4. 15 EVs Waiting Time in the Queue.....	111

LIST OF TABLES

Table 2. 1 Specification of the Proposed On Board Charger	16
Table 2. 2 Parameters of various controllers	22
Table 3. 1 Coding Rate.....	38
Table 3. 2 IEEE 802.16-2004 (Fixed WiMAX).....	50
Table 3. 3 Path Loss Simulation Parameters for WiMAX.....	51
Table 3. 4 IEEE 802.16e (Mobile WiMAX).....	57
Table 3. 5 Values of Path Loss Exponent	60
Table 3. 6 Terrain category [Vinko et al. 1999].....	61
Table 3. 7 Path loss parameters [Hamid and Kostanic2013]	79
Table 3. 8 Types of Antenna	86
Table 3. 9 Parameters for 802.11	96

ABBREVIATIONS

3GPP	:	Third Generation Partnership Project
BER	:	Bit Error Rate
CP	:	Cyclic prefix
DAC	:	Digital-to-Analog Converter
eNodeB	:	Base station node
EV	:	Electric Vehicle
EVPL	:	Electric Vehicle Parking Lot
FDD	:	Frequency Division Duplex
G2V	:	Grid to Vehicle
LOS	:	Line of Sight
LTE	:	Long Term Evolution
M/M/m	:	Inter-arrival time distribution/ Service time distribution/ Number of Server
MIMO	:	Multiple-Input-Multiple Output
NLOS/NOLOS	:	Non Line of Sight
OFDM	:	Orthogonal Frequency Division Multiplexing
QAM	:	Quadrature Amplitude Modulation
QPSK	:	Quadrature Phase Shift Keying
SC-FDMA	:	Single carrier frequency division multiple access
SISO	:	Single-Input-Single-Output
SNR	:	Signal-to-Noise Ratio
TDD	:	Time Division Duplex
UE	:	User equipment
V2G	:	Vehicle-to-Grid
V2H	:	Vehicle-to-Home
V2V	:	Vehicle-to-Vehicle
WiFi	:	802.11 Networking
WiMAX	:	Worldwide Interoperability for Microwave Access

CHAPTER 1

INTRODUCTION

1.1 VEHICLE-to-GRID (V2G)

The restructuring policy of power system network and depleting fossil fuels have motivated private players to participate in power generation using renewable energy resources . With the developments in power grid technology from conventional to Smart grid, the concept of Distributed Generation (DG) along with bidirectional power flow evolved. With rapid integration of DGs like photovoltaics (PV), wind turbines, micro turbine, fuel cell (FC) and internal combustion(IC) engine in the distribution network and for the stabilized system operation in terms of voltage and frequency during peak and off peak hours, the need for distribute energy storage systems (DESS) aroused. Also the intermittent sources like PV and Wind systems supplement the concept of storage systems.

EV battery is one among the storage system. Due to growing oil demand and serious environmental concerns even the Car manufacturers and associated entities are promoting the Plug-in electrical vehicle (PHEV) or pure electrical vehicle (PEV) or Electrical Vehicles (EV) which can be used as transportation tool along with power transaction unit. With this the concept of V2G has become a reality. EVs are usually parked for 90-95% of the time in residential buildings, office complex, parking lots etc. and this parking time can be used to for power transaction with the grid. EV connected to home grid is termed as Vehicle-to-Home (V2H), EV connected to other EV is Vehicle-to-Vehicle (V2V) and the group of EVs connected to the grid for power transaction is Vehicle-to-Grid (V2G).

A single EV can consume but cannot deliver power to the grid but the group of EVs makes a sizeable difference and delivers power to the grid [Liu et al. 2013]. V2G supports and contributes power to the grid in order to meet the time varying load demand and helps in maintaining stability of the power system for a shorter duration of time. V2G is economical, effective and efficient solution for peak shaving and valley filling in comparison to other existing methods [Wang and Wang 2013; Wu et al. 2011]. EVs need bidirectional charger to sell or buy power from the grid. Further the bidirectional charger has the direct current (dc) link capacitor which inherently provides the reactive power support to the grid [Yilmaz and Krein 2013].

The conceptual framework of V2G is shown in Figure 1.1 [Liu et al. 2013] and it depicts EVs connected to the grid through charging stations which are located at the Medium Voltage (MV) network and Low Voltage (LV) network. The medium scale generation is connected to MV network and small scale generation is connected to the LV network. The smart buildings, commercial complexes with dedicated parking lot facilitate EVs to get connected to the grid.

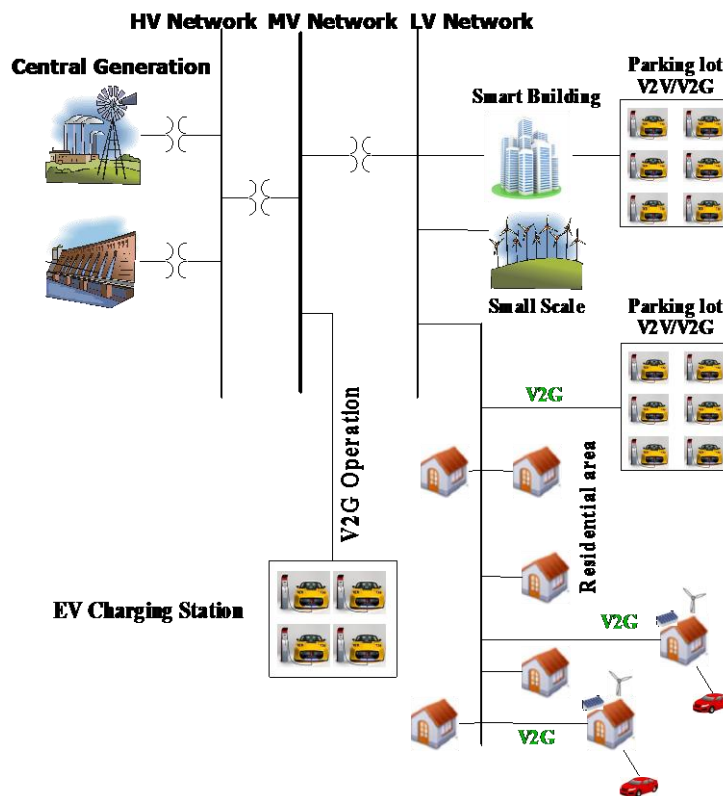


Figure 1. 1 Conceptual framework of V2G.

EV can be connected to home grid or other interface using the On-Board or Off-Board bidirectional chargers or V2G integrators. The On-Board V2G integrator is suitable for V2H and V2V whereas, Off-Board is for V2G. Both the integrators have to comply with IEEE 1547 Standards. These integrators are used for both charging and discharging of EV batteries.

For smooth functioning and better battery life, the state of charge (SOC) of EV battery should be between 20 - 90%. EV acts as connected load if the SOC is less than 60% and DER if SOC is in the range of 80 - 95% [Diyun et al. 2011]. EV action is based on SOC of EV battery i.e. either to sell (discharge) or buy (charge) power from the grid as shown in Figure 1.2. The group of EV batteries can be used to meet the grid requirements accordingly and in order to facilitate this, we need communication between the grid and EVs.

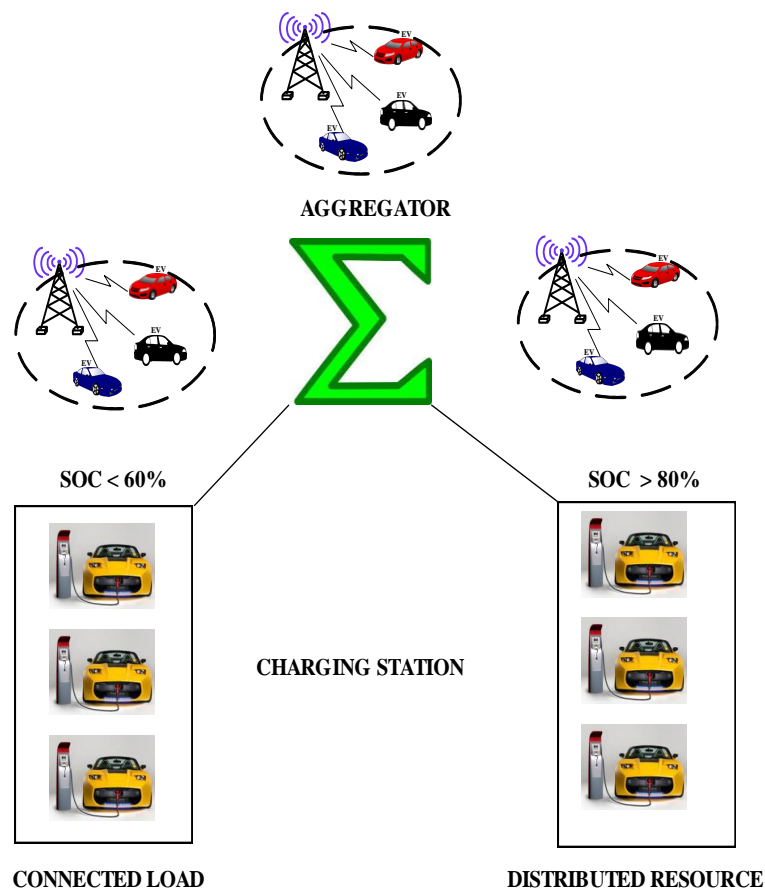


Figure 1. 2 EV action based on SOC of a battery.

The communication model of V2G is shown in Figure 1.3. The Grid Control Center (GCC), Aggregator and EV are three essential entities of V2G communication and operation. The GCC provides the information about the electricity requirements to Aggregator and in turn the Aggregator after receiving the information, communicates to EVs. The Aggregator aggregates EVs and facilitates them to contribute power to the grid.

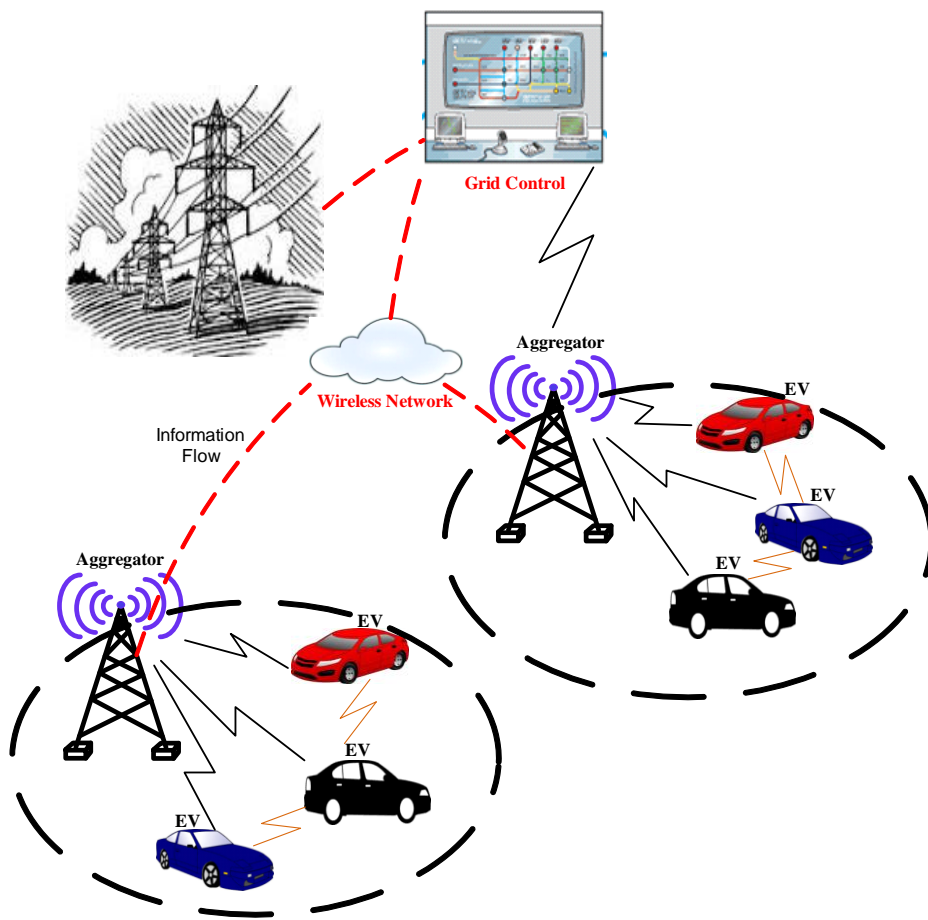


Figure 1. 3 Communication Model of V2G.

In V2G environment, wireless communication protocols are adopted due to the fact that moving EVs can't be communicated with wired communication. Hence, establishing wireless links for GCC to EV communication is very important for smooth functioning of V2G operation. Along with the communication, mobilizing EVs at Aggregator and facilitating them to participate in power transaction with grid is another key issue.

1.2 WIRELESS COMMUNICATION

To develop a robust wireless communication network, proper planning is required and in order to address this issue Channel modeling will come into picture. The wireless channel is the variation in the channel strength over time and frequency. The variations may be due to path loss, shadowing and small scale fading.

1.2.1 Path Loss

The propagation models are used to calculate the electrical field strength and predict the path loss which is very crucial in planning wireless network. The information in wireless communication system is transmitted from the transmitter to the receiver by the means of electromagnetic waves and in the process of propagation they come across lot of obstacles in the environment which causes the Path Loss [Josip et al. 2007; Mohammad and Abdulla 2009]. It is defined as the difference between the transmitted power and the received power measured in terms of dB. The Propagation models are split in to three categories:

- i. Deterministic model: site specific theoretical
- ii. Empirical models: based on measurements, antenna height, frequency and distance
- iii. Stochastic models: based on series of random variables.

1.2.2 Shadowing

The signal loss occurs due to buildings, trees, hills and walls. The power loss in dB is random and is given by:

$$L_p = E\{L_p\} + \chi \quad (1.1)$$

where, E is expected value and χ is random, zero mean approximately gaussian with $\sigma = 6-12$ dB and represents the effect of shadowing. The log normal distribution better describes the statistical properties of shadowing.

The average Loss is given by:

$$E\{L_p\}=10\gamma\log_{10}\left(\frac{d}{d_0}\right)+L_0 \quad (1.2)$$

1.2.3 Small Scale Fading

The multipath will cause short term fluctuations in the signal amplitude which leads to small scale fading. The small scale fading is categorized into flat, frequency selective, slow and fast fading. If the channel bandwidth is larger than the signal bandwidth then the received signal undergoes flat fading otherwise frequency selective fading. In both the flat and frequency fading, signal is distorted and dispersed due to attenuation, different versions of transmitted signals and delay in time. This is known as inter symbol interference (ISI). Doppler spread causes frequency dispersion and results in fast or slow fading. The Rayleigh and Rician distribution describes the statistical nature of the NLOS and LOS [Theodore 1999].

1.3 LITERATURE REVIEW

The first article on the concept of V2G was coined by Prof. Willet Kempton, University of Delaware, USA. The recent research studies have reported on various components of V2G such as opportunities and challenges of V2G and V2G integrators, communication aspects of V2G and stochastic modeling of EVPL occupancy and Queuing. A brief description of the same is presented below:

The various opportunities and challenges of V2G are articulated in [Liu et al. 2013] with the emphasis on the framework for V2H, V2V and V2G systems, power electronics for V2G systems, battery technology and optimisation of power quality issues. The existing techniques available for V2G integration are reviewed in [Yilmaz and Krein 2013] focussing on V2G system requirements and potential economic benefits of V2G. Willett Kempton, Jasna Tomi are pioneers of the V2G concept and their research articles are serving as base papers for the researchers in this area. In the year 2005 they articulated two papers: first briefed the basics of V2G and the revenue

generation associated with it [Willet and Jasna 2005] and in the second paper they explained the complexities involved in implementation of V2G [Willet and Jasna 2005]. The potential benefit and sustainability of V2G in Smart Grid Environment is discussed in [Dallinger and Link 2014] and the detailed conceptual frame work of V2G is presented in [Christope and George 2009]. The impact of V2G on distribution grid is discussed in [Robert et al. 2011] and the experimental verification and difficulties of V2G are expressed in [Mendoza et al. 2013]. The contactless charger suitable for Indian Power Grid environment and benefits are projected in [Thirugnanam et al. 2014] and requirements of bidirectional charger for V2G are discussed in [Khan et al. 2012]. The new approach to V2G connection is proposed in [Kyu et al. 2012] and economic opportunities related to V2G aspect is presented in [Esmailian et al. 2012]. Aggregator agent role for EV in the Energy Market and the framework for the Aggregator activity are presented in [Ricardo and Manuel 2010] and the role of Aggregators in Smart Grid Demand Response Markets and the operation for the day ahead market are discussed in [Lazaros et.al 2013]. The optimal charging of EV in Smart Grid with valley filling algorithms are presented in [Niangjun et.al 2012] and load model for prediction of EV charging demand is discussed in [Kejun et.al 2010]. Integration of Power Systems, transport systems and vehicle technology for electrical mobility impact assessment and control is presented in [Matthia et.al 2012].

In [Kisacikoglu et.al 2015] have discussed on the usage of bidirectional converter for reactive power support in V2G integration and the design aspects of off board V2G integrator are comprehensively presented in [Kesler et.al 2014].

In the existing literature only few papers discuss about the V2G communication. The GCC to aggregator and aggregator to EV communication are discussed in [Zountordonio et.al 2011]. In this paper fixed WiMAX protocol is proposed for the GCC to aggregator communication and the 802.11p protocol is proposed for aggregator to EV communication. Performance is analysed using BER v/s SNR curves. The Bluetooth protocol for EV to Smart Grid communication is presented in [Massimo et.al 2011] where the link is established between the charging station,

vehicle and Smart phone. The SystemC architecture and user vehicle charging station system with Bluetooth and CAN protocol is developed. The message propagation model for vehicular communication protocols is furnished in [Anna et.al 2010] which demonstrate the need of vehicular adhoc networks (VANET) for intelligent transportation system (ITS). V2G communication interfaces are discussed in [Kovacs et al. 2013] and HPGP (Home Plug Green PHY) is presented in [Cheol et al. 2012]. A secured communication protocol is described in [Huei 2012] for EV integration to grid. Unique batch authentication protocol is proposed in [Huei 2012]. Multiagent based system developed for EV integration to grid and simulating G2V and G2V charging strategies for large vehicle fleet is presented in [Sachin et.al 2011; Stefan and Matthias 2013]. Agent based impact analysis of EV rural MV network using traffic survey data is discussed in [Matthias et.al 2013].

EV demand model for load flow studies based on queuing model is developed and discussed in [Rodrigo and John, 2009] and optimising the PHEV charging queues is presented in [Hesam and Xavier 2015]. Probabilistic power flow calculation for PHEV charging demand is modeled and presented in [Gan and Xiao-Ping 2012]. Markov chain is used to simulate the charging and driving behaviour of EV presented in [Hill and Blythe 2012] and plug in mobility and charging flexibility Markov model for driving behaviour is discussed in [Pia et al. 2012]. Stochastic model quantifies the energy requirement from the grid and the EV mobilisation in [Soares et.al 2011] and M/M/m queuing model is developed for EVs charging at supply station in [Dhaou et al. 2013]. A stochastic model for EV charging is exclusively discussed in [Csaba and Laszlo 2012]. Markov model developed for EV battery storage through the PV system is discussed in [Junseok et al. 2012].

In existing literature, only one research paper reports the application of WiMAX and 802.11p wireless protocols excluding path loss for GCC to Aggregator and Aggregator to EV communication respectively and two papers discuss the concept of Queuing strategies for EV charging in V2G environment. After reviewing the articles it is observed that there is no mention of wireless protocols with path loss models for EV to EV and EV to Smart Meter Communication in V2G. Also, Stochastic Model of

EVPL occupancy has not been discussed. Based on above research scope the problem statement is given as: the Performance Investigation of Applicable Wireless Communication Protocols for GCC to Aggregator, Aggregator to EV, EV to EV, EV to Smart Meter and stochastic modelling of EVPL occupancy, queuing model for EV charging in V2G for Smart Grid Environment.

1.4 RESEARCH OBJECTIVES

V2G supports the grid requirements by shaving peak, filling valley and leveling the load demand. The key requirements for V2G operation are:

- i. Information transfer: The information sent by GCC should reach aggregator and aggregator has to send this information to EVs. The fading channel is a big challenge in case of wireless communication as the information is transmitted from transmitter to receiver by the means of electromagnetic waves and in the process of propagation they come across lot of obstacles in the environment which causes the Path Loss.
- ii. Facilitating EVs to participate in power transaction with the grid. The EV requirements are SOC of EV battery, parking lot/charging slot availability and recharge stations availability.

The applicable wireless communication protocols have to be selected and suitable empirical path loss models have to be considered to address and mitigate the issue of channel fading. The management of EV arrivals and departure is taken care for charging and discharging operation in EVPL. With this background the following objectives were set for the thesis:

- 1 Performance analysis and comparison of path loss models for the wireless communication protocols considered for V2G communication using MATLAB.
- 2 Modeling of Physical layer in MATLAB/SIMULINK and to investigate the performance of the applicable wireless communication protocols for Grid control center to aggregator communication.

- 3 Modeling of Physical layer in MATLAB/SIMULINK and to investigate the performance of the applicable wireless communication protocols for Aggregator to EV communication.
- 4 Modeling of Physical layer in MATLAB/SIMULINK and to investigate the performance of the applicable wireless communication protocols for EV to EV communication.
- 5 Modeling of Physical layer in MATLAB/SIMULINK and to investigate the performance of the applicable wireless communication protocols for EV to Smart Meter Communication.
- 6 Stochastic Modeling Of EV Parking Lot Occupancy And Queuing
 - i. EVPL Occupancy.
 - ii. Markov Chain Based Queuing Model.

1.5 THESIS ORGANISATION

This thesis is organised as follows:

Chapter 1 deals with the introduction to the topics covered in this thesis namely V2G and V2G communication. The existing literature survey on these topics is reported and the objectives of the work are specified. The organization of the thesis is covered at the end.

Chapter 2 is dedicated to the modelling and simulation of V2G integrators. The V2G and G2V power flow performance are discussed.

Chapter 3 exclusively proposes wireless access support for GCC to Aggregator, Aggregator to EV, EV to EV and EV to Smart Meter communication in V2G for Smart Grid application. The path loss models are analysed and compared for the selected protocols. The Physical layer of applicable wireless communication protocols (fixed/mobile WiMAX, WiFi, LTE) are developed using MATLAB/SIMULINK and their performance is investigated using BER v/s SNR curves.

Chapter 4 focuses on the development of Stochastic model for EVPL occupancy and EV Queuing. EVPL utilisation, EVs waiting time in system and queue are discussed.

Chapter 5 covers the summary of the work carried out and briefly outlines the main contributions carried out in the thesis. It also enlists the scope for future investigations in the area of V2G communication.

1.6 CONTRIBUTIONS OF THE THESIS WORK

The main contributions of this thesis work are development of wireless infrastructure for V2G communication and stochastic modeling of EVPL occupancy and EV queuing for charging/discharging. The wireless link is established between GCC to aggregator, aggregator to EV, EV to EV and EV to Smart Meter communication. Following are the applicable protocols considered for V2G communication:

- i. Fixed WiMAX protocol is proposed for GCC to aggregator communication and performance is analysed using BER v/s SNR curves. Also the path loss models are analysed and compared.
- ii. Mobile WiMAX protocol is proposed for aggregator to EV communication and performance is analysed using BER v/s SNR curves.
- iii. LTE protocol is proposed for EV to EV communication and performance is analysed using BER v/s SNR curves.
- iv. WiMAX/WiFi is proposed for Smart Meter to EV communication and performance is analysed using BER v/s SNR curves. Also the channel models for 802.11 protocol are analysed for indoor environment.
- v. Queuing model and stochastic model for EVPL occupancy is developed to facilitate EV charging. The simulations are carried out using MATLAB and EVs waiting in queue and waiting in system are presented.

CHAPTER 2

MODELING OF V2G INTEGRATORS

2.1 INTRODUCTION

EV can be connected to the home grid or other interface using the On-Board or Off-Board bidirectional charger or integrators. The chargers have to comply with IEEE 1547 standard. Basically a charger is an interface between EV battery and the grid for power transaction.

It is possible to have bidirectional power flow by incorporating the charger to operate in different modes. Generally, transaction of power from vehicle to the grid is called V2G and the vice-versa is called G2V. This has led to several economic and technical benefits and has become a hot spot for research in the last decades [Letendre and Willet 1999, 2002]. The integrators for power transaction are broadly classified into

- a) On-board integrator and
- b) Off-board integrator.

As shown in Figure 2.1, each EV is provided with a permanent integrator and is called an On-board integrator [Kisacikoglu et al. 2015]. They convert AC grid voltage into DC, and they have unidirectional power transfer capability. It can also be provided to support ancillary services of power quality functions like voltage regulation, reactive power compensation (inductive or capacitive), power factor correction and harmonic filtering.

In an Off-board integrator, the interface for EV and the grid is made available only at the charging stations [Kesler et al. 2014]. A DC bus is created in the charging station by converting the available AC grid voltage to DC to which EVs are coupled.

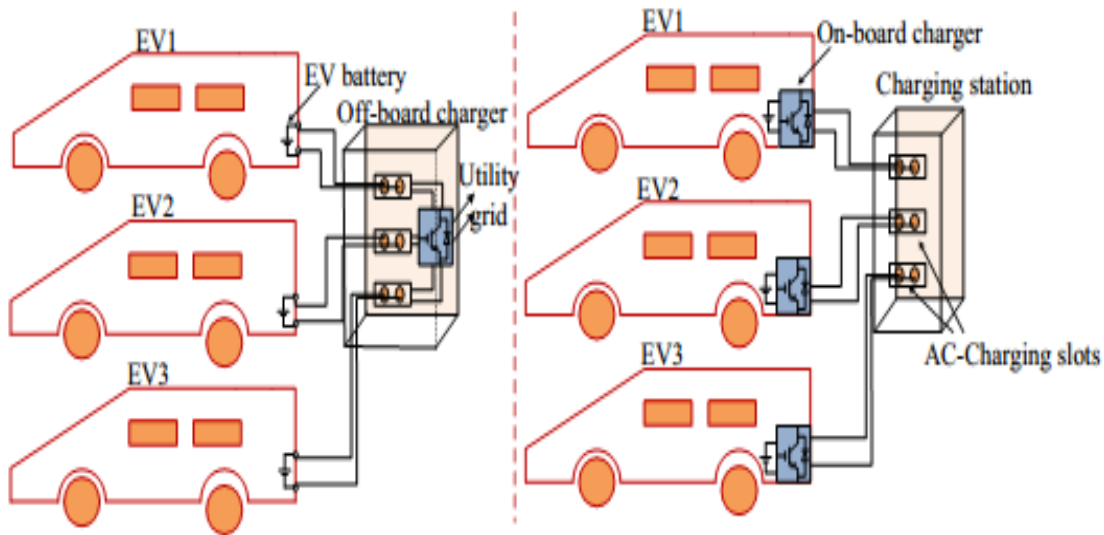


Figure 2. 1 Off-board and On-board integrator.

2.2 MODELING OF V2G INTEGRATOR

This section describes topological details of the proposed integrator and also control aspect of the same is presented. A two stage power processing is employed for V2G and G2V operation of the integrator. The on-board chargers typically include two stages: 1) the AC–DC rectification and 2) DC–DC conversion. The first stage is bidirectional DC-DC converter and the second stage is a bidirectional DC-AC converter. The direction of power flow is dictated by the operating mode. The power flows from EV batteries to the DC link and then to the grid during V2G mode of operation and in the opposite direction during G2V mode of operation. The configuration of V2G integrator is shown in Figure 2.2.

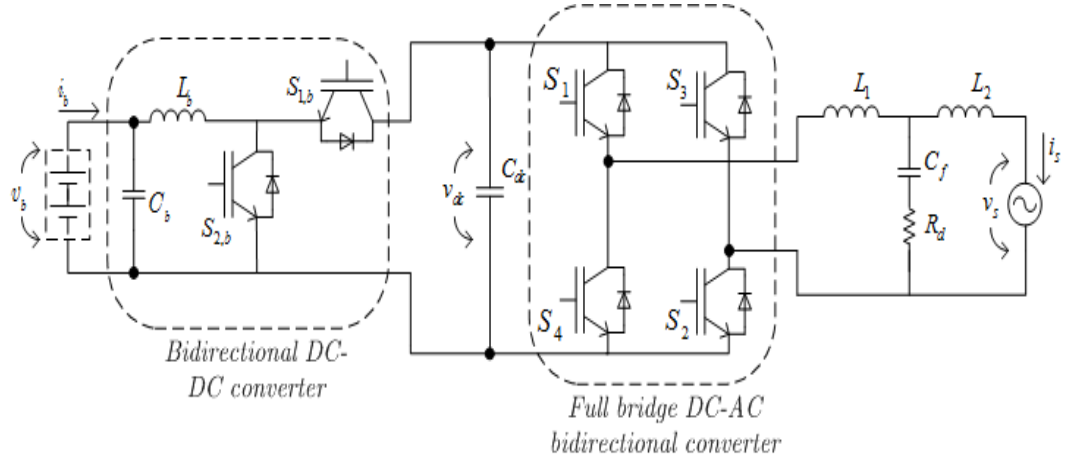


Figure 2. 2 Configuration of the system under study.

The system parameters considered are listed in Table 2.1. The sizing of DC-link capacitor plays a vital role in decoupling the power and thus a suitable value of capacitor has to be chosen for proper operation of the system. The capacitor is chosen based on the power level, voltage ripple, and double frequency of the grid voltage. Considering the grid voltage and current to be sinusoidal

$$v_g(t) = v_m \sin(\omega t) \quad (2.1)$$

$$i_g(t) = i_m \sin(\omega t - \phi) \quad (2.2)$$

The instantaneous power will have terms corresponding to the average and double-line frequency power. This can be written as

$$P_{out(t)} \cong V_{dc}(t)i_{dc}(t) \cong S \cos(\phi) + S \cos(2\omega_g t - \phi) \quad (2.3)$$

Where S is the apparent power in VA, and the DC-link current $i_{dc}(t)$ consists of DC and AC component. Thus the value of capacitance can be obtained using the relation

$$C_{dc} = \frac{S}{2\omega_g V_{dc} \Delta v_{dc}} \quad (2.4)$$

By substituting, the values corresponding to the specifications considered

$$C_{dc} = \frac{8000}{2 * 2 * \pi * 50 * 400 * 40} \cong 1\text{mF} \quad (2.5)$$

A full bridge bidirectional converter with SPWM (sinusoidal pulse width modulation) unipolar voltage switching scheme is used as a switching circuit of the inverter. The bidirectional DC-DC converter is capable of boosting the battery voltage during V2G operation and step down the voltage suitable for battery during G2V operation.

Table 2. 1 Specification of the Proposed On Board Charger

<i>Parameter</i>	<i>Value</i>	<i>Unit</i>
Grid voltage (RMS)	230	V
Grid frequency	50	Hz
Maximum input current (RMS)	35	A
Maximum input power	8	KVA
Output voltage range (DC)	190-270	V
Maximum output current (DC)	30	A
Inductor L_1	0.3	mH
Inductor L_2	0.5	mH
Capacitor C_f	2	μF
Capacitor C_b	800	μF
Capacitor C_{dc}	1000	μF
Switching frequency of DC-AC converter	10	kHz
Switching frequency of DC-DC converter	25	kHz

2.2.1 Grid-to-Vehicle (G2V) mode of operation

In this mode of operation, DC-AC bidirectional converter acts as an active rectifier drawing sinusoidal current from grid in phase with the grid voltage. The bidirectional DC-DC converter operates as a buck converter in current control mode.

2.2.2 Three-level bidirectional DC-AC converter control

In grid connected mode, converter operates in current controlled mode as the voltage across it is maintained by the infinite grid. Thus for the proper operation, synchronization with the grid voltage is mandatory. This is achieved using a phase locked loop (PLL) which generates an in phase component of the grid voltage and eliminates the harmonics present. An LCL filter acting as an interface between DC-AC converter and the grid reduces harmonic distortion in the injected grid current. The amount of attenuation provided over high frequency range is more even with the smaller value of passive components as the filter is of third order. However the filter possesses a significant problem due to its low or zero impedance at the resonant frequencies making the current controller design complicated. A general approach to damp the resonance oscillations is to add a damping resistor in series with the filter capacitor. Even though the method seems to be effective in stabilizing the overall filter characteristics, it suffers from the increased power loss.

As an alternative to passive damping, an approach to introduce the same effect using feedback of the parameters which can serve as damping term and is known as active damping. Bode plot of LCL filter for various value of damping is shown in Figure 2. 3. For an application with a stiff grid, a passive damping method is often preferred for its simplicity and low cost. The control of DC-AC converter is achieved through two loops with outer loop for voltage control loop and the inner loop for current control. The block diagram of LCL filter with the inner current loop is shown in Figure 2.4. Various controllers like stationary frame control, dq frame control and abc frame controllers can be employed to maintain the sinusoidal grid current with lower harmonic distortion. A proportional resonant (PR) compensator is used to track a sinusoidal current reference signal with zero steady state error, as the controller introduces an infinite gain theoretically at the grid frequency.

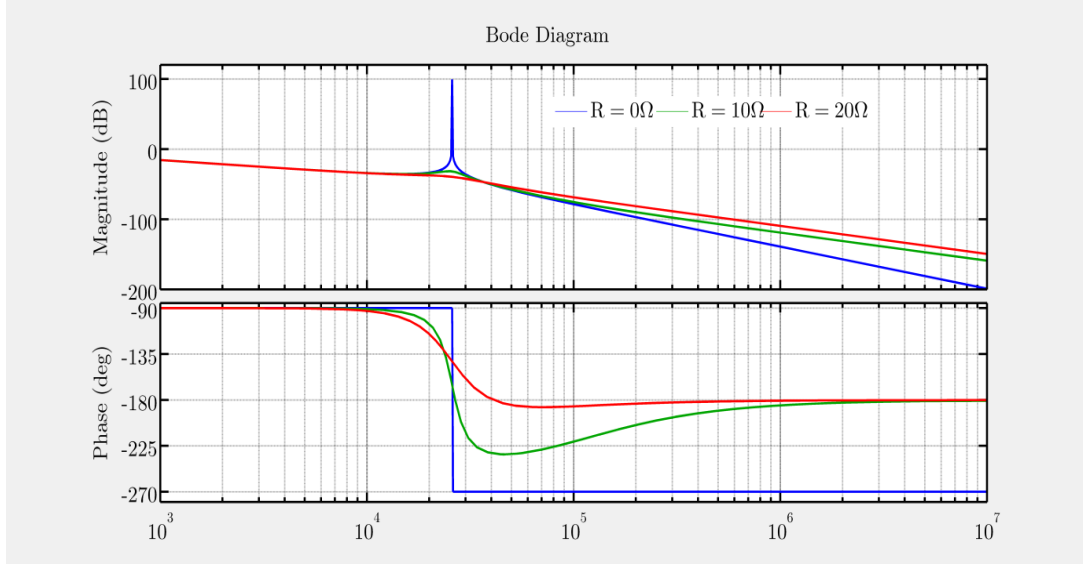


Figure 2. 3 Bode diagram of LCL filter.

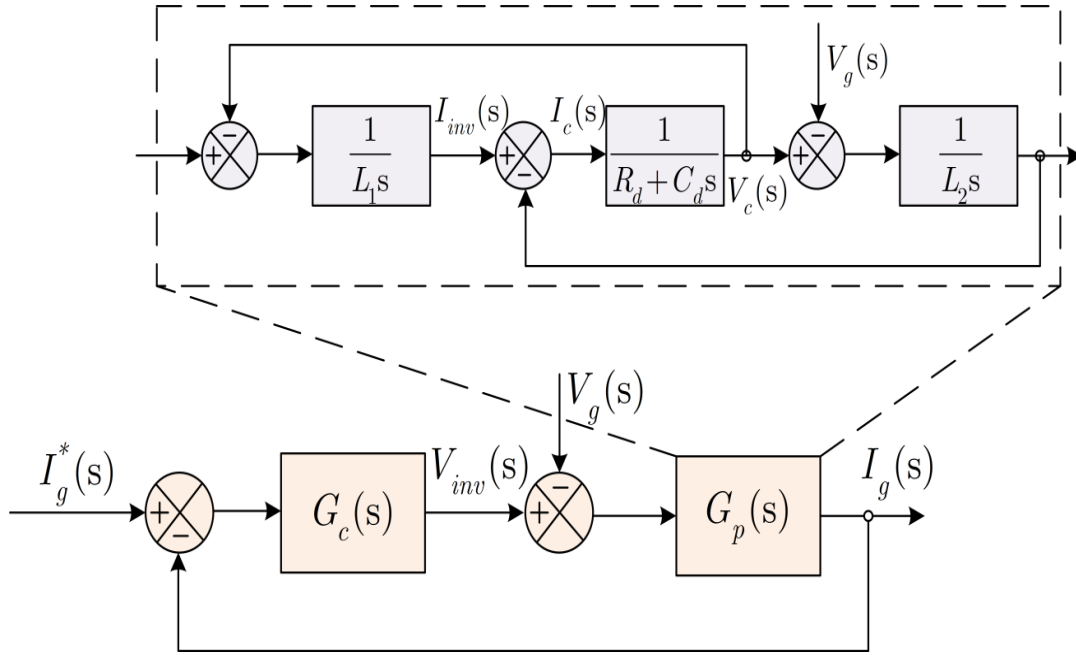


Figure 2. 4 Block diagram of LCL filter.

The expression for the grid current from the above block diagram can be obtained as

$$I_g(s) = G_p(s) \left(\frac{s^2 L_1 C_d + s C_d R_d + 1}{s C_d R_d + 1} V_g - V_{inv} \right) \quad (2.6)$$

Since, the magnitude and phase response of $\frac{s^2 L_1 C_d + s C_d R_d + 1}{s C_d R_d + 1}$ are 0 dB and 0° at the fundamental frequency of the grid. Therefore, equation (2.6) can be simplified to equation

$$I_g(s) = G_p(s)(V_{inv} - V_g) \quad (2.7)$$

The input-output relation of the current loop can be derived as:

$$I_g(s) = H_1(s) \cdot I_g^*(s) + H_2(s) \cdot V_g(s) \quad (2.8)$$

where,

$$H_1(s) = \frac{G_c(s) \cdot G_p(s)}{G_c(s) \cdot G_p(s) - 1} s$$

$$H_2(s) = \frac{G_p(s)}{1 - G_c(s) \cdot G_p(s)}$$

To successfully track the $i_g^*(t)$ signal without steady state errors, the magnitude of $H_1(j\omega)$ in equation (2.8) has to be equal to 1 at the fundamental frequency of $i_g^*(t)$. Thus, it is clear that if $G_c(j\omega)$ has infinite gain at fundamental frequency, $H_1(j\omega)$ would have a unity gain. On the other hand, if $G_c(j\omega)$ has infinite gain at fundamental frequency, $H_2(j\omega)$ in equation (2.8) results in 0. So, $H_2(j\omega)$ term can be neglected. Therefore, it is not necessary to have the grid voltage feed-forward in the current control loop. To conclude, the controller, $G_c(j\omega)$ has to have an infinite gain at fundamental frequency in order to track the current reference $i_g^*(t)$.

The control structure of a PR controller is given by equation (2.9).

$$G_c(s) = K_p + \frac{K_i \cdot 2 \cdot \xi \cdot \omega_o \cdot s}{s^2 + 2 \cdot \xi \cdot \omega_o \cdot s + \omega_o^2} \quad (2.9)$$

Where $\omega_o = 2\pi f_o$, K_i is the fundamental harmonic gain, and ξ is the damping factor.

The bode diagram for the uncompensated and compensated current control loop is shown in Figure 2.5. It can be seen that after compensation the overall bandwidth of the system is increased which makes the system to respond faster. The gain of around 82 dB at the grid frequency (50 Hz) leads to zero steady state error in tracking of the reference current generated.

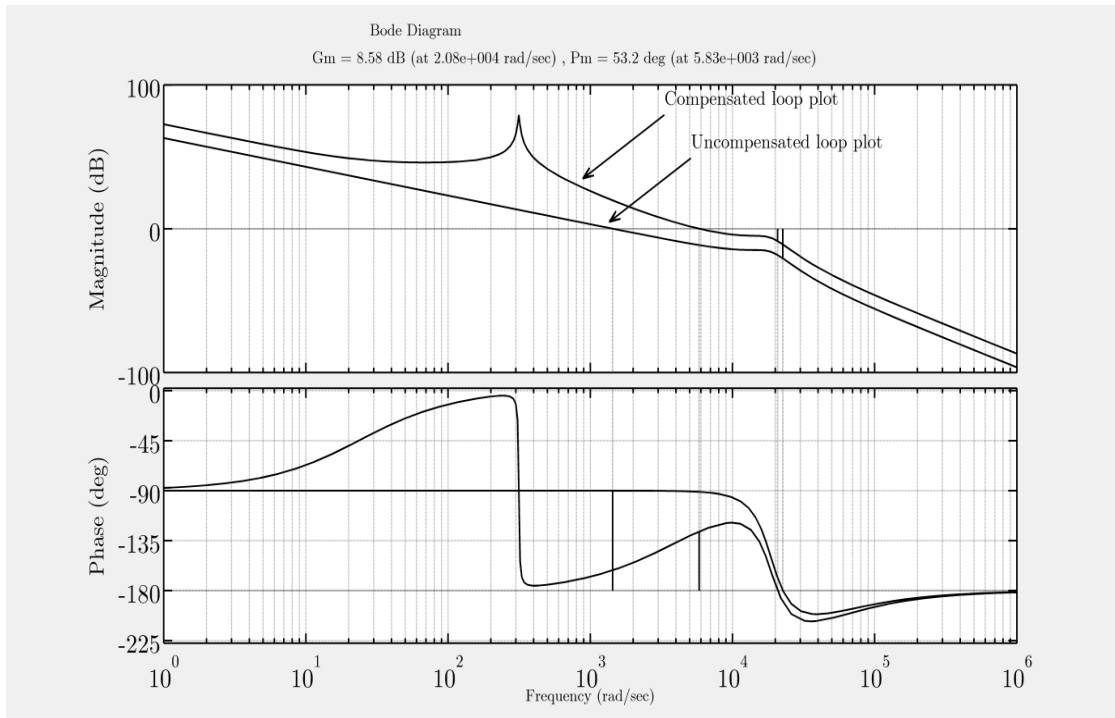


Figure 2. 5 Bode diagram of uncompensated and compensated current control loop.

The overall control structure with outer voltage loop embedded is shown in Figure 2.6. The converter DC link voltage should be greater than peak value of the grid voltage, so that the power can be transferred from EVs to grid. Assuming that the

sinusoidal current is being pumped to the grid, the DC link voltage will have a second harmonic component. This leads to control system instability if it is not filtered out before using for control purpose. Thus, band stop filter (BSF) is used to remove 100 Hz component in V_{dc} . The unipolar pulse width modulation scheme is employed for gating the power switches.

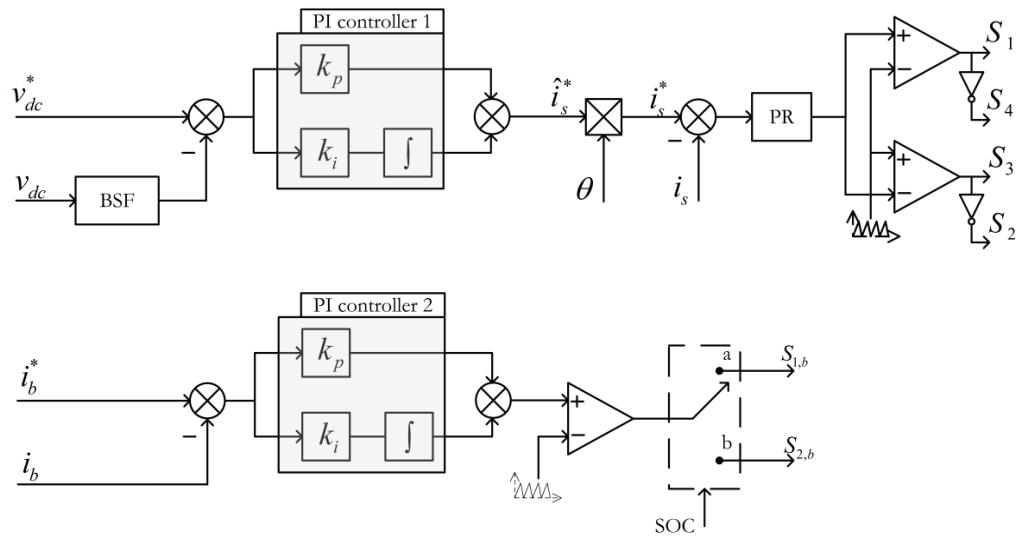


Figure 2. 6 Control block diagram of the bidirectional DC-AC & DC-DC converter.

2.2.2.1 Bidirectional DC-DC converter control

The DC link voltage is maintained constant by the DC-AC converter. The DC-DC converter acts as a buck converter during G2V mode of operation. The control structure for accomplishing the above tasks is shown in Figure 2.6. As per recommendations by the EV manufacturers generally a constant current charging is done first until the battery voltage reaches recommended maximum value and followed by a constant voltage charging. A proportional integral controller (PI) is used for regulating both DC link voltage and current (charging/ discharging) of the EV battery.

2.2.3 Vehicle-to-Grid (V2G) mode of operation

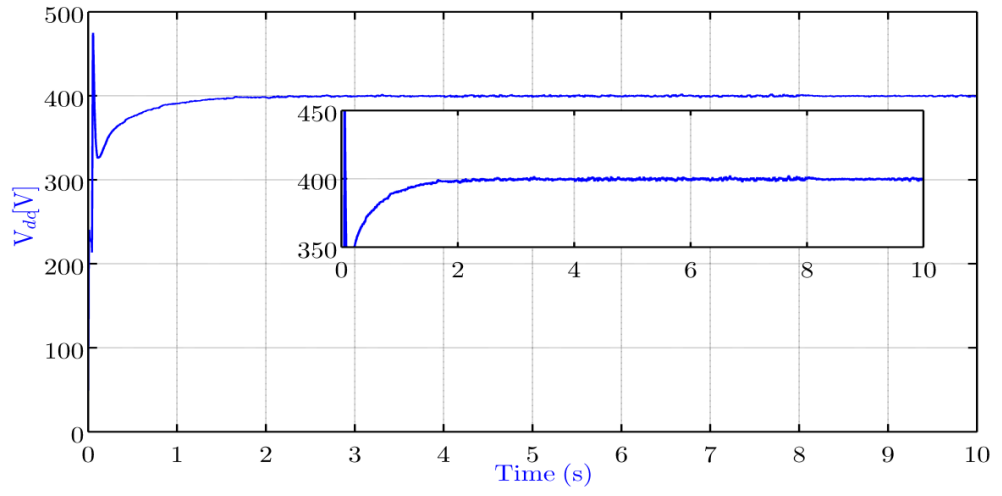
In this mode of operation, DC-AC bidirectional converter injects the sinusoidal current in phase with the grid voltage. The reference current generated by PI controller1 is compared with actual grid current and error is processed through the PR controller. DC-DC converter acts as a boost converter by stepping up the battery voltage and draws a constant current from the battery. The specification of the various parameters of the system and the controller are listed in Table 2.2.

Table 2. 2 Parameters of various controllers

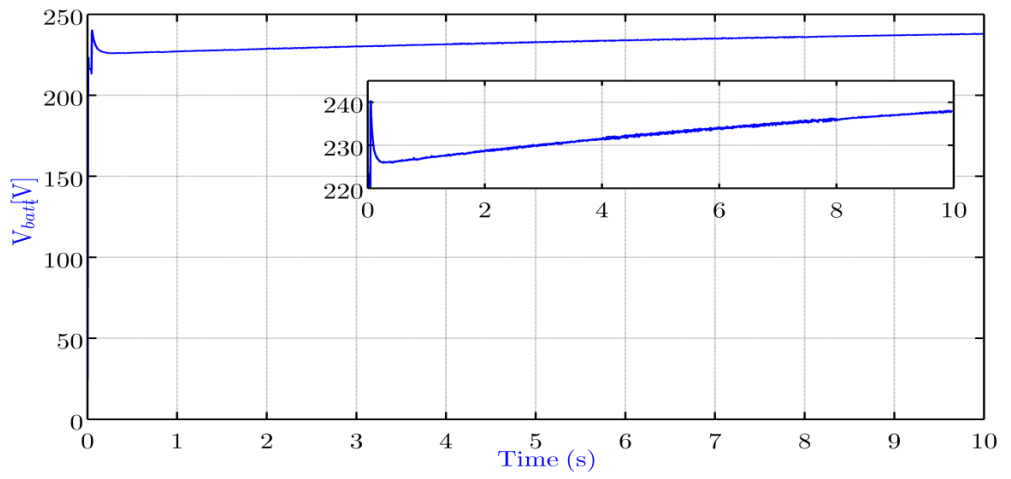
	K_P	K_I
PI controller 1	0.3	2
PI controller 2	0.75	5
PR controller	3	10000

2.3 SIMULATION RESULTS

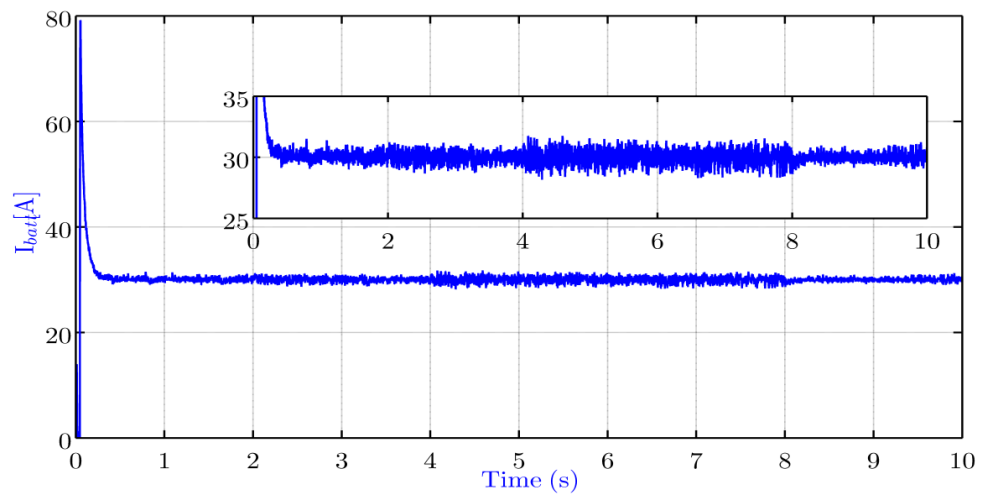
Simulations are carried out using MATLAB/SIMULINK with the parameters listed in the Table 2.1 and 2.2. System operation during V2G and G2V are presented. Figure 2.7 shows the waveforms corresponding to G2V operation. Figure 2.7(a) shows DC link voltage waveform being regulated at 400 V. Figure 2.7(b-c) depict the battery voltage and current during constant charging mode. Figure 2.7(d) portraits the grid voltage and sinusoidal current being absorbed by DC-AC converter. It is observed that the current drawn is in phase with the grid voltage ensuring unity power factor operation. The battery is supplied with a constant active power ($P = 7$ kW) and zero reactive power ($Q = 0$) as shown in Figure 2.7(e). The harmonic level in the grid current being drawn is found to be 1.83% which comply with IEEE 1547-2003 standard. The harmonic spectrum of the grid current is shown in Figure 2.7(f).



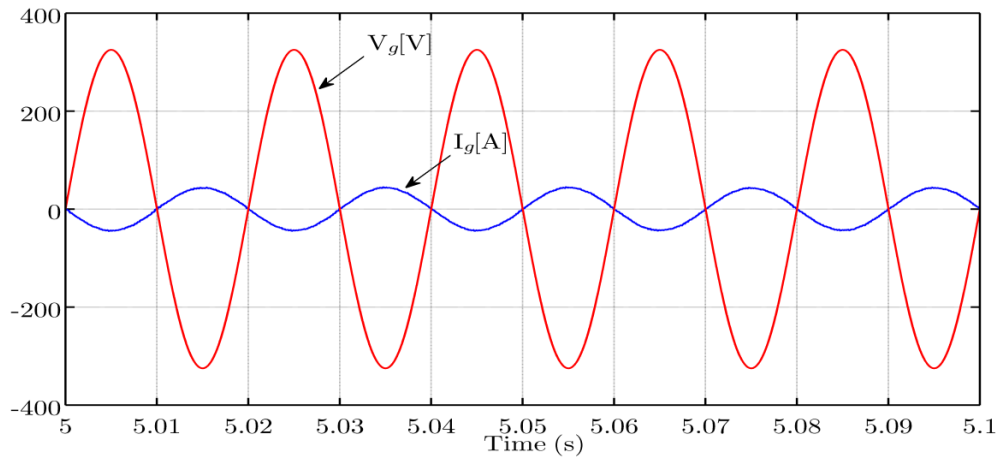
(a)



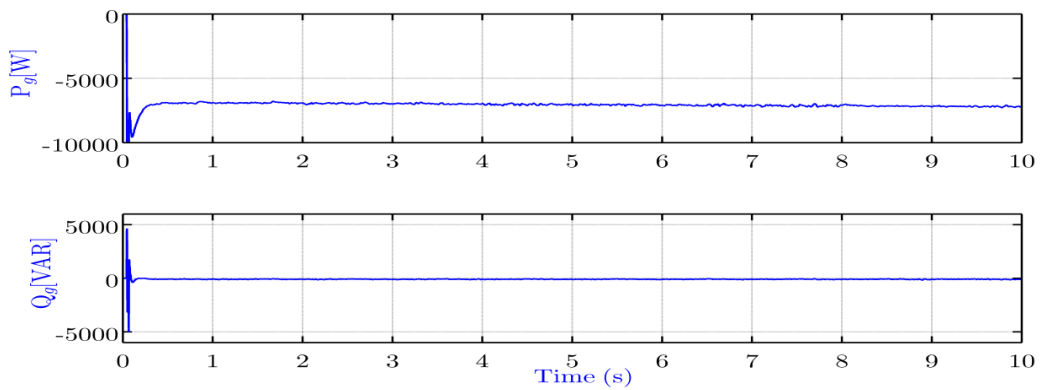
(b)



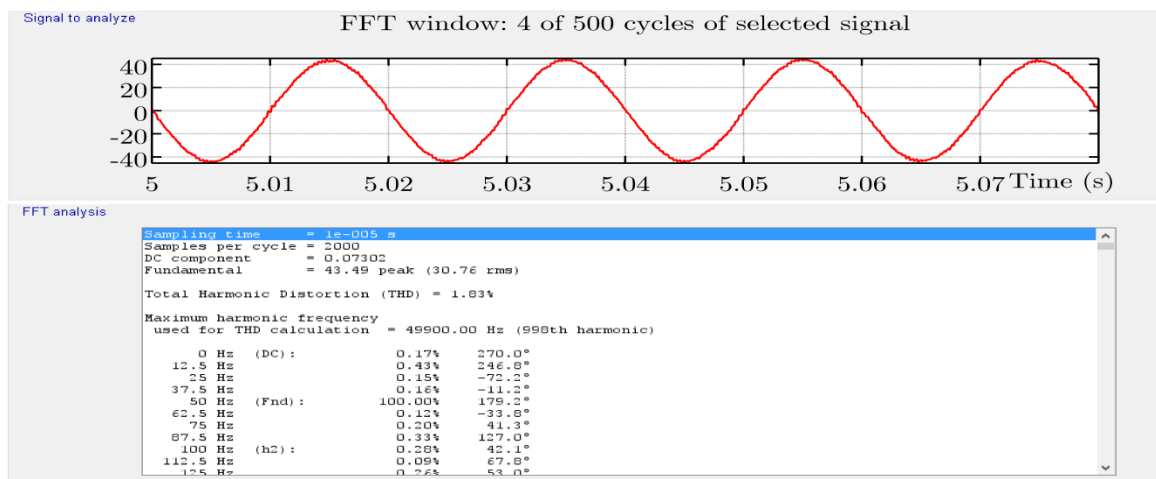
(c)



(d)



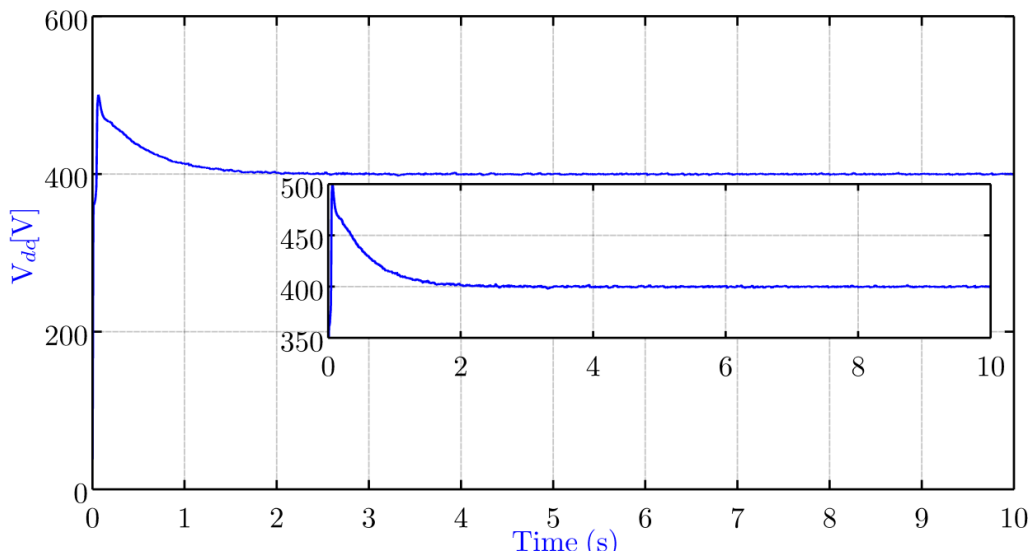
(e)



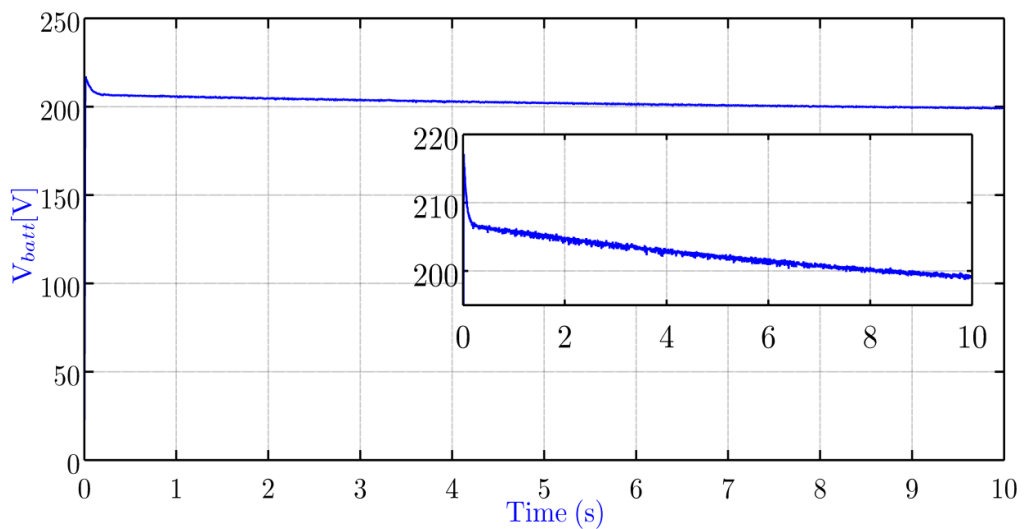
(f)

Figure 2. 7 Operating waveforms during V2G operation (a) DC link voltage (b) Battery voltage (c) Battery current (d) Grid voltage and current (e) Active and reactive power (f) Harmonic spectrum of grid current (1.83% THD).

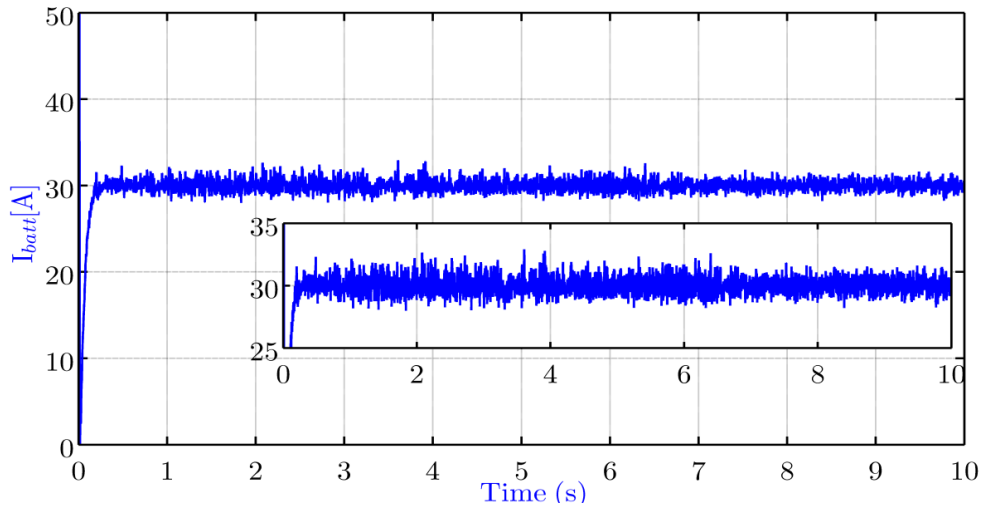
Figure 2.8(a-b-c) depict the regulated DC link voltage, battery voltage and constant battery current during V2G operation and the bidirectional DC-DC converter acts as a boost converter during this mode. Figure 2.8(d) shows sinusoidal current being injected and the grid voltage. It is observed that current injected is in phase with the grid voltage ensuring unity power factor operation. The battery is supplied with a constant active power ($P = 6 \text{ kW}$) and zero reactive power ($Q = 0$) as shown in Figure 2.8(e). The harmonic level in the grid current being drawn is found to be 2%. The harmonic spectrum of the grid current is shown in Figure 2.8(f).



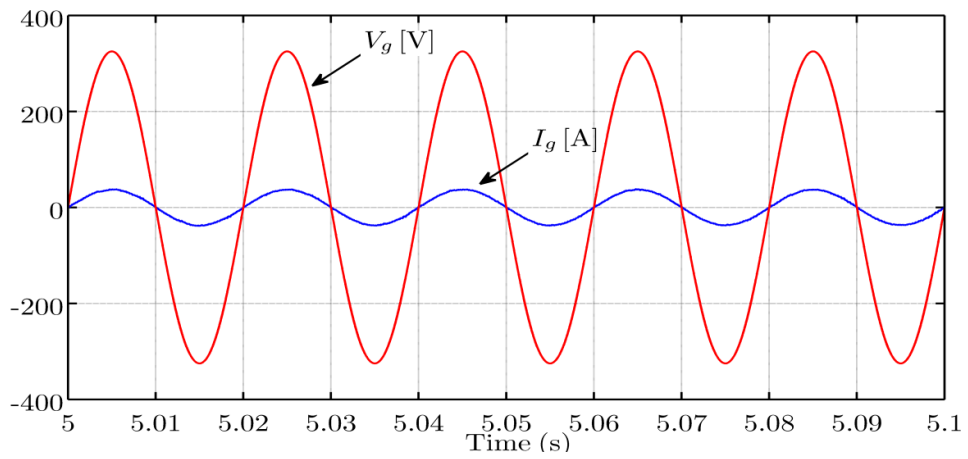
(a)



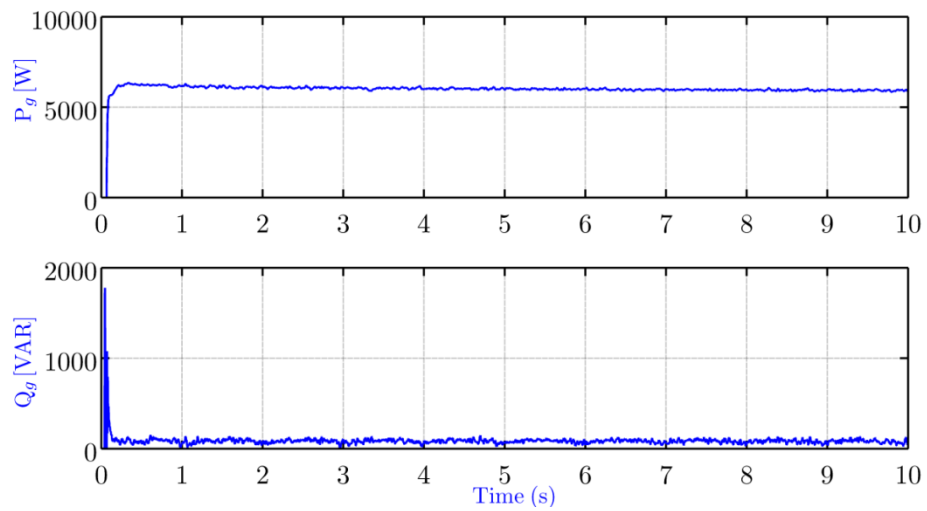
(b)



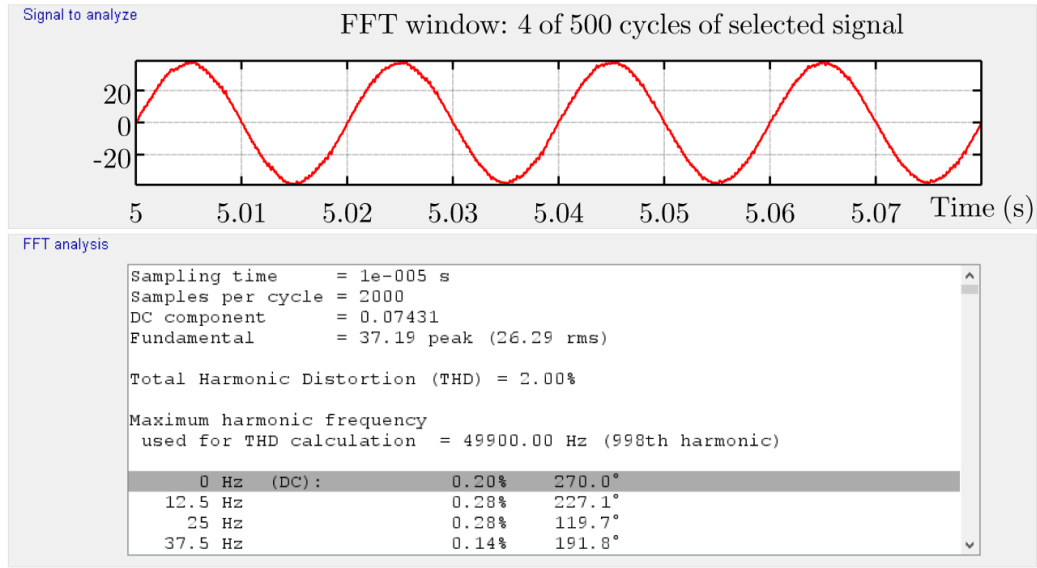
(c)



(d)



(e)



(f)

Figure 2. 8 Operating waveforms during G2V operation (a) DC link voltage (b) Battery voltage (c) Battery current (d) Grid voltage and current (e) Active and reactive power (f) Harmonic spectrum of grid current (2% THD).

2.4 CONCLUSION

A single-phase integrator for EVs is presented and the proposed system allows the integration of EV battery to the grid through two stage power processors. The power flows from vehicle battery to the grid during V2G and from grid to vehicle during G2V mode of operations. The grid current being injected/absorbed is maintained with low harmonic distortion and unity power factor. Design details of the current controller are discussed and simulation results demonstrating both the operating modes are presented. MATLAB/SIMULINK is used for simulation studies and the results show that harmonic analysis of the grid current is found to be within the prescribed power quality limits of IEEE. The proposed integrator is suitable for On-board and can also be employed as an Off-board by eliminating the DC-DC converter stage with small changes in the control law enforced.

CHAPTER 3

WIRELESS ACCESS SUPPORT FOR V2G COMMUNICATION

In the last chapter modeling of V2G integrator and power flow performances of V2G and G2V are discussed. The developed integrator allows EVs to get connected to the grid and participate in power transaction. In order to mobilize EVs to participate in power transaction, communication between the grid and EV owner is essential.

Wireless communication infrastructure for information transfer plays crucial role in V2G operation for smart grid environment. In order to develop the wireless infrastructure for V2G communication, three key entities: GCC, Aggregator and EV are considered. In this case GCC and Aggregator are only fixed entities. So, fixed WiMAX protocol is proposed for GCC to Aggregator communication. Whereas, mobile WiMAX protocol is proposed for Aggregator to EV communication as EVs are mobile in nature. A moving EV may not receive the exact information as it experiences several fades in the process of signal propagation and sometimes EV might be located in a deeply faded region. To overcome this and support the grid requirements efficiently, EV to EV communication link is necessary. LTE protocol is proposed for EV to EV communication. Once the information from GCC is passed to EVs through Aggregator, interested EV owners take part in power transaction with the grid. For the accountability of power transaction between EV and grid, Smart Meter comes in to picture and acts as communication interface. Wi-Fi and WIMAX protocols are proposed for EV to Smart Meter communication. The protocols have different layers: Physical layer, Data link layer, Network layer, Transport layer and Application layer. In this study Physical layer is considered for performance investigation of applicable protocols as it deals with the transfer of bits from

transmitter to receiver with special emphasis on signal attenuation, distortion and transmission media carrying a signal (Multipath and Doppler shift).

3.1 GENERAL STRUCTURE OF PHYSICAL LAYER COMMUNICATION SYSTEM

The Figure 3.1 and 3.2 shows the general overview of physical layer communication system. The source information bits are converted to symbols using digital modulation and further these symbols are converted to pulses using DAC to transmit over the communication channel. The goal is to achieve bit error rate within acceptable limits and permissible power [Roberto 2009].

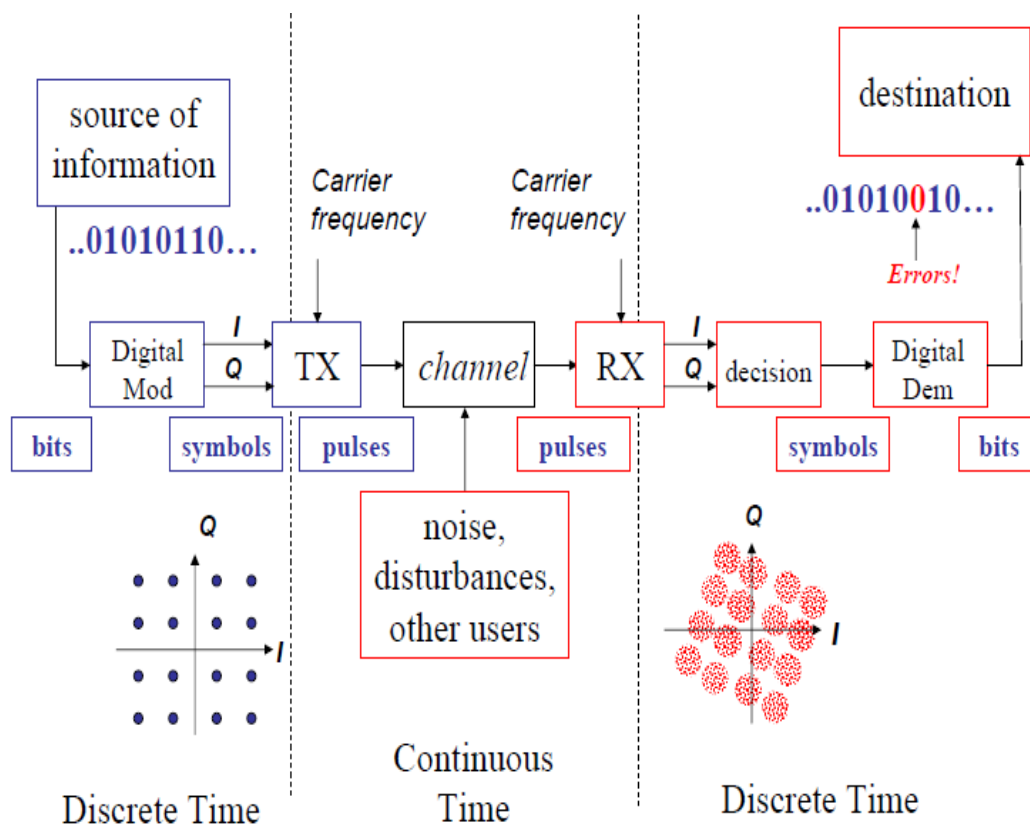


Figure 3. 1 Overview of physical layer communication system.

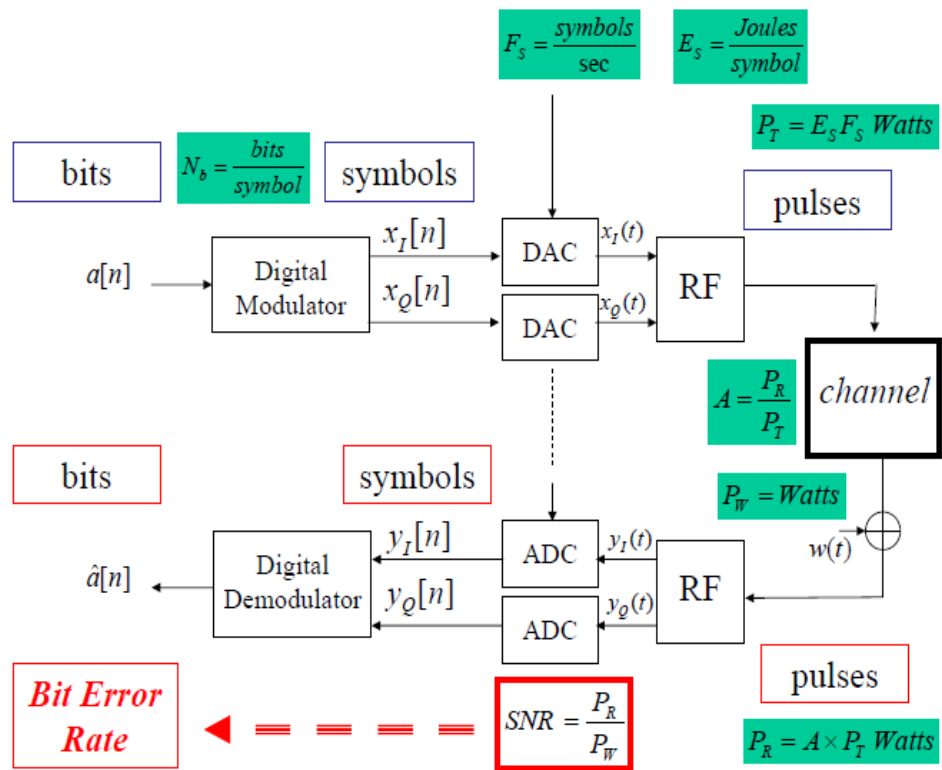


Figure 3. 2 Steps involved in physical layer communication system.

3.1.1 Digital Modulation:

The digital modulation is considered for following reasons: more information capacity, higher data security, better quality communications and quicker system availability.

The quadrature signals are based on complex numbers and also complex signal. For a 2-D signal the Real part is In-Phase Component and Imaginary is Quadrature phase component. Two quadrature signals can be considered as tips of two phasors rotating in opposite direction. The sum of these phasors is always a real number. Thus, the real signals can be transmitted over co-axial cable or digitised or stored in computers memory can be represented in complex number notation [Raveendranathan 2011].

I and Q components are rectangular representation of the polar diagram. The signals in the I/Q are separated by 90° means they are in orthogonal or quadrature. Most digital modulation maps the data as number of discrete points on the I/Q plane as shown in Figure 3.3 and 3.4. These are called as constellation points. As signal travels from one point to another it usually results in simultaneous amplitude and phase modulation.

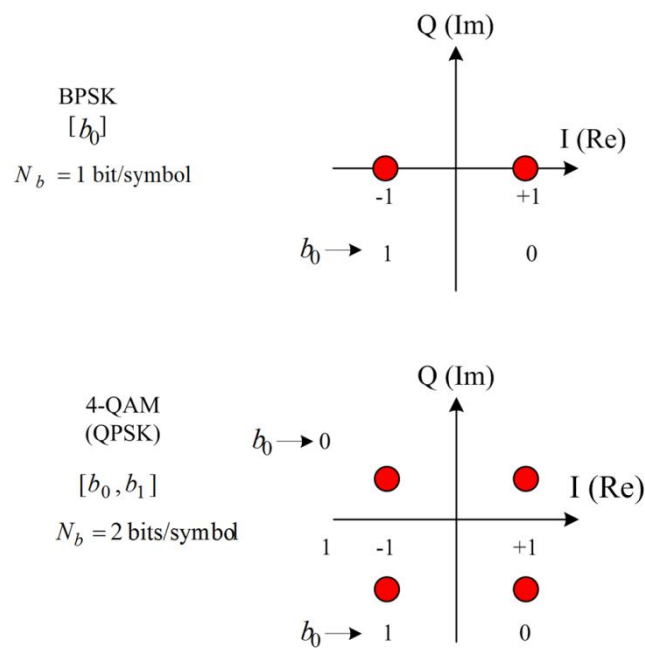


Figure 3. 3 BPSK and 4-QAM Modulation.

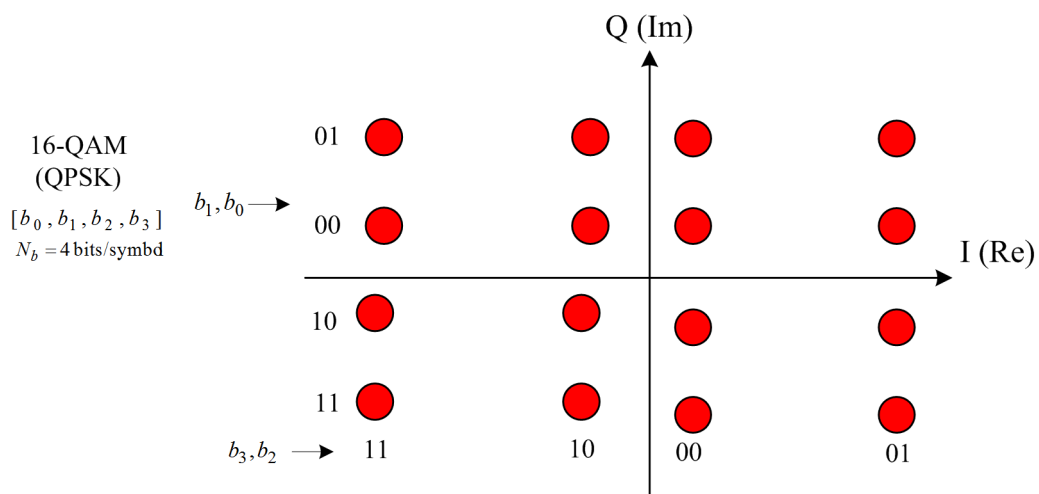


Figure 3. 4 16-QAM Modulation.

The problems associated with the transmitted pulses to received pulses through channel are: attenuation, noise, multipath and Doppler shift and due to this Signal-to-Noise Ratio (SNR) will come in to picture. In evaluating system performance, the quantity of greater interest is the SNR, since a major concern is to detect the signals in the presence of noise with an acceptable error probability. Bit error rate (BER) is defined as the ratio of number of error bits to the total number of bits transmitted during a specific period. The information is expressed in terms of phase of the carrier in modulation schemes.

3.2 GCC TO AGGREGATOR COMMUNICATION

GCC has the information about the power requirements based on energy market or load demand. Energy market is categorized in to two types:

- i. Real Time Markets (instantaneous): can sell or buy power
- ii. Day-ahead Markets (forward): participants may submit bids to buy or sell defined amount of electricity.

GCC plays a prominent role in directing all of the short-term and day-to-day electricity trading activities with utilities, marketers, brokers, power pools and other counter-parties to meet the time varying load demand [Lazaros et al. 2013]. The Aggregator is one among the broker which supports the grid requirements by mobilizing group of EVs to transact power with the grid. GCC will send the information about the power requirements to the aggregator and aggregator in turn sends this information to EVs. The wireless communication system model for GCC to Aggregator is shown in Figure 3.5. In this section, fixed WiMAX and 3GPP LTE communication protocols are proposed for GCC to aggregator communication in V2G.

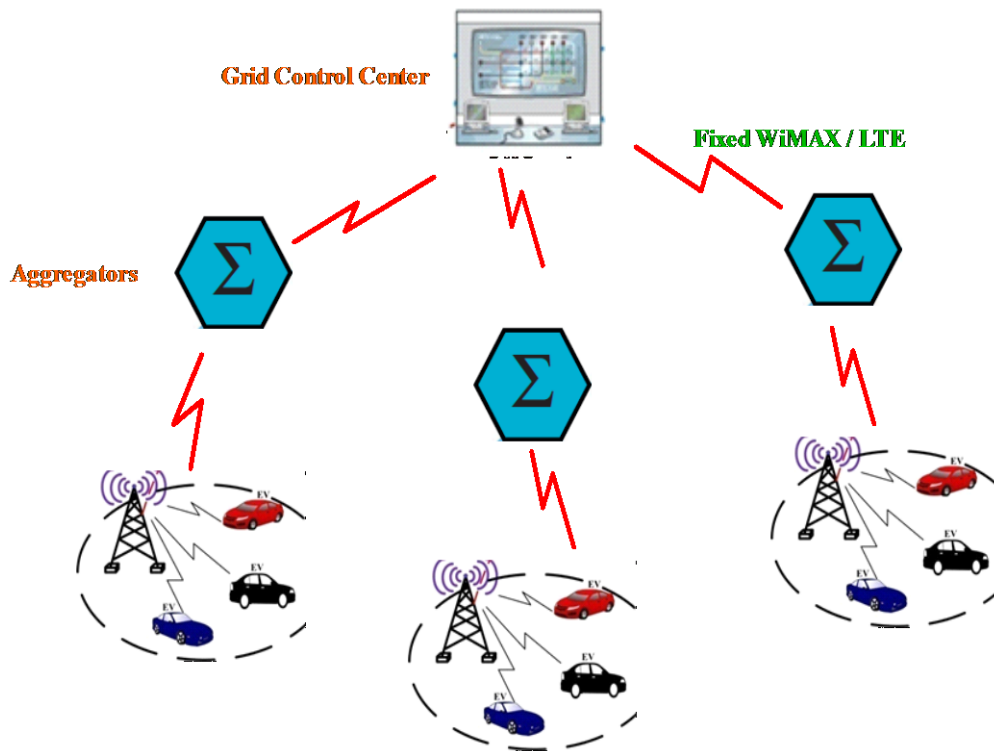


Figure 3. 5 Wireless Infrastructure Framework for V2G.

3.2.1 Fixed WiMAX Protocol for GCC to Aggregator Communication

WiMAX standard defines air interface for frequency range of 2-6 GHz in for IEEE 802.16 [Zountouriou et al. 2011]. The WiMAX standard defines the ideal profiles using 256-FFT OFDM Physical layer specification and supports up to 50km coverage area and data flow up to 70Mbps. In practice, the coverage area is 5-7 Km and 7Mbps. An OFDM has three subcarriers i) data, ii) pilot and iii) null.

For line-of-sight (LOS) transmissions, single carrier air interface is used and for the non- line-of-sight (NLOS) transmissions two OFDM schemes are used. The mobile WiMAX standard defines the ideal profiles using 256-FFT/ OFDM PHY layer specification and supports up to 50 Km coverage area and data flow up to 70Mbps. In practice, the coverage area is 5-7 Km and 7Mbps [Zountouriou et al. 2011].

3.2.1.1 Physical Layer for WiMAX

WiMAX physical layer block diagram is shown in the Figure 3.6 for GCC to Aggregator communication. The physical layer of WiMAX has three parts: transmitter, receiver and communication channel.

3.2.1.1.1 WiMAX Transmitter:

The transmitter of physical layer data vectors include (randomization, error correction, RS coding and interleaving) for different coding rates (concatenated Reed Solomon and Convolution coding) and modulation schemes (M-QAM) [Roberto 2009].

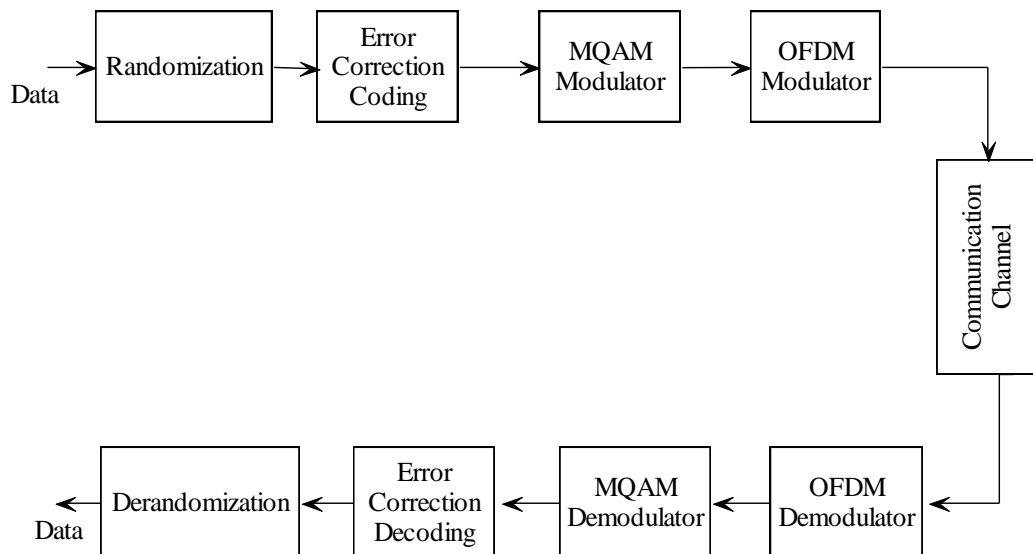


Figure 3. 6 Block diagram of Physical Layer Fixed WiMAX.

The physical layer is modeled in MATLAB/SIMULINK and following are the steps involved:

3.2.1.1.1.1 Randomisation:

Randomisation is a first step in physical layer modeling after burst of data packets received from higher layers. Individual burst is randomised in Downlink and Uplink.

Bit by bit of the data is scrambled to improve the coding performance. Random binary sequence generator is main component of data randomisation which is implemented using Linear Feedback Shift Register as shown in Figure 3.7 [Muhammad and Ghauri 2008].

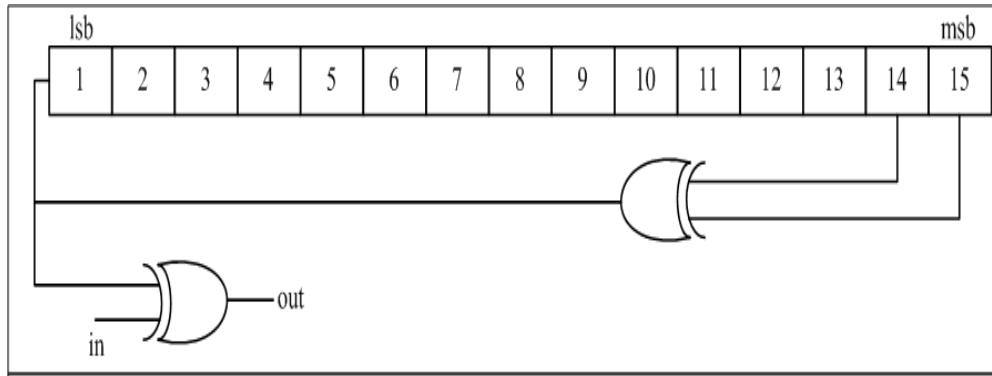


Figure 3. 7 Block Diagram of Randomizer Chain.

3.2.1.1.1.2 Error Correction Code:

Forward Error Correction(FEC) is done on both downlink bursts and consists of RS Outer Code and a rate compatible Convolution Inner Code.

3.2.1.1.1.3 Reed Solomon (RS) Encoding:

RS codes are non binary cyclic codes with symbols which are made up of m-bit sequences, where, $m \geq 2$. R-S (n,k) codes m-bit symbols exist for all n and k for which $0 < k < n < 2^m + 2$ where, k is number of data symbols and n is total number of code symbols [Bernard 1987].

For most conventional R-S (n,k) code ,

$$(n, k) = (2^m - 1, 2^m - 1 - 2t) \quad (3.1)$$

where, t is symbol error correcting capability and $n - k = 2t$ is the number of parity symbols. For the RS codes the code minimum distance is given by:

$$d_{\min} = n - k + 1 \quad (3.2)$$

RS code is used to append redundancy to the data sequence in order to correct block errors. RS encoding is based on Galois Field(GF) computations to calculate the redundant bits and is defined by GF (2^m) [Muhammad and Ghauri 2008]. GF is useful in representing data in error control coding.

WiMAX uses a fixed RS Encoding technique RS ($n = 255, k = 239, t = 8$) where eight tail bits are appended to data before it is presented to RS Encoder stage as shown in Figure 3.8. Code and field generator polynomials are required for generating GF array and to calculate redundant bits respectively.

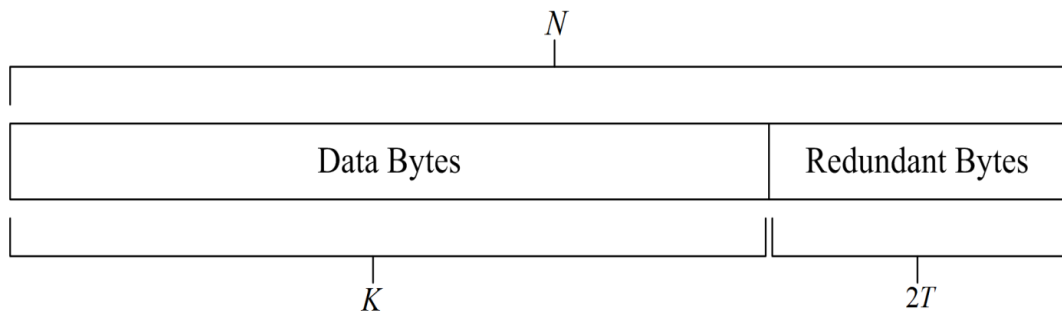


Figure 3. 8 RS coding.

3.2.1.1.1.4 Convolution Encoding (RS Code)

To correct the random errors in the data transmission, Convolution codes are used and is specified by CC (m, n, k) in which each m -bit information symbol is transformed into an n -bit symbol, where m/n is the code rate ($n > m$) [Bernard 1987]. To encode data, k memory registers which hold 1 input bit. All memory registers start with a value of 0. The encoder has n modulo-2 adders, and n generator polynomials, one for each adder.

In WiMAX Physical Layer, each RS block is encoded by the binary convolutional encoder with coding rate $1/2$ and a constraint length equal to 7. Encoder has two binary adders and two generator polynomials. These generator polynomial codes are:

$$A = 171 \text{ octal } 11111100 \text{ 1 binary for X}$$

$$B = 133 \text{ octal } = 1011011 \text{ binary for Y}$$

The output of the convolution encoder is then punctured to remove the additional bits from the encoded stream. The number of bits removed is dependent on the code rate used. The FEC convolution and puncturing is shown in Figure 3.9.

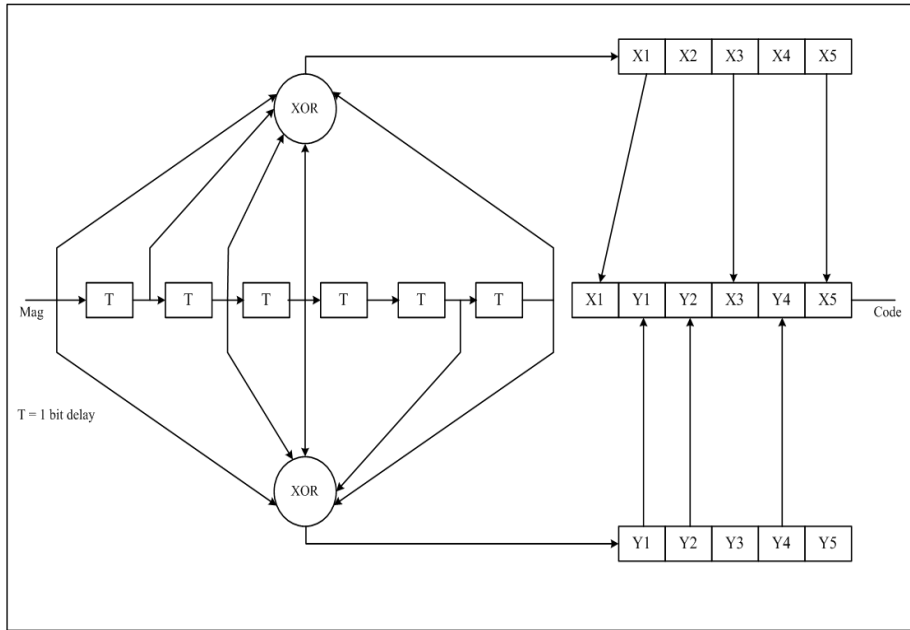


Figure 3. 9 FEC Convolution and Puncturing.

The procedure for puncturing in CC is as follows: For Rate $\frac{3}{4}$ CC, X2 and Y3 are omitted from transmission, there by changing the rate to $\frac{3}{4}$. In Table 3.1, ‘1’ denotes the transmitted bit, and ‘0’ denotes the omitted bit.

Table 3. 1 Coding Rate

	Code Rate			
Rate	1/2	2/3	3/4	5/6
d_{free}	10	6	5	4
X	1	10	101	10101
Y	1	11	110	11010
XY	X_1Y_1	$X_1Y_1Y_2$	$X_1Y_1Y_2X_3$	$X_1Y_1Y_2X_3Y_4X_5$

3.2.1.1.1.5 Interleaving:

Interleaver works on the bit positions and is done by spreading the coded symbols in time before transmission. The data incoming to the interleaver is randomised in two permutations. First permutation ensures that adjacent bits are mapped onto non-adjacent subcarriers and second maps the adjacent coded bits onto less or more significant bits of constellation.

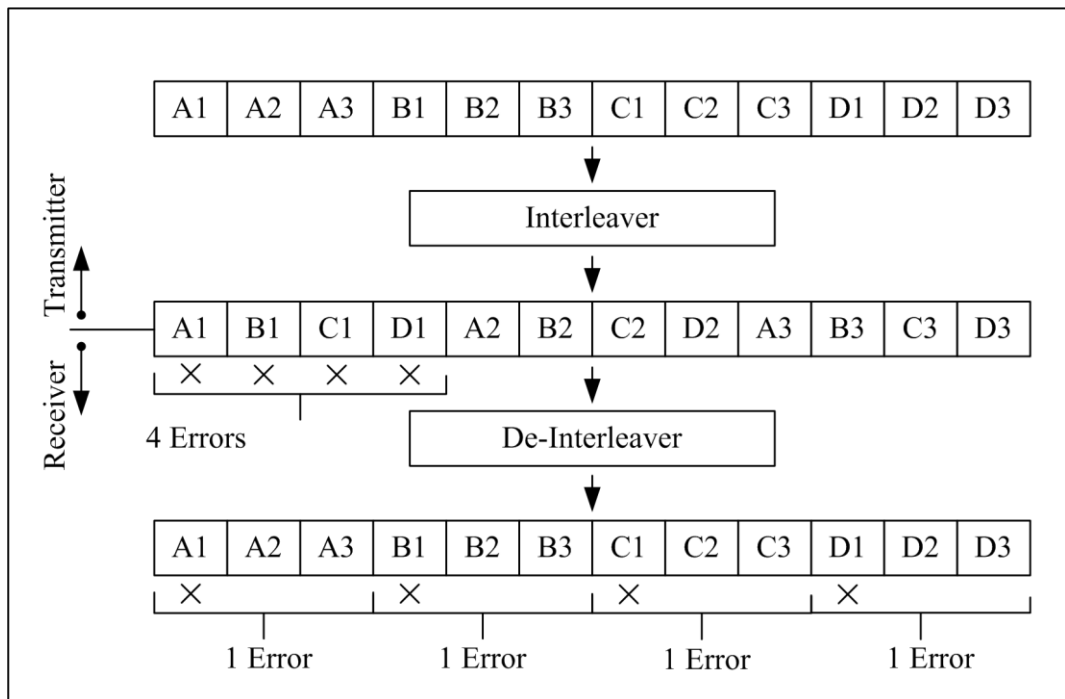


Figure 3. 10 Subblock interleaving.

WiMAX 802.1 6 supports 4 modulation techniques. The sub block interleaving is shown in Figure 3.10. WiMAX 802.1 6 defines two permutations for the interleaver.

The first permutation is defined by the formula:

$$mk = (N_{cbps} / 12) * \text{mod}(k, 12) + \text{floor}(k / 12) \quad (3.3)$$

The second permutation is defined by the formula:

$$s = \text{ceil}(N_{\text{cpc}} / 2)$$

$$jk = s * \text{floor}(mk / s) + (mk + N_{\text{cbps}} - \text{floor}(12 * mk / N_{\text{cbps}})) \text{mod}(s) \quad (3.4)$$

Where, N_{cpc} = Number of coded bits per carrier

N_{cbps} = Number of coded bits per symbol

k = index of coded bits before first permutation

mk = index of coded bits after first permutation

jk = index of coded bits after second permutation

3.2.1.1.1.6 Modulation

The interleaver reorders the data and sends the data frame to the IQ mapper. IQ mapper maps the incoming bits of data from interleaver onto a constellation and mapped data is subsequently modulated onto all allocated data carriers to increase frequency offset index.

Guard band, pilot carriers and DC carrier are inserted before using IFFT to convert the frequency domain signals into time domain as shown in Figure 3.11 (256 point). Figure 3.12 shows the generic placement of Guard band, pilot carriers and DC carrier for OFDM symbol. These time domain signals are then transmitted through the channel [Roberto 2009].

The signal is distorted when the information is transmitted via a wireless channel because of multipath. Usually there is a Line of Sight (LOS) path between transmitter and receiver. The other alternative paths are created by signal reflections due to vehicles, buildings, and obstacles are called as Non-LOS (NLOS). The signals travelling along these paths reach the receiver at different times based on the distance travelled along each path.

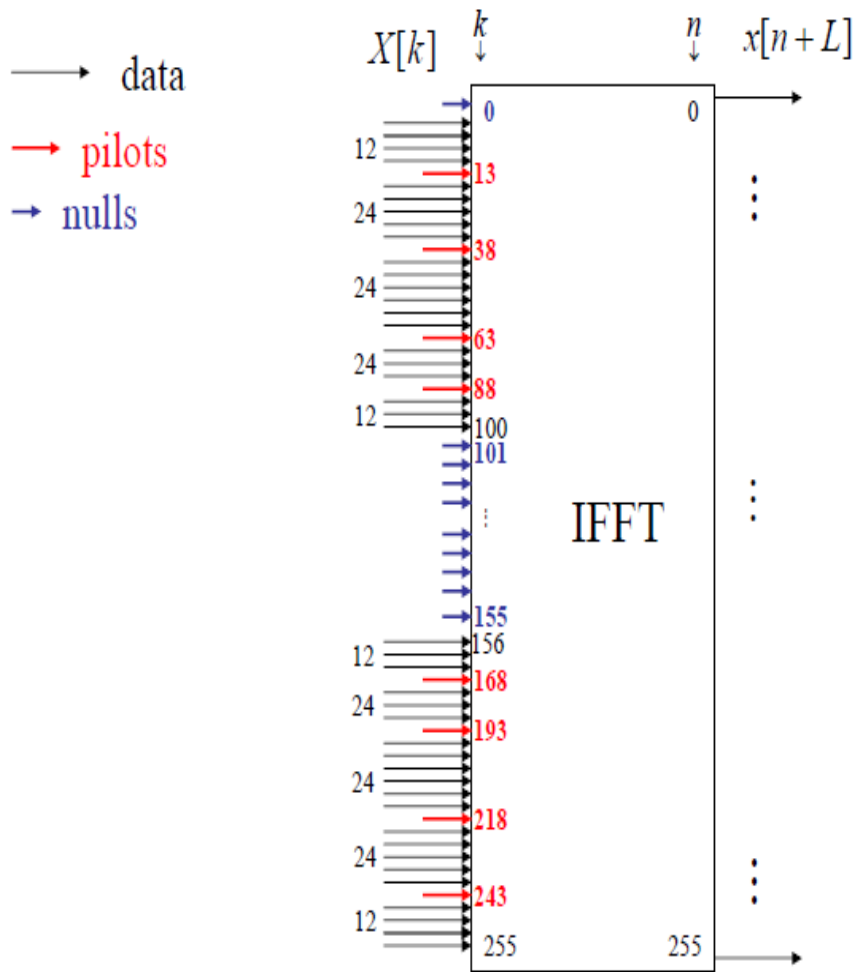
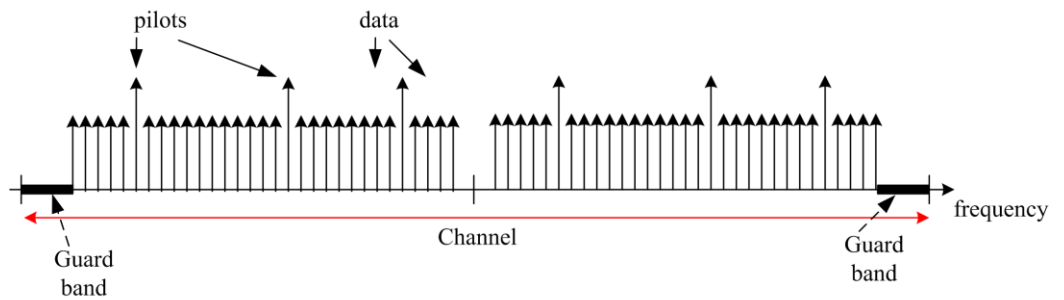


Figure 3. 11 OFDM Symbol.



N_{guards} = to provide frequency guards between channels

$N_{nulls} = N_{guards} + 1$ (DC subcarrier is always zero)

N_{pilots} = pilots for channel tracking and synchronization

N_{data} = data subcarriers

$N_{used} = N_{pilots} + N_{data}$

Figure 3.12 Guard band, pilot carriers and DC carrier.

Previously, single carrier modulation scheme was used in cellular systems and the delay spread due to multipath caused a symbol to "bleed" in to the subsequent symbol reaching the receiver via direct path and is known as inter-symbol interference (ISI) [Jim 2007; Tara 2011]. The effect of multipath distortion in frequency domain is shown in Figure 3.13.

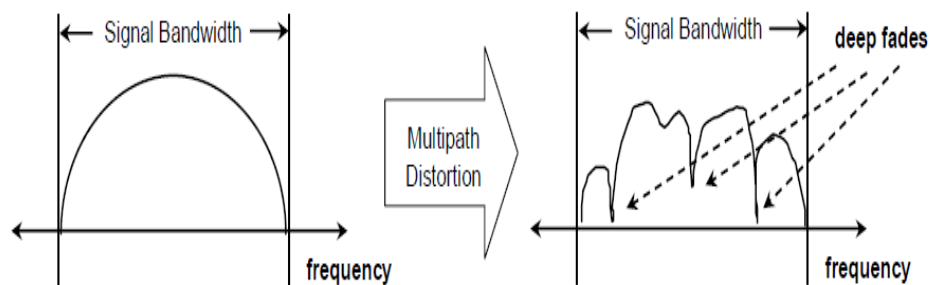


Figure 3. 13 Frequency selective fading.

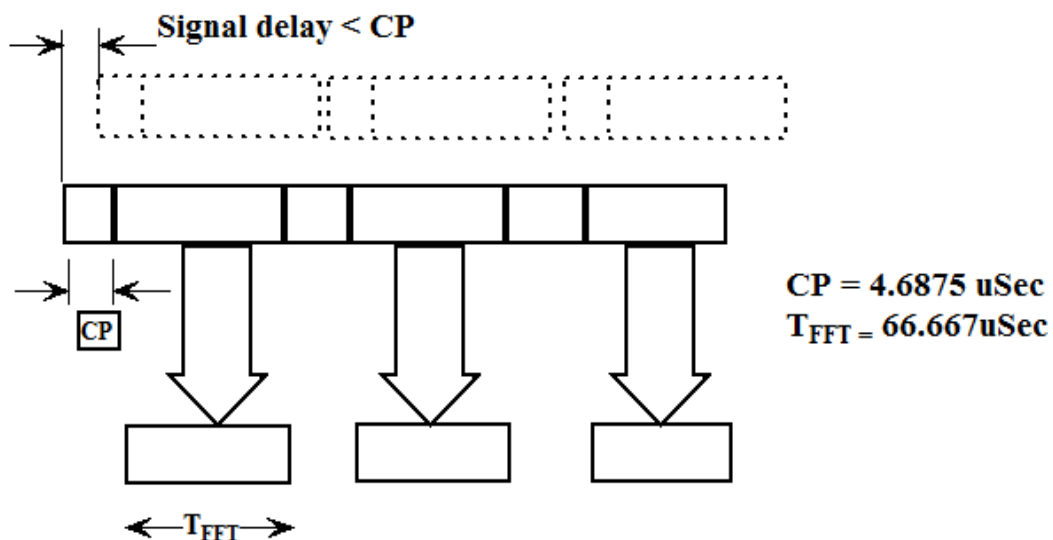


Figure 3. 14 OFDM Symbol.

The time domain equalizers methods are used to compensate the channel distortion. The methods are a) channel inversion and b) rake equalizers are employed to resolve individual path (CDMA systems). The increase in data rate leads to implementation complexities and shorter symbol time. The OFDM eliminates ISI caused due to multipath with the help of longer symbol periods and a cyclic prefix.

Unlike single carrier system, to achieve higher data rates it does not require increased symbol rates. The cyclic prefix (CP) and the FFT period are two components of OFDM symbol. The Figure 3.14 shows the OFDM symbol period (longer) and cyclic prefix to eliminate the ISI. The WiMAX is based on the OFDM technology and helps to tackle the ISI. The disadvantages of OFDM are i) highly sensitive to frequency offset and ii) high peak-to- average power ratio (PAPR).

3.2.1.1.2 Channel:

The problems associated with the transmitted pulses to received pulses through channel are: attenuation, noise, multipath and Doppler shift and due to this Signal-to-Noise Ratio (SNR) will come in to picture. In evaluating system performance, SNR is a major concern which detects the signals in the presence of noise with an acceptable error probability.

3.2.1.1.3 WiMAX Receiver Model:

It is the reverse of all the functions of transmitter. The data is extracted from OFDM symbols, demodulate waveform, deinterleave decode (Viterbi and RS) and inversion of the bit scrambling operation. Simulation is carried out using AWGN channel.

3.2.1.2 Path Loss Models

The path loss models are used to calculate the electrical field strength and predict the path loss which is very crucial in planning wireless network. The information in wireless communication system is transmitted from the transmitter to the receiver by the means of electromagnetic waves and in the process of propagation they come across lot of obstacles in the environment which causes the Path Loss [Josip et al. 2007; Mohammad and Abdulla 2009]. It is defined as the difference between the transmitted power and the received power measured in terms of dB.

The Propagation models are split in to three categories:

- i. Deterministic model: site specific theoretical
- ii. Empirical models: antenna height, frequency and distance (based on measurements,)
- iii. Stochastic models: based on random variables.

The empirical models are considered for analysis and are as follows:

3.2.1.2.1 Free Space Path Loss Model

It is the amount of signal strength lost during propagation from transmitter to receiver. The free space path loss is calculated using the following equation [Josip et al.2007]:

$$PL_{FSPL} = 32.45 + 20 \log_{10}(d) + 20 \log_{10}(f) \quad (3.5)$$

where, f: frequency in MHz; d:distance in m; Power is usually expressed in decibels (dBm).

3.2.1.2.2 COST 231 Hata Model

The COST 231 model is used in urban areas at higher frequencies ranging from 1500 MHz - 2000 MHz. This models calculate the path loss and contains corrections urban, suburban and rural environments. Although 3.5GHz frequency range is beyond its frequency range but still its simplicity and correction factors allows to predict path loss in higher frequency ranges [Abhayawardhana et al. 2005]. The equation for COST 231 Hata Model is given by:

$$PL = 46.3 + 33.9 \log_{10}(f) - 13.82 \log_{10}(h_b) - ah_m + (44.9 - 6.55 \log_{10}(h_b)) \log_{10} d + c_m \quad (3.6)$$

3.2.1.2.3 Stanford University Interim (SUI) Model

IEEE 802.16 working group proposed the standards for the frequency below 11GHz containing the channel models developed by Stanford University (SUI) model. The IEEE 802.16 has adopted the Erceg C [Vinko and Larry 1999] model as the reference propagation model for WiMAX system evaluation. This model can be applied in three different environments: Type A, B and C terrain regions.

By using this model the total attenuation PLs(d) is given by:

$$\begin{aligned} PL_s(d) &= PL_{s0}(d) + s \\ &= 20 \log_{10} \left(\frac{4\pi d_0}{\lambda} \right) + 10\gamma \log_{10} \left(\frac{d}{d_0} \right) + X_f + X_h + s \end{aligned} \quad (3.7)$$

3.2.1.2.4 Hata Okumara extended model or ECC 33 Model

This model is most extensively used empirical propagation model based on Okumura Model. The path loss for this model is given by:

$$PL = A_{fs} + A_{bm} - G_b - G_r \quad (3.8)$$

where, A_{fs} : Free space attenuation [dB]; A_{bm} Basic medium path loss [dB]; G_b : Transmitter antenna height gain factor; G_r : Receiver antenna height gain factor.

3.2.1.2.5 COST 231 Walfish-Ikegami Model (W-I) Model

This model is extension of COST 231 and is well suitable for flat suburban and urban areas with uniform building heights. This gives precise path loss.

For LOS condition

$$PL_{LOS} = 42.6 + 26 \log(d) + 20 \log(f) \quad (3.9)$$

and for NLOS condition

$$PL_{NLOS} = \begin{cases} L_{FSL} + L_{rts} + L_{msd} & \text{for urban and suburban} \\ L_{FS} & \text{if } L_{rts} + L_{msd} > 0 \end{cases} \quad (3.10)$$

where, L_{FSL} : Free space loss; L_{rts} : Roof top to street diffraction; L_{msd} : Multi-screen diffraction loss.

3.2.1.2.6 ERICSSON Model

The network planning engineers use software to predict the path loss developed by Ericsson Company Ltd. The path loss for this model is given by

$$PL = a_0 + a_1 \cdot \log_{10}(d) + a_2 \cdot \log_{10}(h_b) + a_3 \cdot \log_{10}(h_b) \cdot \log_{10}(d) - 3.2 \left(\log_{10}(11.75h_r)^2 \right) + g(f) \quad (3.11)$$

3.2.2 3GPP LTE PROTOCOL FOR GCC TO AGGREGATOR COMMUNICATION

The LTE wireless communication standard is a successor of GSM, EDGE, and UMTS. It is designed for high speed data which results in increased capacity and transmission speed. LTE can be used for different radio interface. The LTE downlink Physical layer conveys data and control related information effectively from base station (eNodeB) to user equipment (UE). The LTE Physical layer employs orthogonal frequency division multiplexing (OFDM) and multiple input multiple output (MIMO) technologies. The orthogonal frequency division multiple access (OFDMA) is used for the downlink and single carrier frequency division multiple access (SC-FDMA) for the uplink. The LTE standard specifies Frequency Division Duplex (FDD) and Time Division Duplex (TDD) to separate uplink and downlink traffic. The majority of the systems use FDD. The LTE system compared to the

previous wireless cellular standards have following superior features: i) peak data rates up to 100Mbps in 20 MHz channel for downlink and 50Mbps in 20MHz channel for uplink, ii) less than 10 msec for data transfer(less than 100 ms for initial connection setup), iii) performance is optimized for low speeds and higher for speeds above 120km/hr, whereas the link is maintained up to 350 km/hr speed, iv) the coverage is full performance oriented up to 5 km, slightly degraded between 5-30km and operational up to 100km, v) it is flexible for spectrum usage up to 20MHz and demonstrates high spectral efficiency[Jim 2007; Brown and Khan 2013].

3.2.2.1 LTE Physical Layer

The LTE Physical layer is designed to accommodate bandwidth from 1.25MHz - 20MHz. The OFDMA downlink multiplexing supports the physical channels and these convey information from higher layers in the LTE stack. The type of modulation and the coding parameters for physical channels and the signals depends on the task assigned. The generic frame structure of LTE physical layer is shown in Fig.3.15. The frame structure is applicable to both downlink and uplink FDD. The frames are of 10msec duration and contain 20 slot periods, each of 0.5msec and again segmented into sub-frames consisting of two slot periods of 1msec duration. The spacing of OFDMA subcarrier is 15 kHz. The physical resource block (PRB) is a slot which has 12 adjacent sub carriers grouped together and it is a smallest unit of base station scheduler assigned bandwidth. The transmitted downlink signal is represented by two dimensional resource grid. The block in each PRB slot represents an OFDM symbol and is called as resource element.

The standard defines physical channel as "a set of resource elements carrying information originating from higher layers". The downlink physical channels are i) Physical downlink shared channel (PDSCH), ii) Physical broadcast channel (PBCH), iii) Physical downlink control channel(PDCCH), iv) Physical control format indicator channel(PCFICH), v) Physical HARQ indicator channel(PHICH), vi) Physical multicast channel(PMCH). The downlink physical layer parameters specified in the

standard are considered for physical layer implementation [Tara 2011]. The PDSCH is used in this paper for modeling LTE downlink physical layer.

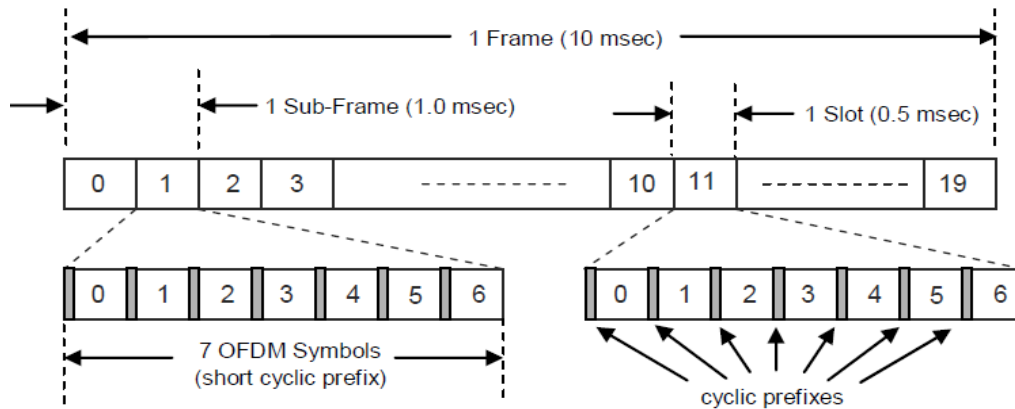


Figure 3.15 LTE Frame structure.

The signal to noise ratio (SNR) is the ratio between the desired signal to the noise. It is given by

$$SNR = P_{signal(dB)} / P_{noise(dB)} \quad (3.12)$$

In dB it is expressed as

$$SNR_{dB} = P_{signal(dB)} - P_{noise(dB)} \quad (3.13)$$

3.2.2.2 Implementation

The LTE downlink physical layer consists of transmitter (channel coding, modulation, layer mapping, precoding, resource element mapping and OFDM modulator), channel (MIMO) and receiver (OFDM demodulator, resource element demapping, decoding, layer demapping, demodulation. descrambling). The simulation is carried out for single downlink from eNodeB (grid control center) to UE (aggregator). The block diagram of LTE physical layer is shown in Figure 3.16.

These are the following steps involved in a downlink physical layer model:

- Scrambling: It scrambles the bits within the codeword.
- Digital Modulation Mapping: The bits are transformed into digital modulated symbols and the modulation is chosen (QPSK, 16-QAM and 64-QAM).
- Precoding and Layer Mapping: The precoding is done to allow UE to separate different antenna streams in MIMO or transmitter diversity. These precoded elements are then mapped onto a number of two-dimensional time-frequency resource elements for transmission.
- OFDM Signal Generation: OFDM symbols are created using the number of subcarriers allocated for the transmission and CP is added to it.

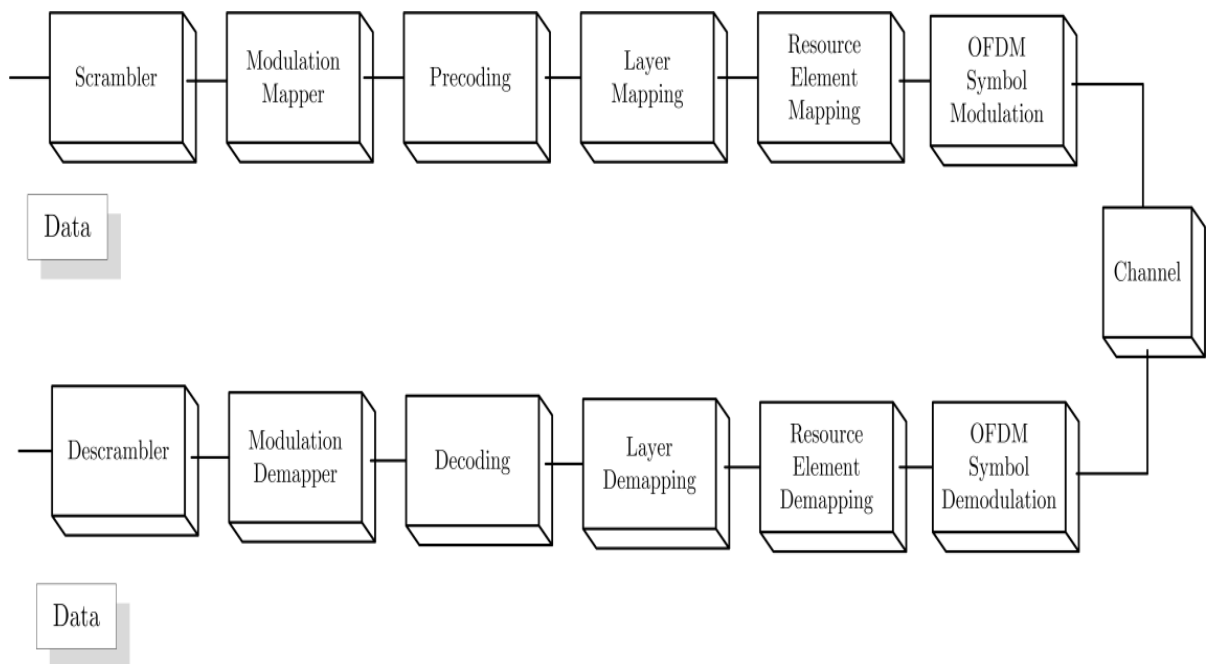


Figure 3. 16 Block diagram of LTE Physical Layer.

3.2.3 Results and Discussion

3.2.3.1 Fixed WiMAX

The GCC to aggregator communication is very crucial in meeting the load demands and contribute to the grid. The aggregator facilitates the EVs by providing parking lot and charging slot for power transaction with the grid. The fixed WiMAX protocol is chosen for the communication. The parameters used for simulation are shown in Table 3.2.

Table 3. 2 IEEE 802.16-2004 (Fixed WiMAX)

<i>Parameters</i>	<i>Value</i>
Frequency Band	2GHz-11GHz fixed
OFDM carriers	OFDM: 256 OFDMA: 2048
Modulation	QPSK, 16QAM, 64QAM
Transmission Rate	1Mbps-75Mbps
Duplexing	TDD or FDD
Channel Bandwidth	(1,2,4,8)x1.75MHz (1,4,8,12)x1.25MHz 8.75MHz

The physical layer of WiMAX protocol is modeled and simulated in MATLAB/SIMULINK. The BERv/s SNR graph is plotted and is shown in Figure 3.19. To achieve the BER of 10^{-2} both BPSK $\frac{1}{2}$ requires 7.5dB, QPSK $\frac{1}{2}$ requires 12dB, QPSK $\frac{3}{4}$ requires about 15dB, 16QAM $\frac{1}{2}$ requires around 16.5dB. The QPSK $\frac{1}{2}$ and 16 QAM $\frac{1}{2}$ are less prone to errors as compared to other modulation schemes.

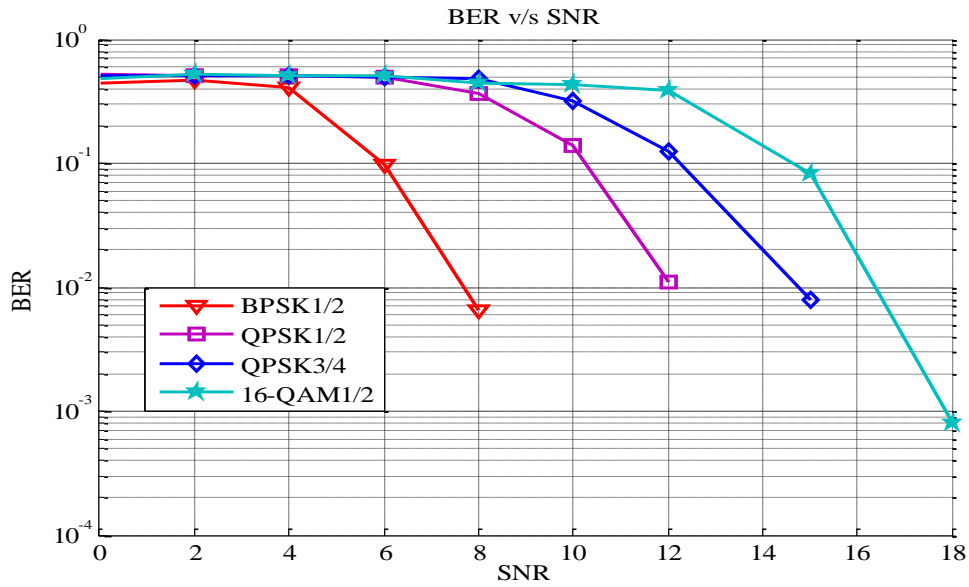


Figure 3. 17 BER v/s SNR for GCC to Aggregator Link.

3.2.3.1.1 Path Loss Results

The simulations were carried out using following parameters as shown in Table 3.3. The metrics prediction error mean (μ) and standard deviation (σ) are used for evaluating the path loss models.

Table 3. 3Path Loss Simulation Parameters for WiMAX

<i>Parameters</i>	<i>Value</i>
Base Station transmitted power	43dBm
Mobile Transmitter power	30dBm
Transmitter Antenna Height	30m
Receiver Antenna Height	6/10m
Operating frequency	3.5GHz
Distance between Tx and Rx	5km
Building to building height	50m
Correction for Shadowing	10.6dB/8.2dB urban/suburban

The positive value of μ means that the model over estimates path loss value and negative value means the model predicts smaller path loss value than the expected. In line with this, a small value of σ indicates a good model prediction and large value indicates less accurate model.

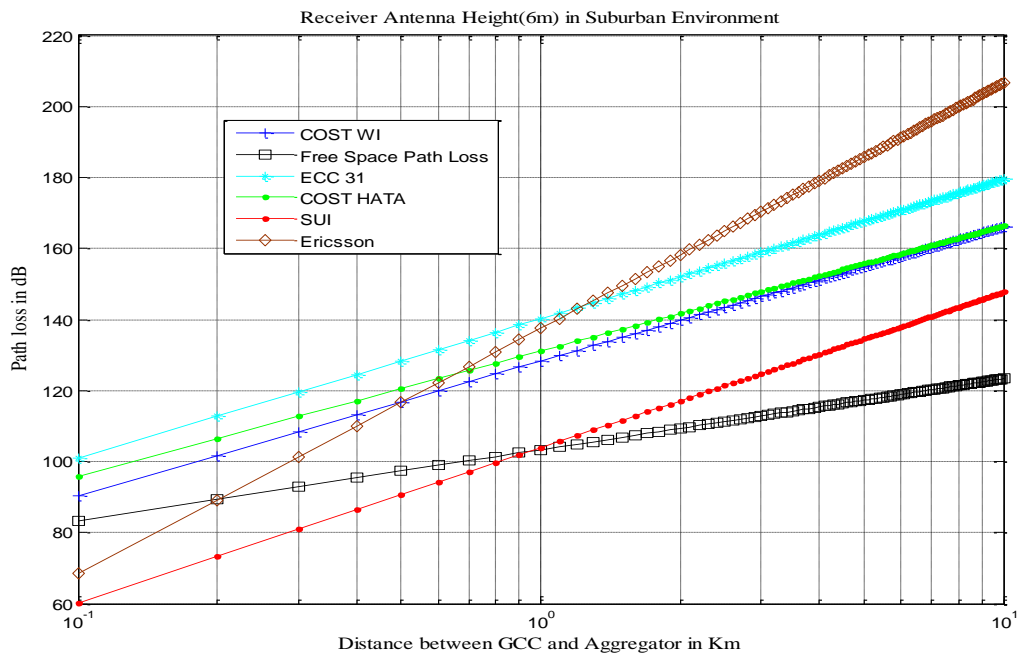


Figure 3. 18 Path loss for the Suburban environment with 6m receiver antenna height.

The transmitter and receiver antenna heights are considered to be 30m and 10m respectively. The transmitter power is 43dBm and the results are shown in Figure 3.18 and Figure 3.19. The SUI model demonstrates lower path loss of 162dB and 142dB for urban and suburban environments respectively. The COST HATA, COST WI and ECC-31 demonstrate path loss of 158dB, 162dB and 164dB respectively and preferred for Suburban environment. The Ericsson model demonstrates comparatively higher path loss of 204 dB for Suburban but it is interesting to note that it demonstrates path loss of 160dB which is less compared to all other models in case of Urban environment. The COST WI and COST HATA exhibits higher path loss of 178 dB and 176dB respectively for Urban environment as compared to other models. This description is for 10 m receiver antenna height.

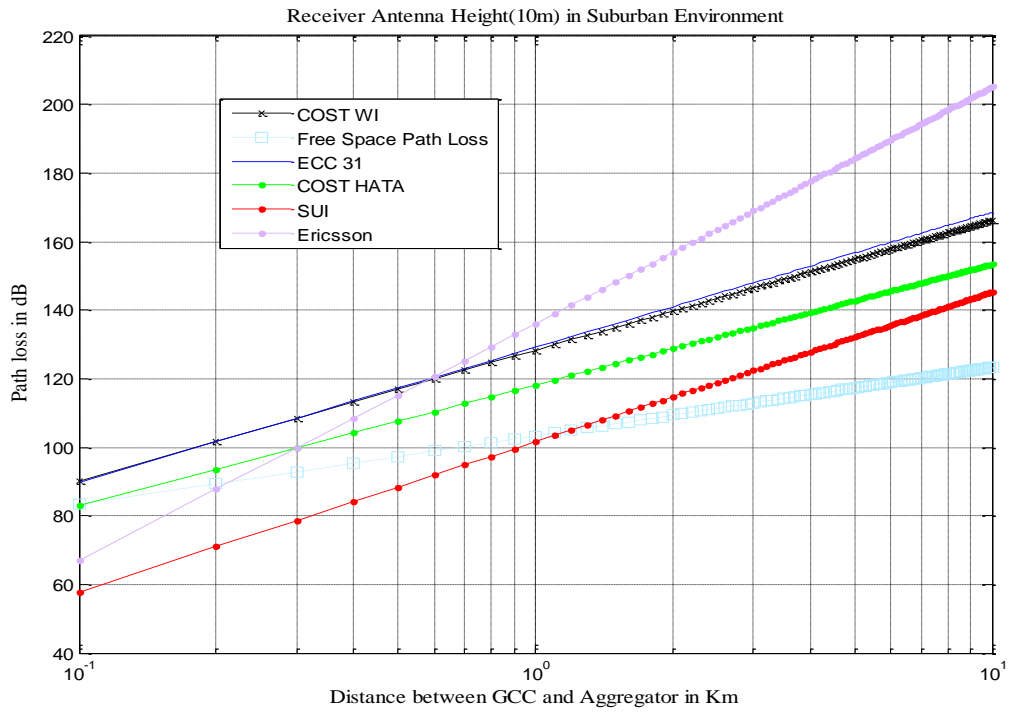


Figure 3. 19 Path loss for Suburban environment with 10m receiver antenna height.

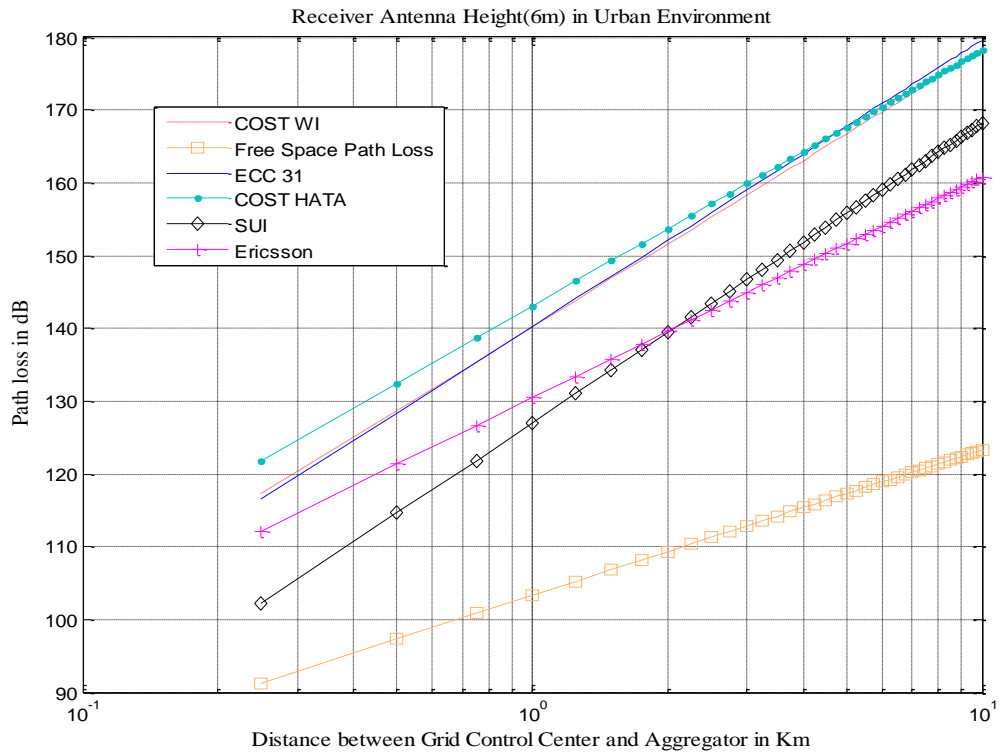


Figure 3. 20 Path loss for the Urban environment with 6m receiver antenna height.

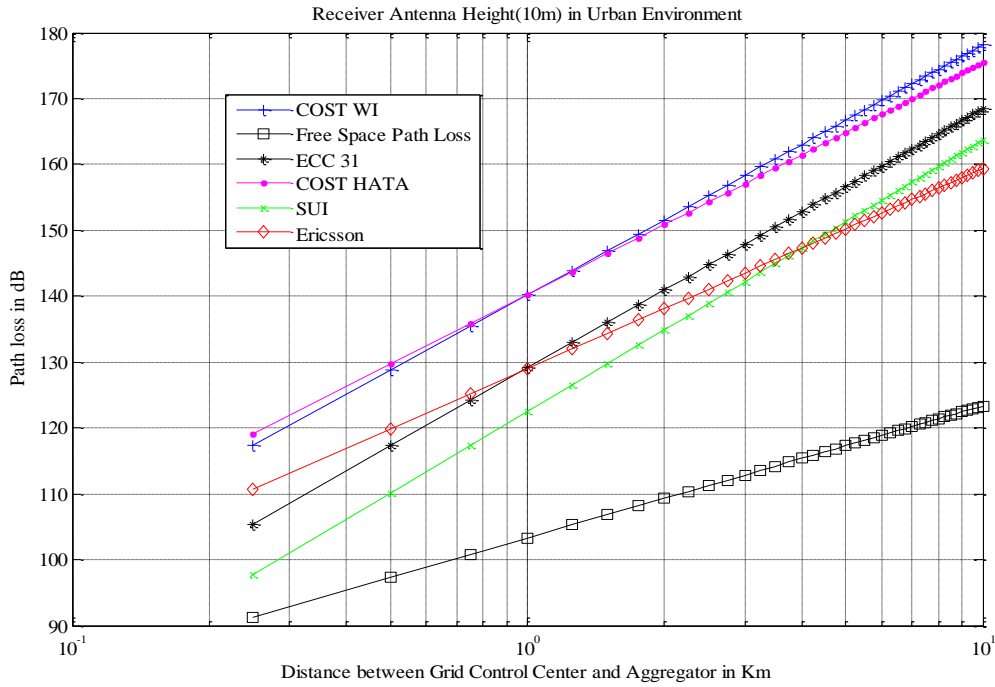


Figure 3. 21 Path loss for the Urban environment with 10m receiver antenna height.

With 6m receiver antenna height for the Urban environment the Ericsson model demonstrates path loss of 160dB and ECC 31 exhibits highest path loss of 180dB. The COST WI and COST HATA demonstrate about 178dB. The SUI is moderate and demonstrates path loss of 168dB as depicted in Figure 3.20. For Suburban with 6m antenna height the SUI demonstrate the lowest path loss of 148dB and Ericsson demonstrate the highest path loss of 208dB. The COST WI and COST HATA demonstrate the path loss of 165dB as shown in Figure 3.21.

3.2.3.2 3GPP LTE

The performance of developed LTE Physical layer is evaluated for different channel models and frequencies. The 16 QAM, 2x2 antenna configurations is considered for analysis. The Figure 3.22.shows the BER v/s SNR plot for 16 QAM, 2x2, static MIMO. The distance between the GCC (eNodeB) and the aggregator (UE) is assumed as 10km. The urban or suburban environments are considered for the performance analysis. To achieve the performance near to 10^{-1} , the 16 QAM requires

15dB for extended pedestrian A model (EPA 5Hz), 18dB for extended vehicular A model (EVA 5Hz), and greater than 25dB for extended typical urban model (ETU 70Hz) as shown in Figure 3.22. From this, we can conclude that the EPA model is relatively energy efficient than the EVA model. The results are validated with the open literature [Hamid and Kostanic 2013].

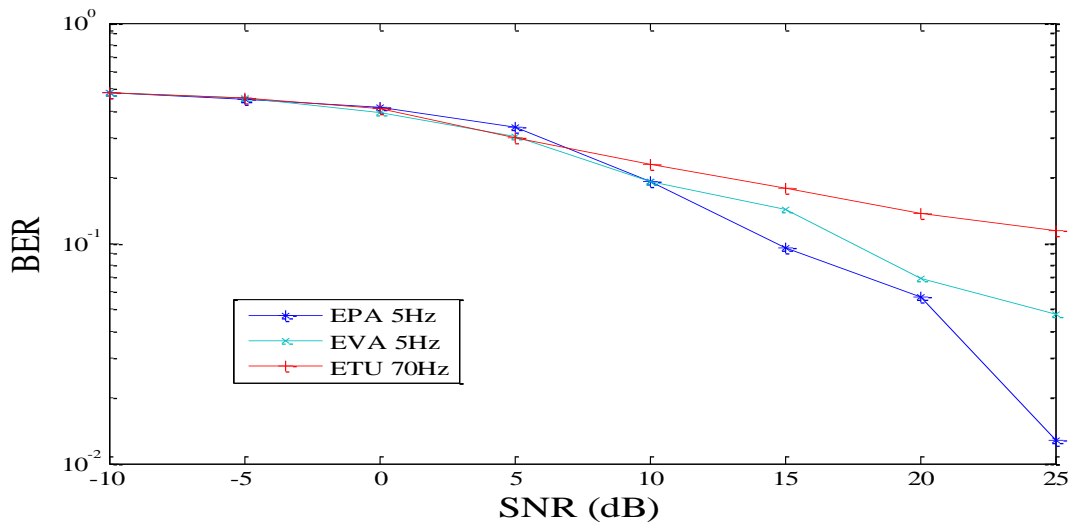


Figure 3. 22 BER v/s SNR for 16QAM different channel models.

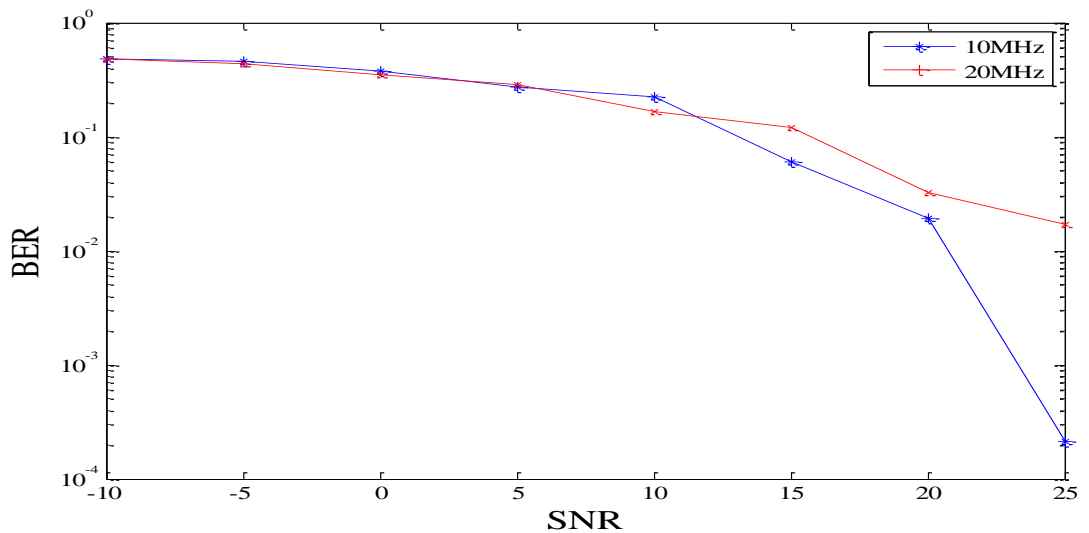


Figure 3. 23 BER v/s SNR for different Bandwidths.

The Figure 3.23 depicts BER v/s SNR for 10MHz and 20MHz bandwidth. To achieve the BER rate of 10^{-1} , the 10 MHz bandwidth signal requires around 14dB and 20MHz signal requires around 17dB. It is observed that the performance is almost the same for 10MHz and 20MHz bandwidth. It can be concluded from the developed model that the performance is found to be same for different channel bandwidth. For the urban environment the ETU model can be adopted for GCC to aggregator communication in V2G operation.

3.3 AGGREGATOR TO EV COMMUNICATION

The aggregator is an intermediate entity between GCC and EVs and promotes participation of EVs in V2G operation. An Aggregator is viewed as a large source of generation or load by GCC, which provides the ancillary services such as spinning and regulatory reserve. The aggregator motivates and attracts the EV owners to contribute power by providing incentives in the form of free parking lot with charging slots. To mobilize EVs in parking lots for grid power transactions, the communication link between the Aggregator and EVs is needed. After receiving the information about the power requirements from GCC, the aggregator will send the same information to EVs. Based on this information, EV owners who are willing can participate in power business with the grid.

As the aggregator is fixed and the EVs are movable, the mobile WiMAX protocol is proposed for aggregator to EV communication in V2G. Also, comprehensive analysis of wireless fading channels is discussed for performance study of the protocol.

3.3.1 Mobile WiMAX Protocol for Aggregator to EV Communication

The communication between aggregator to EV can be accomplished using IEEE 802.16e-2005 the mobile WiMAX. The physical layer WiMAX model is discussed

and presented in section 3.2. The following parameters are considered for the simulation of mobile WiMAX as shown in Table 3.4.

Table 3. 4 IEEE 802.16e (Mobile WiMAX)

<i>Parameters</i>	<i>Value</i>
Frequency Band	2GHz-6GHz mobile
OFDM carriers	OFDM: 256 OFDMA: 128, 256, 512, 1024, 2048
Modulation	QPSK, 16QAM, 64QAM
Transmission Rate	1Mbps-75Mbps
Duplexing	TDD or FDD
Channel Bandwidth	(1,2,4,8)x1.75MHz (1,4,8,12)x1.25MHz 8.75MHz

3.3.2 Wireless Fading Channels for Aggregator to EV Communication

The channel model is a mathematical representation of the relation between the transmitted and received power during transmission in wireless communication. The channel model describes the effects of channel on the transmitted signal. The fading leads to variations in the transmitted signal during propagation over time and frequency. The fading occurs due to large scale and small scale fading. The path loss and shadowing fall in the large scale fading category. The multipath is responsible for small scale fading. The fading channels are categorized as shown in the Figure 3.24 [Raj 2001] below.

The large scale fading occurs due to the path loss and shadowing. The path loss occurs due to the large distance travelled by the transmitted signal and shadowing occurs due to obstacles, building, trees, hills and walls. The variations in the transmitted signal due to the large scale and small scale fading are shown in Figure 3.25 [Theodore 1999; Andrea 2005].

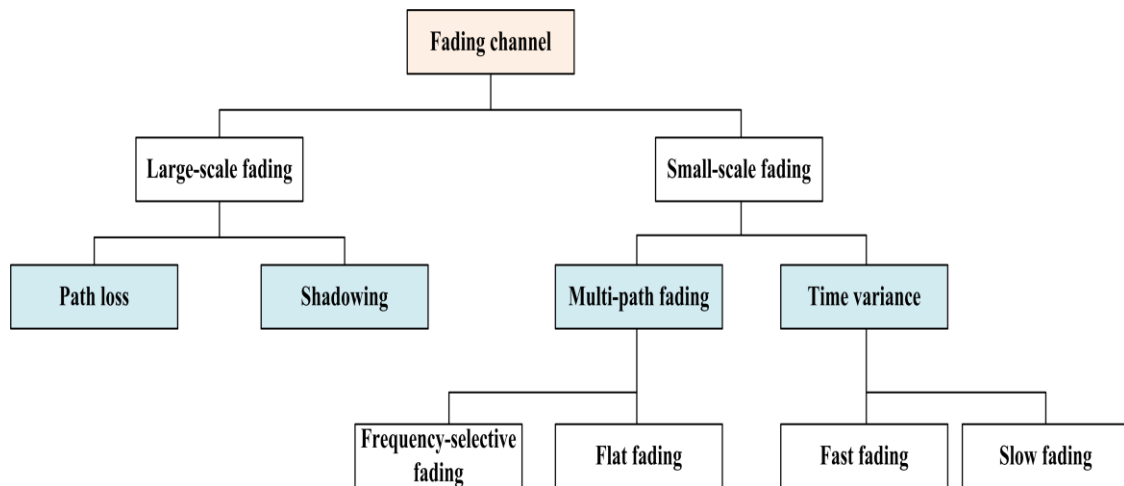


Figure 3.24 Category of Fading Channels.

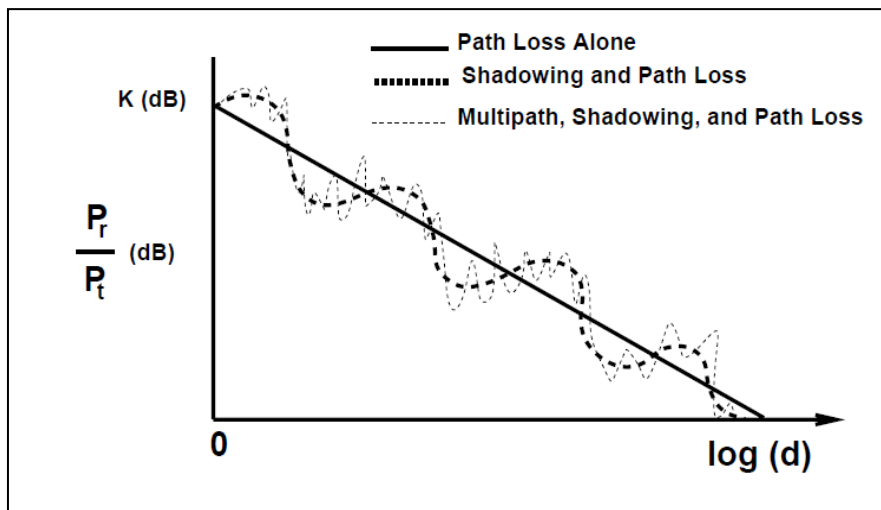


Figure 3. 25 Variations in the transmitted signal due to path loss, shadowing and multipath.

3.3.2.1 Path Loss Models

As discussed in section 3.2 path loss models are used to calculate the electrical field strength and predict the path loss which is very crucial in planning wireless network. In wireless communication systems, the electromagnetic waves carry the information from transmitter to the receiver and come across lot of obstacles in the environment which cause Path Loss. The difference between the power transmitted and the power received in terms of dB is termed as path loss [Mohammad and Abdulla 2009]. The empirical path loss models are considered which are discussed in section 3.2.2.

3.3.2.2 Shadowing

The signal loss occurs due to buildings, trees, hills and walls and is shown in Figure 3.26. The power loss in dB is random and is given by:

$$L_p = E\{L_p\} + \chi \quad (3.14)$$

where, E is expected value and χ is random, zero mean approximately gaussian with $\sigma = 6-12$ dB and represents the effect of shadowing.

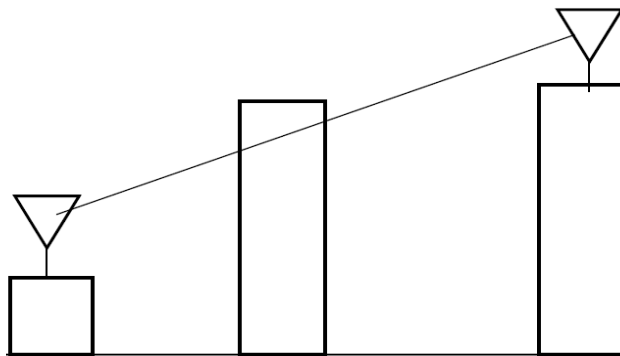


Figure 3. 26 Shadowing.

The average Loss is given by:

$$E\{L_p\} = 10\gamma \log_{10} \left(\frac{d}{d_0} \right) + L_0 \quad (3.15)$$

where,

E is expected value

γ is path loss exponent and the values are:

d_0 is reference distance and for the indoor the value is (1-10m) and for the outdoor, the value is (10-100m). The values of the path loss exponent are shown in Table 3.5.

Table 3. 5 Values of Path Loss Exponent

Values of Path Loss Exponent	
Free Space	2
Urban	2.7-3.5
Indoors(LOS)	1.6-1.8
Indoors (NLOS)	4-6

3.3.2.2.1 IEEE 802.16d Models:

This model is based on log-normal shadowing and is suitable for macro cell suburban area. It is an extension of Hata model. The range of frequency is larger than 1900 MHz and the correction parameters allow this model up to 3.5GHz band. This model can be applied in three terrain regions which are shown in Table 3.6 [Vinko and Larry 1999].

The total attenuation $PL_s(d)$ is given by:

$$\begin{aligned}
 PL_s(d) &= PL_{s0}(d) + s \\
 &= 20 \log_{10} \left(\frac{4\pi d_0}{\lambda} \right) + 10\gamma \log_{10} \left(\frac{d}{d_0} \right) + X_f + X_h + s
 \end{aligned} \tag{3.16}$$

where, $PL_{s0}(d)$ path loss attenuation(fixed), σ_s is shadowing, effect(depends on terrain), d is distance, d_0 is intercept distance, λ is wavelength, γ is path loss exponent, X_f is frequency.

Table 3. 6 Terrain category [Vinko et al. 1999]

Model Parameters	Terrain category		
	Type A	Type B	Type C
d_0	100m	100m	100m
a	4.6	4.0	3.6
b	0.0075m^{-1}	0.0065m^{-1}	0.0050m^{-1}
c	12.6m	17.1m	20.0m
σ_s	10.6dB	9.6dB	8.2dB

Path loss exponent γ depends on station height and terrain category and is given by:

$$\gamma = a - bh_b + \frac{c}{h_b} \quad (3.17)$$

where,

a, b, c are constants of each terrain category

h_b antenna height of base station in meters ($10 \leq h_b \leq 80$ m).

The frequency correction term X_f depends on the carrier frequency f and is given by:

$$X_f = 6\log_{10}\left(\frac{f}{2000}\right) \quad (3.18)$$

The user antenna height correction term X_h depends on user antenna height h_r ($2 \leq h_r \leq 10$ m) and on the terrain category and is given by:

$$\begin{aligned} X_h &= -10.8\log_{10}\left(\frac{h_r}{2}\right) && \text{Type A \& B} \\ &= -20\log_{10}\left(\frac{h_r}{2}\right) && \text{Type C} \end{aligned} \quad (3.19)$$

The indoor reception provides additional path loss (penetration loss) that can be modeled with a random Gaussian noise with following parameters: mean value: $\mu_s = 12$ dB; standard deviation: $\sigma_w = 8$ dB.

So, in case of indoor reception the total attenuation (outdoor + penetration loss) is given by:

$$\begin{aligned}
 PL_z(d) &= PL_s(d) + w \\
 &= PL_{s_0}(d) + s + w \\
 &= PL_{s_0}(d) + z
 \end{aligned}
 \tag{3.20}$$

where, z sum of two random Gaussian variable s and w .

3.3.2.3 Small Scale Fading

The signal is reflected due to objects which come across the propagation path. Few of the reflected waves are received at the receiver and have different amplitude and phase as these take different paths. The multipath is shown in Figure 3.27. The rapid fluctuation in the amplitude of signal over a short period of time or a travel distance is called small scale fading. The flat fading and the frequency selective fading depend on the multipath. The time delay and the doppler spread will result in flat and frequency selective fading respectively [Theodore 1999].

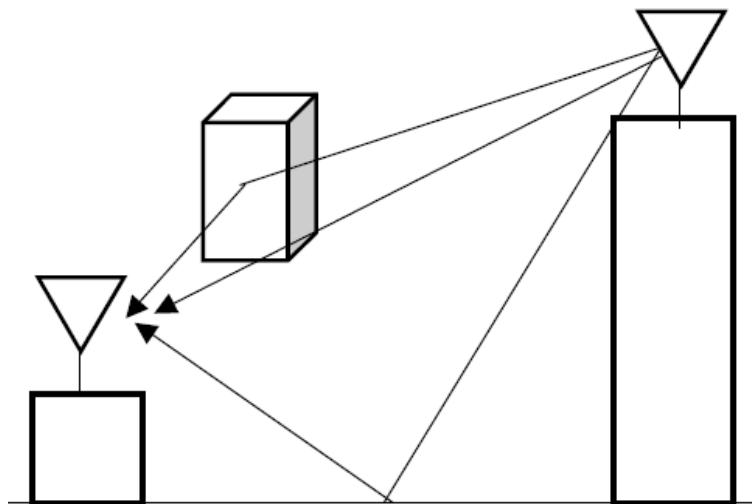


Figure 3. 27 Multipath.

3.3.2.3.1 Spreading in Time:

The traversed paths have different lengths and is shown in Figure 3.28 [Roberto 2009].

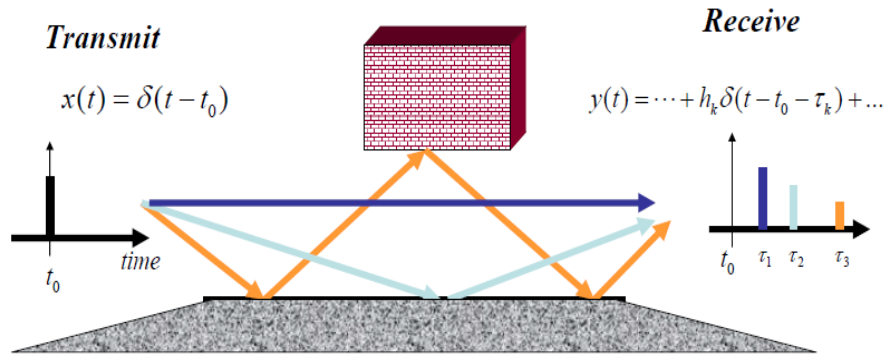


Figure 3. 28 Time Spreading.

3.3.2.3.2 Spreading in Frequency:

The motion causes frequency shift called as Doppler effect and is shown in Figure 3.29.

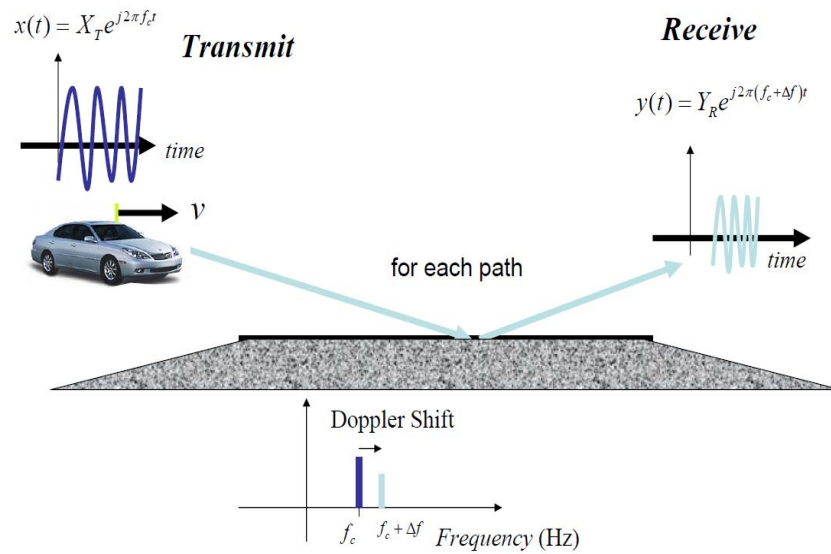


Figure 3. 29 Spreading Frequency.

Each path has

$$y(t) = \text{Re} \left\{ \sum_{\substack{k \\ \text{paths}}} a_k x(t - \tau_k) e^{j2\pi(F_c + \Delta F_k)(t - \tau_k)} \right\} \quad (3.21)$$

where, a_k is attenuation, ΔF_k is shift in frequency and T_k is shift in time.

3.3.2.3.3 Models of Fading Channel:

Doppler spread causes frequency dispersion and results in fast or slow fading. The Rayleigh and Rician distribution describes the statistical nature of the NLOS and LOS respectively [Theodore 1999]. The Rayleigh distribution describes the statistical time varying nature of the received envelope of a flat fading signal (LOS). The sum of the two quadrature gaussian noise signals obeys a Rayleigh distribution. The Rayleigh distribution is shown in Figure 3.30.

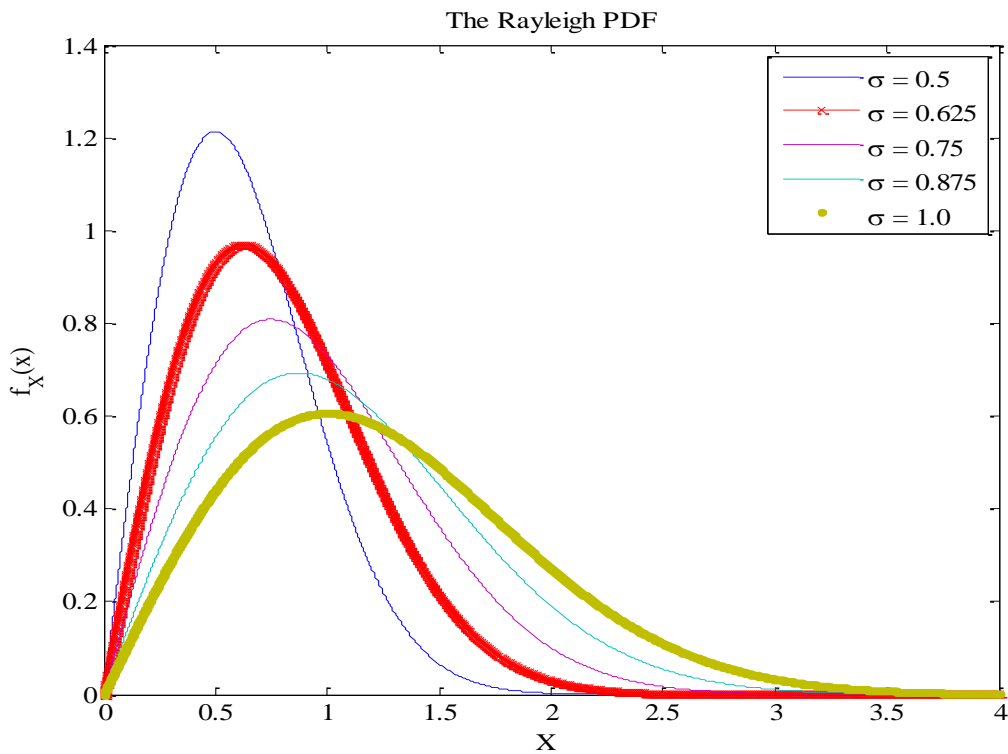


Figure 3. 30 Rayleigh distribution.

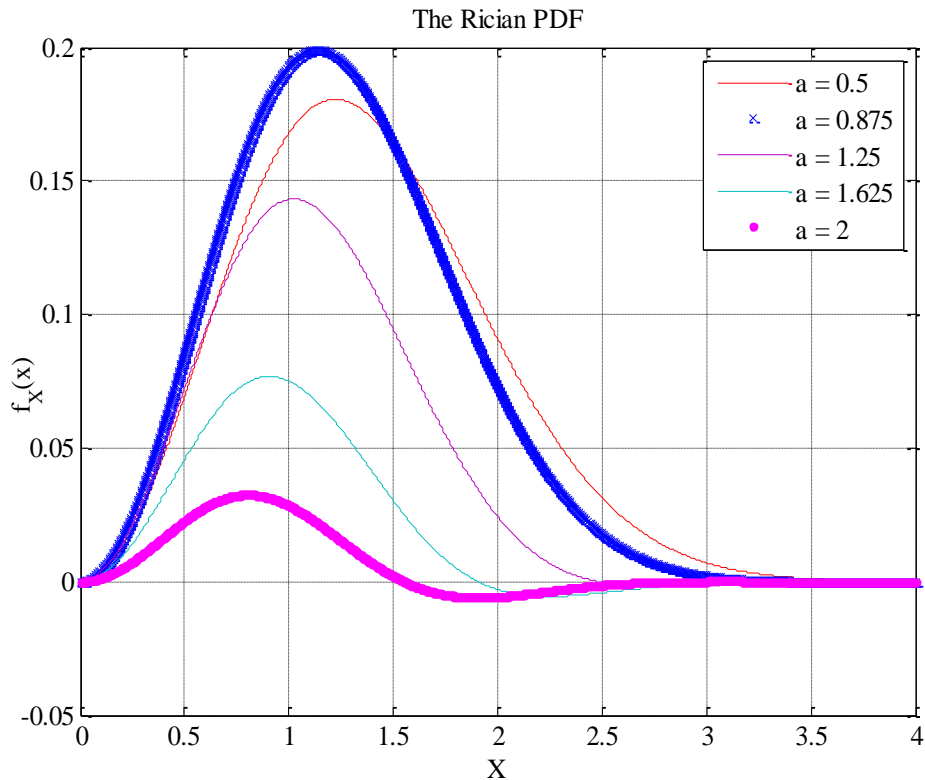


Figure 3. 31 Rician distribution.

The Rician distribution describes statistical nature of the received envelope of a non fading signal (LOS).The Rician distribution is shown in Figure 3.31 [Raveendranathan 2011].

3.3.3 Results and Discussion

3.3.3.1 Mobile WiMAX

The Physical layer of WiMAX is simulated using MATLAB coding in order to investigate the performance of the protocol used for the aggregator to EV communication in V2G. Following are the parameters considered for simulation purpose: The distance between the transmitter and receiver antenna is 5 Km, the operating frequency is 3.5GHz, 10 OFDM symbols per burst, transmitter antenna height is 30m and the receiver antenna height is 10m. The graph is shown in Figure 3.32.

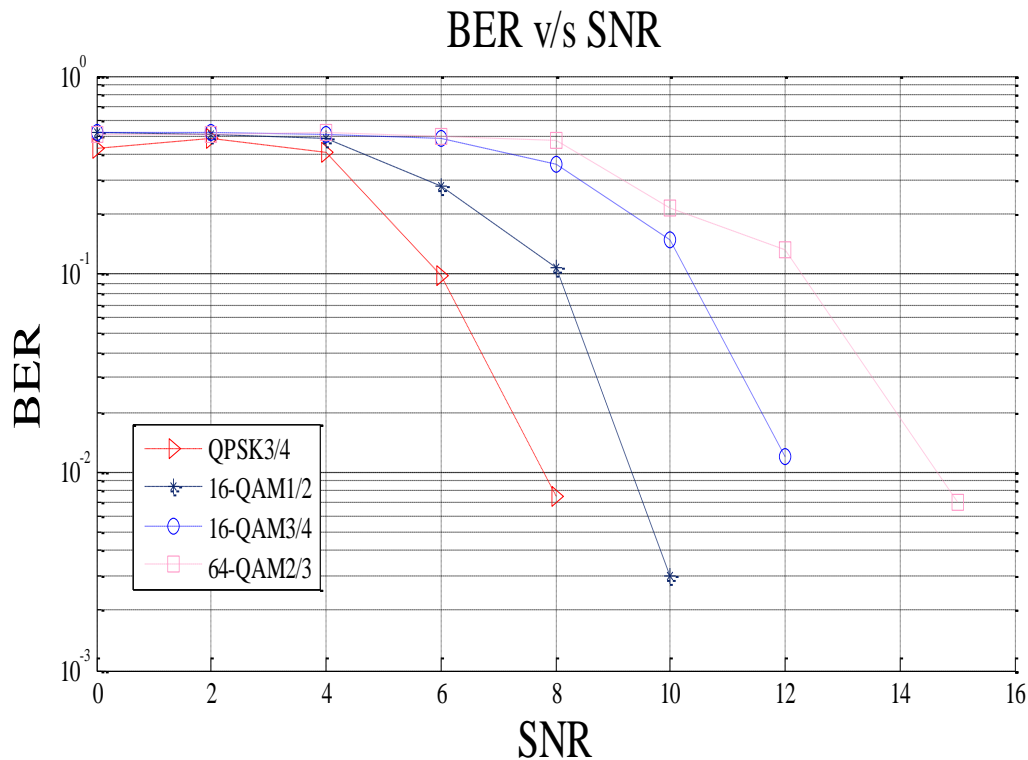


Figure 3. 32 Simulated graph for the Aggregator to EV Communication.

The results depict that to achieve BER of 10^{-2} : QPSK $\frac{3}{4}$ requires 6.8 dB, 16 QAM $\frac{1}{2}$ requires around 9.4 dB, 16 QAM $\frac{3}{4}$ requires, 64 QAM $\frac{2}{3}$ requires 14.8 dB. The 16 QAM $\frac{1}{2}$ is found to be superior as compared to other modulation schemes.

3.3.3.2 Channel Fading

3.3.3.2.1 Large scale fading: (Outdoor –to- Outdoor scenario)

In the large scale fading the signal fades due to large distance. The aggregator is fixed in our case and the EV is either moving or parked in open space. The free space path loss is a standard considered for LOS as discussed in section 3.2.2.3.1. For this scenario, the Cost WI, Cost Hata and Hata Okumara models are considered to analyse the path loss. We have assumed the transmitter antenna height to be 30m and the receiver antenna height to be 10m and 6m for the Urban and Suburban environment respectively.

From Figure 3.33 it is observed that for the receiver at a distance of 6 km in Urban environment: the free space path loss is 119 dB, Cost WI is 170 dB, Cost Hata is 168 dB and Hata Okumara is 160 dB. The Hata Okumara is comparatively less as compared to the Cost Hata and Cost WI. The Cost Hata falls in between the two. The Cost WI exhibits the highest path loss of 170 dB. GCC is transmitter and aggregator is receiver as it is outdoor –to- outdoor scenario.

For the Suburban environment, the Figure 3.34 depict that Cost WI exhibits 158 dB, and Cost Hata demonstrates 159 dB and Hata Okumara projects 171 dB. The path loss of Hata Okumara is higher as compared to the other two models. It is also noticed that the Hata Okumara model demonstrates the highest path loss for Suburban and Cost WI exhibits highest path loss for Urban environment. The Hata Okumara model is preferred for Urban environment and Cost Hata and Cost WI are considered for the Suburban environment. The IEEE 802.16d is obvious choice in hilly or terrain regions.

3.3.3.2 Shadowing: Hilly regions

The aggregator is fixed and the EV is either moving or parked inside the multi storied buildings, shopping complex and in the basement of apartments or is in the hilly regions. In IEEE 802.16d the three terrain regions A, B and C are specified.

From the Figure 3.35 it is clear that the IEEE 802.16d demonstrates 135 dB in Suburban environment and 154 dB for Urban environment. The path loss models for terrain regions A, B and C are shown in Figure 3.36. In this case the transmitter antenna is considered as 10m and receiver antenna as 6m.

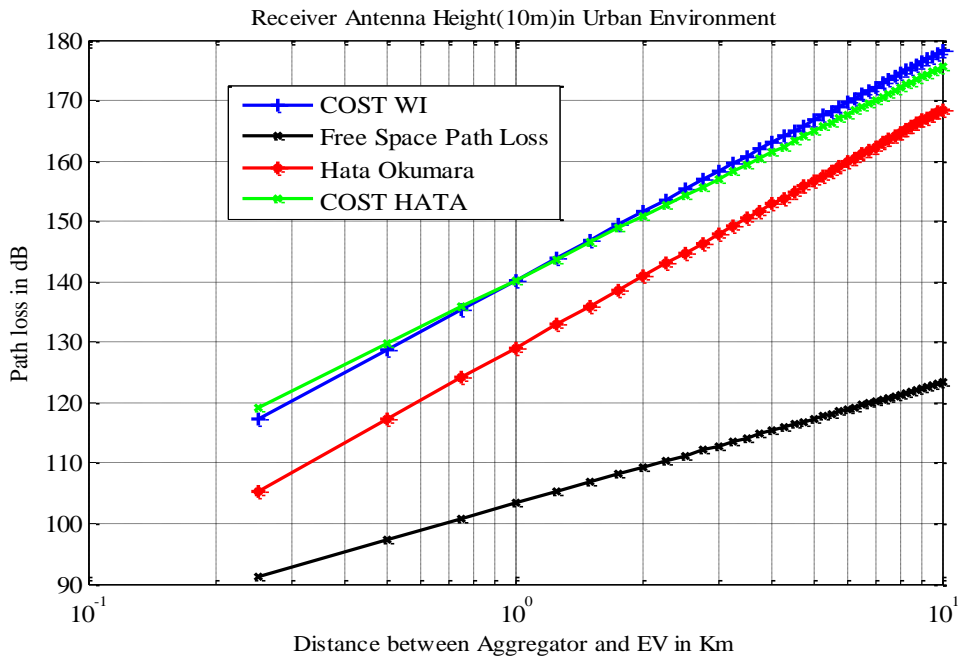


Figure 3. 33 Path Loss for Urban environment at 6 m receiver antenna height.

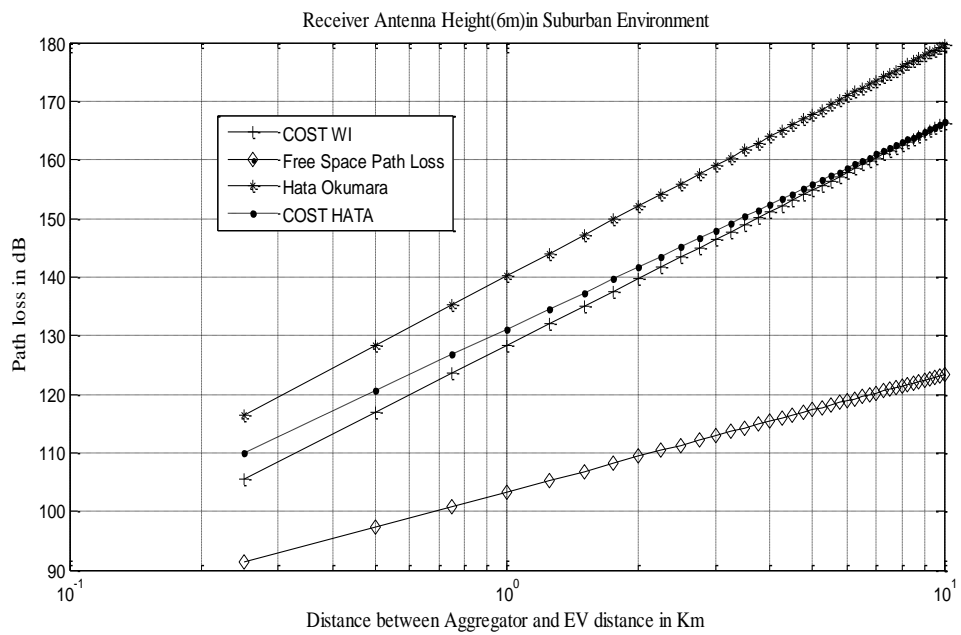


Figure 3. 34 Path Loss for Suburban environment at 6m receiver antenna height.

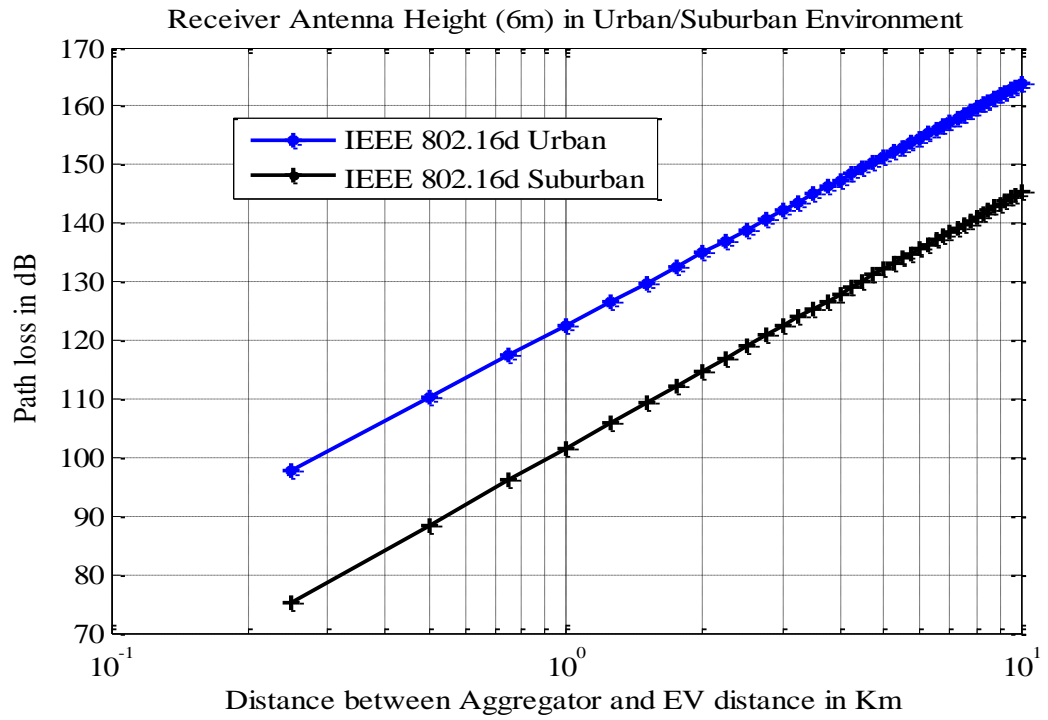


Figure 3. 35 Path Loss for Urban/Suburban Environment with IEEE 802.16d Model.

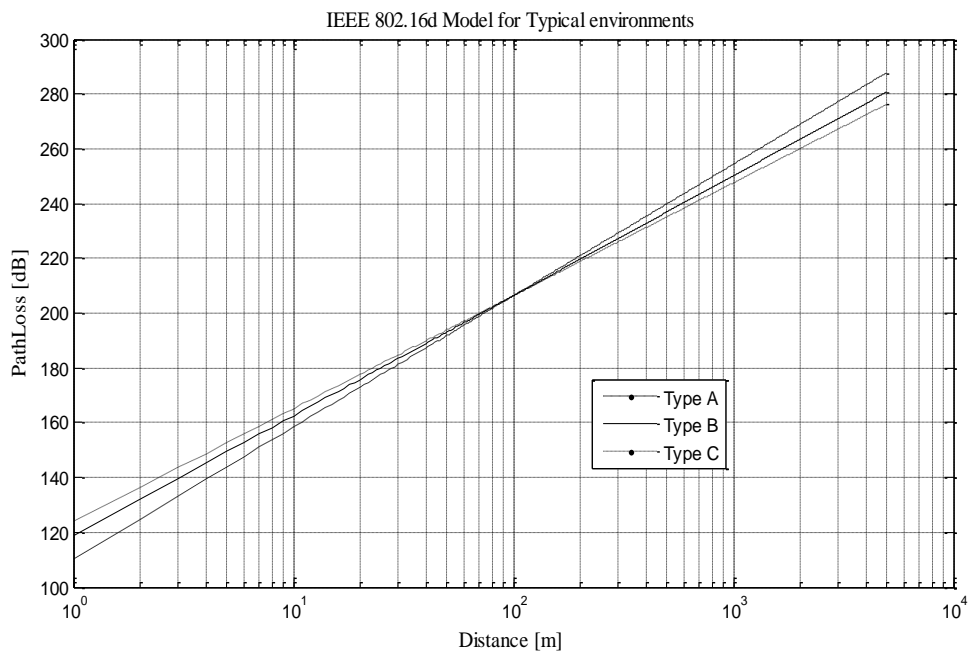


Figure 3. 36 Path Loss for Terrain Regions with IEEE 802.16d Model.

3.3.3.2.3 Small Scale Fading

The MATLAB/SIMULINK model is developed for the flat and frequency selective fading. The simulations are carried out for both Non LOS and LOS conditions. The received power spectrum for flat and frequency selective fading are shown in Figure 3.37 and Figure 3.38 respectively.

3.3.3.2.3.1 Flat Fading

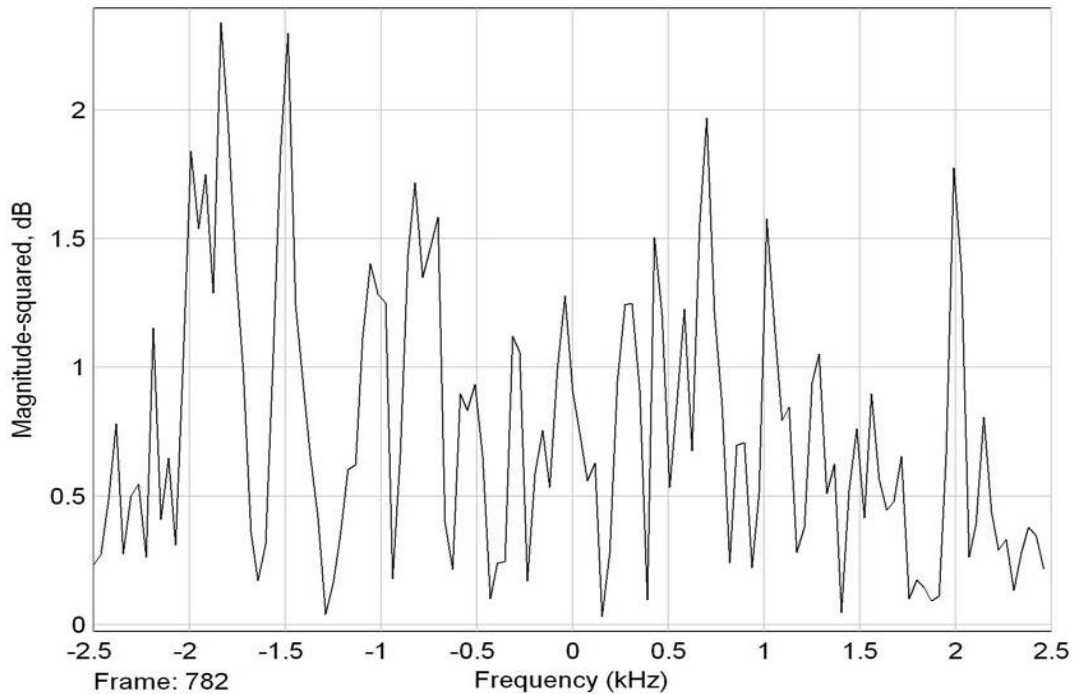


Figure 3. 37 Flat Fading Received Power Spectrum.

The received power spectrum is found to be fairly uniform and is shown in the Figure 3.37. It is observed that the signal attenuates and no distortion is observed. The average attenuation is observed from 1.5 dB to 0.5 dB.

3.3.3.2.3.2 Frequency Selective Fading

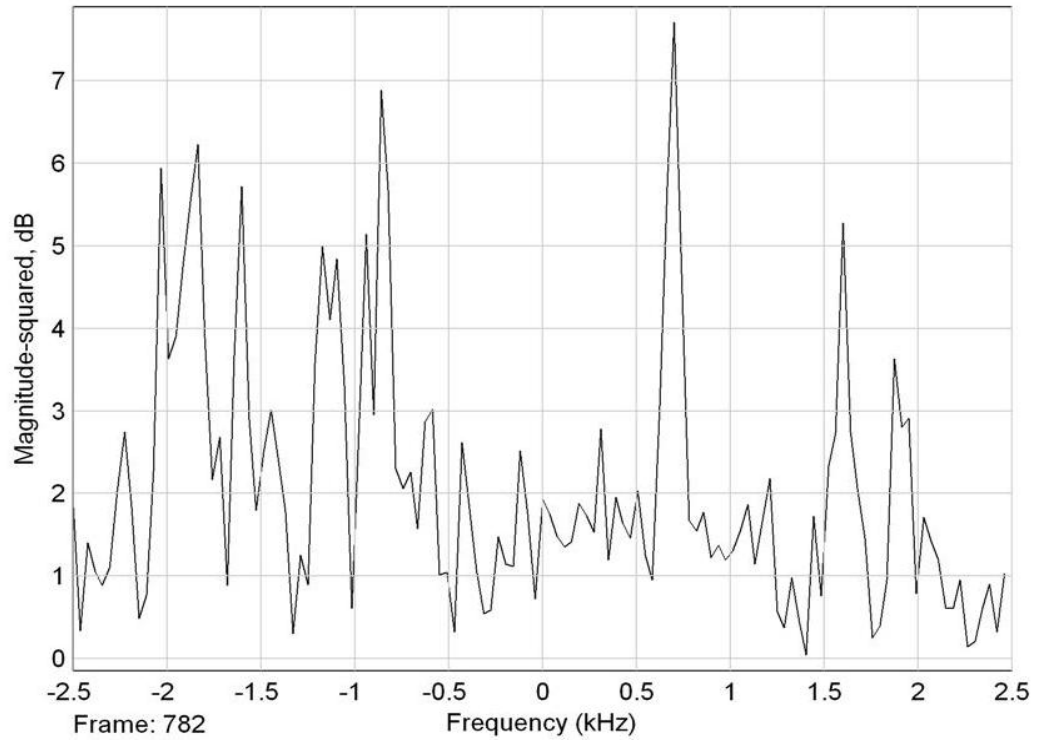


Figure 3. 38 Frequency Selective Fading.

In the frequency selective fading the signal distorts and deep variations are observed from 7 dB to almost 0 dB as shown in Figure 3.38.

The Rayleigh fading with QAM and QPSK modulation schemes were considered for NLOS simulation and are shown in Figure 3.39 and Figure 3.40 respectively. The Rician fading with QPSK modulation for LOS is shown in Figure 3.41. It is observed from the Figure 3.39, 3.40 and 3.41 that the power received at LOS is obviously higher as compared to the NLOS.

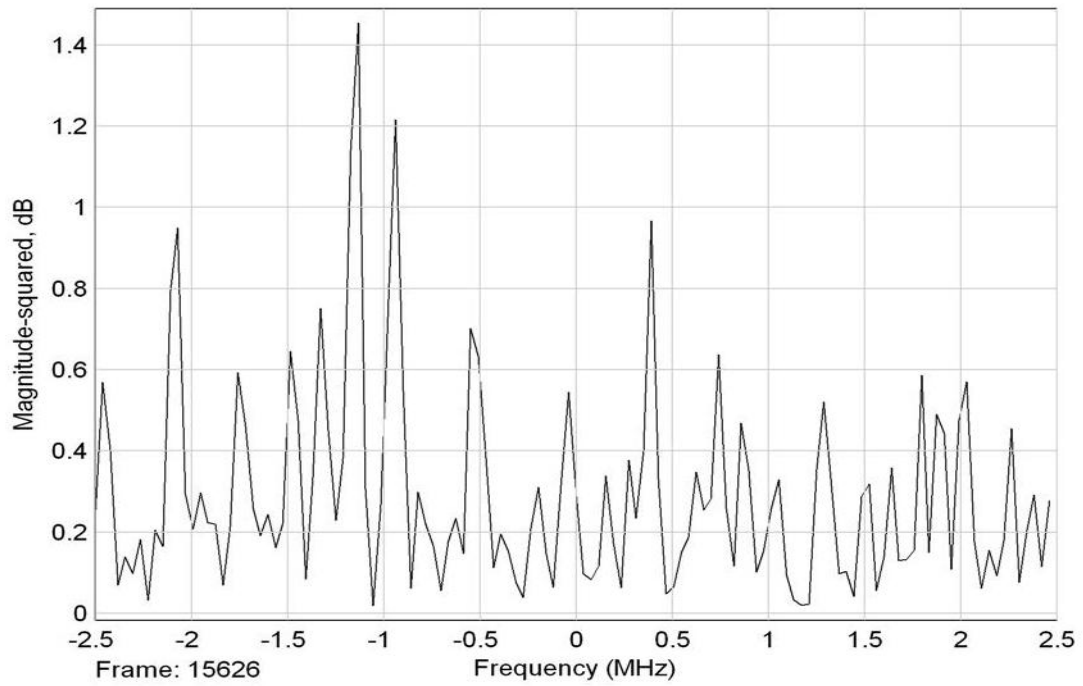


Figure 3. 39 NLOS Rayleigh Fading (QAM).

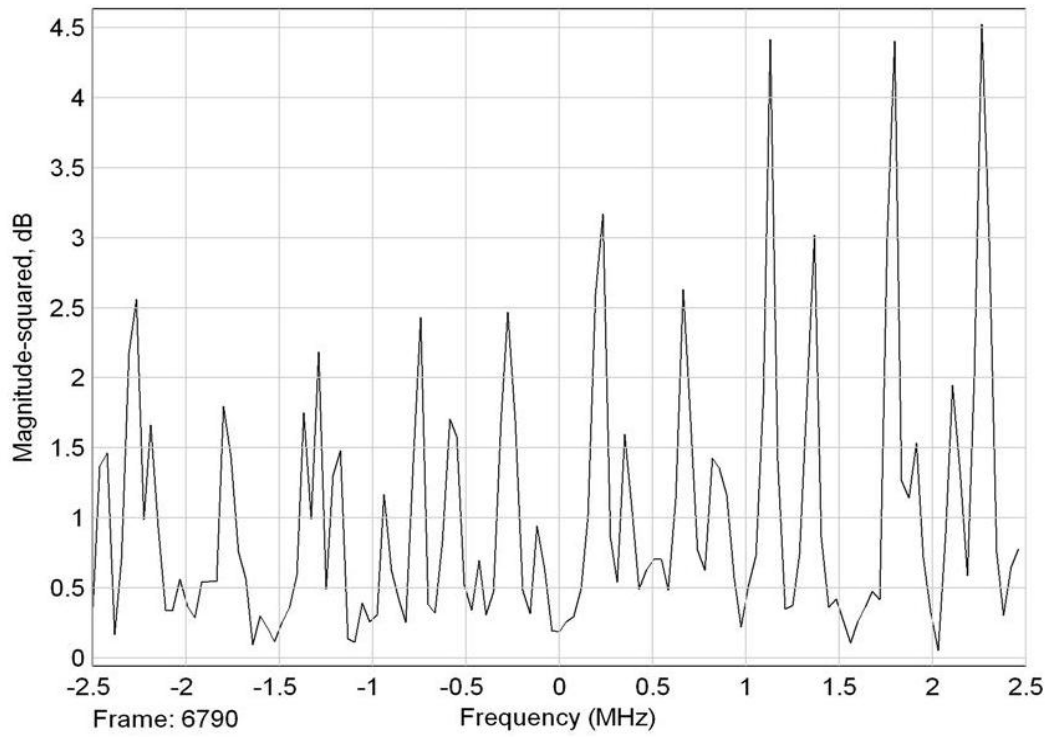


Figure 3. 40 NLOS Rayleigh Fading (QPSK).

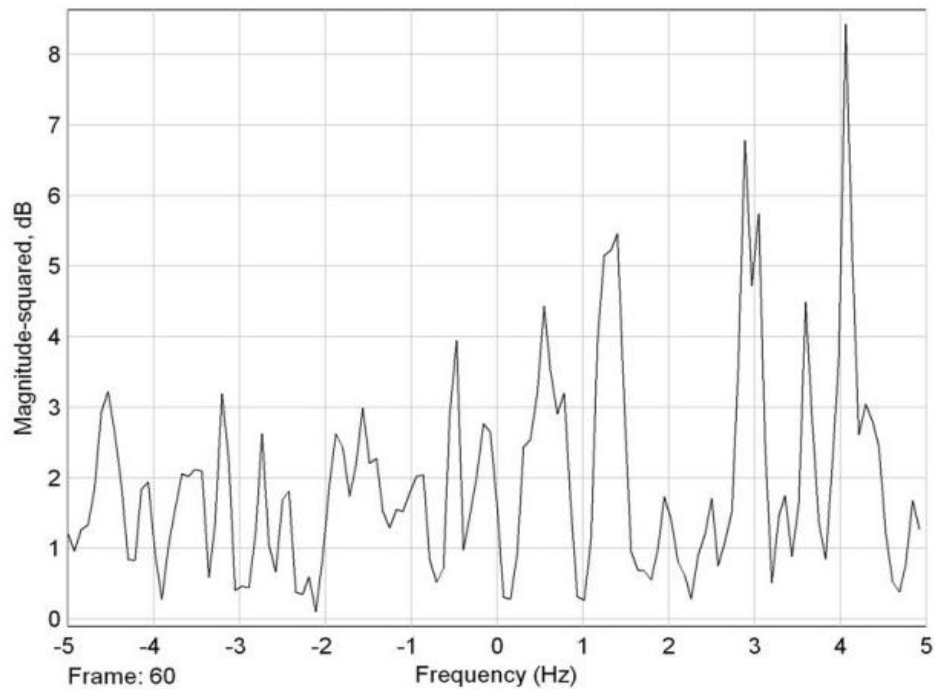


Figure 3.41 LOS Rician QPSK.

The analysis helps to model the suitable fading channel for aggregator to EV communication in V2G.

3.4 EV TO EV COMMUNICATION

The information (signal) propagates through wireless media and comes across obstacles like buildings, trees, hills and walls. Because of large distance and multipath the transmitted signal fades at the receiver. Due to this effect of multipath, a moving EV or receiver can experience several fades in a very short duration along with it EVs might be located in deeply faded region. It becomes difficult to maintain communication link between aggregator and EV and it is an issue of great concern [Gayatri and Mohana 2002].

EVs which have received the information already from the aggregator can forward it to other EVs which fall in their communication range. In V2V communication road safety, traffic flow management, vehicle optimal routing information, automatic fare

collection, consumptions and emissions issues are considered [Luigi Atzori and Alessio Meloni 2012]. Whereas in case of EV to EV communication, SOC of EV battery, Parking lot and charging slot availability are considered. The communication system model of V2G is shown in Figure 3.42.

In this chapter, LTE protocol is presented for EV to EV communication. The LTE downlink physical layer is modeled in MATLAB/SIMULINK for performance investigation. Already the path loss models for LTE protocol are discussed in section 3.3 and here the Small Scale fading is considered for signal strength analysis.

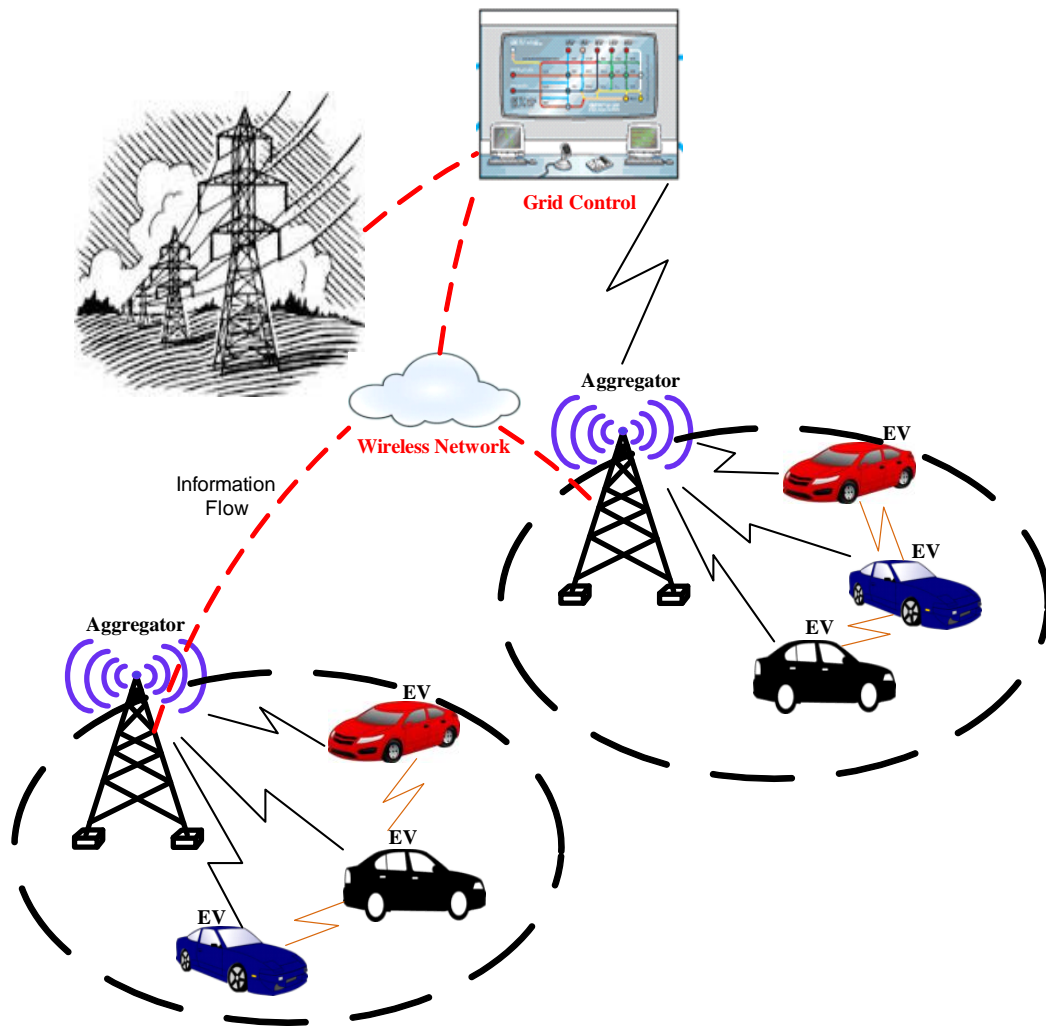


Figure 3. 42 Communication Model of V2G.

3.4.1 Path Loss Models for LTE

The concept of path loss models are already discussed in the sections 3.2 and 3.3. The path loss models applicable for LTE protocol are presented in this section. Six different path loss models are considered and are as follows [Hamid and Kostanic 2013; Houman 2014]:

3.4.1.1 3GPP Model:

The 3GPP has specified different propagation models for predicting the path loss at 2GHz band and for the NLOS the path loss can be determined using:

$$PL_{3GPP} = 125.2 + 36.3 \log(d) \quad (3.22)$$

where, d distance in [m]

3.4.1.2 WINNER B5f Model:

This model was developed by IST-WINNER project and covers a wide range of scenarios. This model considers both line-of-sight (LOS) and NLOS conditions.

$$PL_{WINNER} = 57.5 + 23.5 \log(d) + 23 \log\left(\frac{f}{5}\right) \quad (3.23)$$

where, d ($30\text{m} < d < 1.5\text{km}$) and f frequency in [GHz] ($2\text{GHz} < f < 6\text{GHz}$)

3.4.1.3 COST 231 Hata model:

This model is used in urban areas at the frequencies ranging from 1500 MHz - 2000 MHz. This model calculates the path loss and contains the corrections required for different environments.

The path loss can be determined by:

$$PL = 46.3 + 33.9 \log_{10}(f) - 13.82 \log_{10}(h_b) - ah_m + (44.9 - 6.55 \log_{10}(h_b)) \log_{10} d + c_m \quad (3.24)$$

3.4.1.4 Standard university interim (SUI) model:

The SUI model is an extension of Hata model and developed by Stanford University. The range of frequency is larger than 1900 MHz and the correction parameters allow this model up to 3.5GHz band. This model can be applied in three terrain regions.

The total attenuation $PL_s(d)$ is given by:

$$\begin{aligned} PL_s(d) &= PL_{s_0}(d) + s \\ &= 20 \log_{10} \left(\frac{4\pi d_0}{\lambda} \right) + 10\gamma \log_{10} \left(\frac{d}{d_0} \right) + X_f + X_h + s \end{aligned} \quad (3.25)$$

Path loss exponent γ depends on station height and terrain category and is given by:

$$\gamma = a - bh_b + \frac{c}{h_b} \quad (3.26)$$

3.4.1.5 Lee model

It is one of the popular and widely accepted path loss model. It is simple and reasonable prediction accuracy. The path loss is calculated using the equation

$$PL_{Lee} = PL_0 + m \log \left(\frac{d}{d_0} \right) - H_T - H_R \quad (3.27)$$

3.4.1.6 Vehicular Test Environment:

The vehicular test environment (VTE) consists of large cells with antennas transmitting at high power. The path loss for NLOS is given by:

$$PL_{VTE} = 128.1 + 37.6 \log_{10}(d) \quad (3.28)$$

3.4.2 LTE Protocol for EV to EV Communication

The LTE physical layer details are presented in section 3.2 and in this section the LTE protocol physical layer is developed for:

- i. MIMO 2x2, 4x4 configurations
- ii. Precoding – SU –MIMO-Mode 4 transmission : code book based precoding for 4x4 system, without CDD and selects a random codebook run.

3.4.2.1 LTE Physical Layer

These are the following steps involved in a downlink physical layer model:

- Scrambling: It scrambles the bits within the codeword to a specific.
- Digital Modulation Mapping: The bits are transformed in to digital modulated symbols and the modulation is chosen among QPSK,16-QAM and 64-QAM.
- Precoding and Layer Mapping: The pre coding is done to allow UE to separate different antenna streams in MIMO or transmitter diversity. These pre coded elements are then mapped on to a number of two dimensional time-frequency resource elements for transmission.
- OFDM Signal Generation: OFDM symbols are created using the number of subcarriers allocated for the transmission and CP is added to it.

The LTE Physical layer block diagram is shown in Figure 4.3. The receiver block process is reverse of the transmitter.

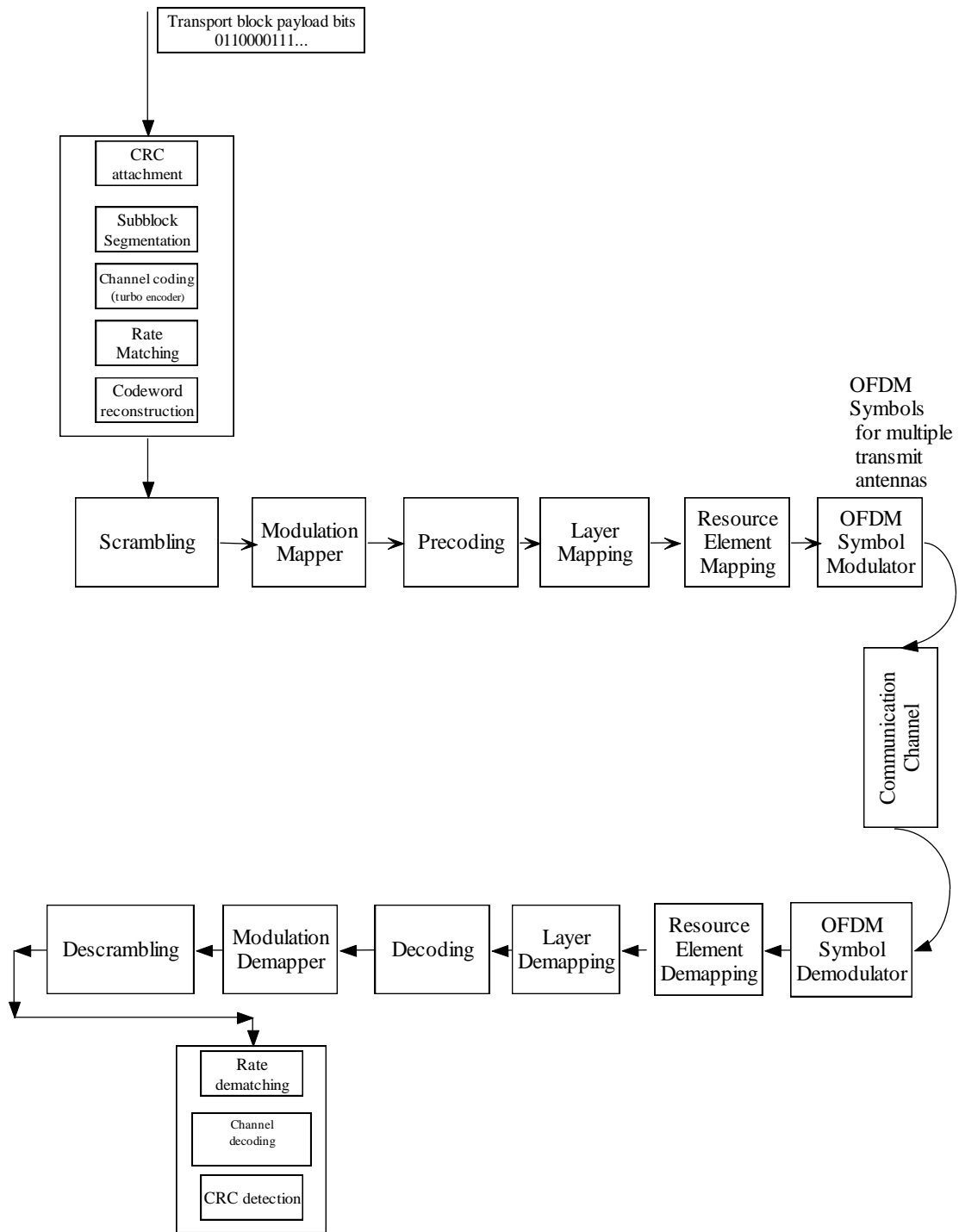


Figure 3. 43 Block diagram of LTE Physical Layer.

3.4.3 Results and Discussion

3.4.3.1 Path Loss Models

The propagation path loss models are analyzed and compared for LTE. The simulations were carried out using following parameters as shown in Table 3.7. The metrics prediction error mean (μ) and standard deviation (σ) are used for evaluating the path loss models [Vinko and Larry 1999]. The positive value of μ means that the model over estimates path loss value and negative value means the model predicts smaller path loss value than the expected. In line with this, a small value of σ indicates a good model prediction and large value indicates less accurate model.

Table 3. 7 Path loss parameters [Hamid and Kostanic2013]

<i>Model</i>	<i>f</i> (GHz)	<i>Tx- antenna height[m]</i>	<i>Rx- antenna height[m]</i>	<i>Distance-d [km]</i>
3GPP	2	30	10	--
WINNER B5f	2-6	25	15	0.03-1.5
SUI	2-11	10-80	3-10	0.1-8
COST 231 Hata	1.5-2	30-200	1-10	1-20
Lee	0.85-2	20-100	1-15	Up to 20
VTE	2	0-50	10	--

The transmitter and receiver antenna heights are considered to be 30m and 10m respectively. The transmitter power is 43dBm and the results are shown in Figure 3.44 and Figure 3.45. The Lee model demonstrates lower path loss 128dB for both urban and suburban environments as compared to other path loss models. Apart from the Lee model, in case of urban environment WINNER (142dB) and 3GPP (154dB) models are preferred whereas in case of suburban environment SUI and WINNER

models. The Vehicular Test Environment (VTE) demonstrates higher path loss compared to both environments.

The 3GPP and WINNERB5f models need no particular parameters to be defined. The COST 231-Hata Model is suitable for both environments depending on the height correction factor $a(h_m)$ and can be used to predict path loss at higher frequencies. The SUI model is undoubtedly the best choice for suburban environment. The results are validated with the open literature [Hamid and Kostanic 2013]. The path loss estimates for Urban/Suburban environment at 10m Receiver antenna height. These estimates will help to plan the Wireless network for V2G communication.

The statistical properties better describe the fading. EV instead of receiving the signal over LOS, receives different versions of information because of varying path lengths and random phases. Lognormal distribution describes the shadowing and we considered carrier frequency of 900 MHz, 10 multi paths and 8 scatters for the simulation purpose and is shown in Figure 3.46.

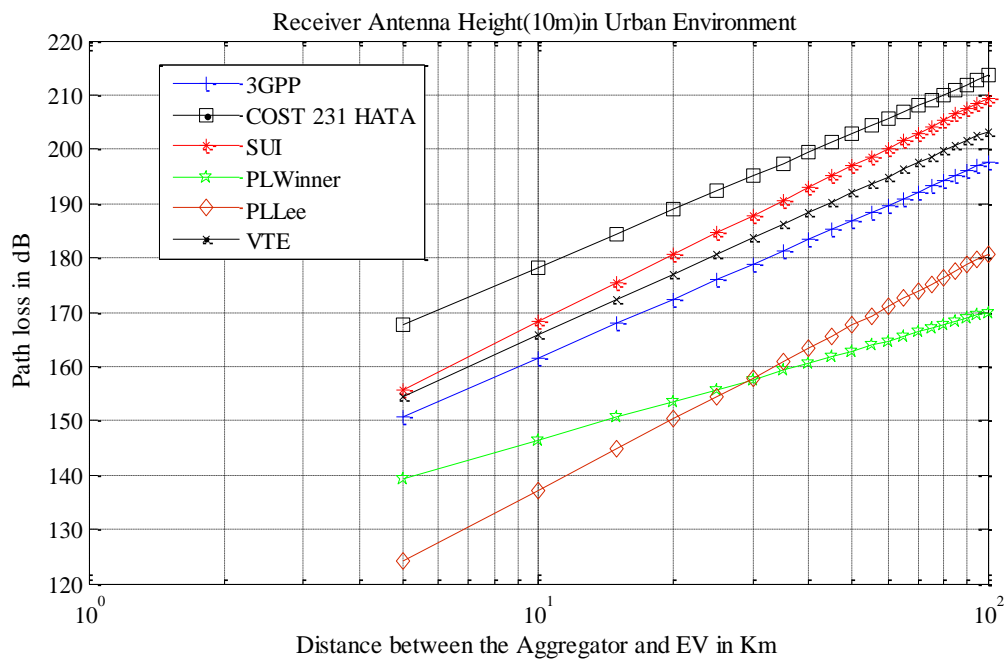


Figure 3. 44 Path loss for Urban Environment.

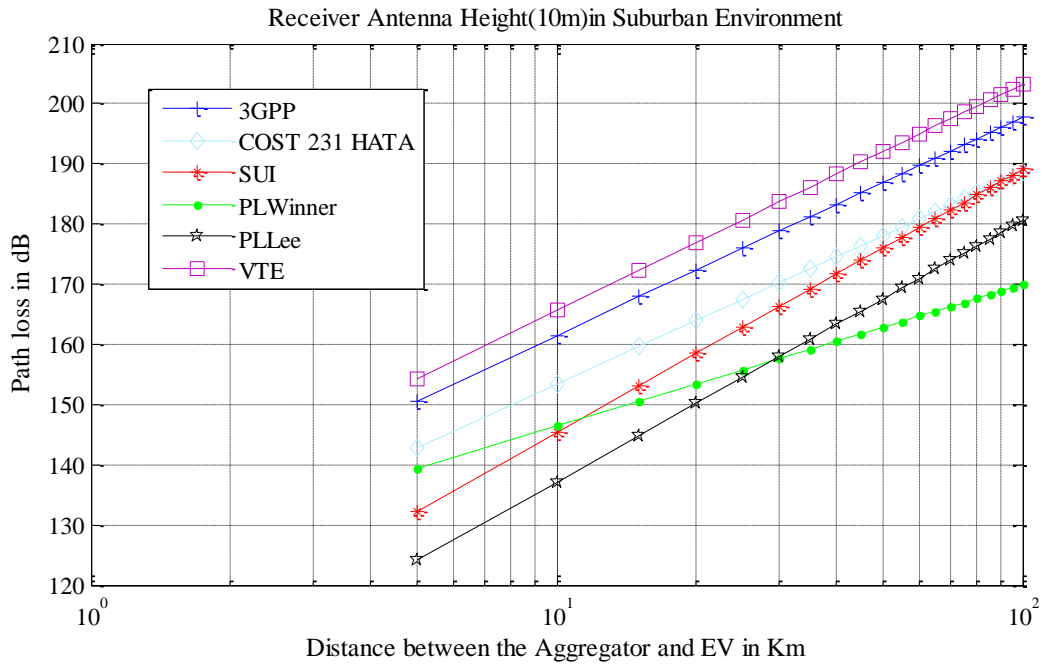


Figure 3. 45 Path loss for Suburban Environment.

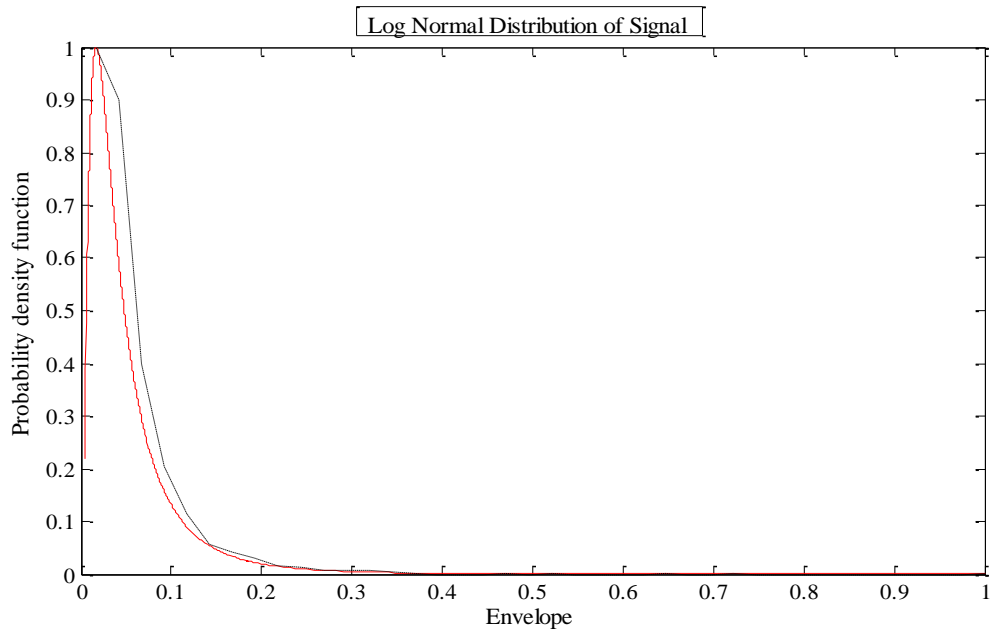


Figure 3. 46 Lognormal distribution of a signal.

3.4.3.2 Shadowing

The concept of shadowing is discussed in section 3.3.2.2. The Rayleigh and Rician distributions are considered for NLOS and LOS respectively. The EV is moving at 50m/sec and the received envelope demonstrates that the average of volts received is 2.6125V (Rayleigh) and 3.5827V (Rician) shown in Figure 3.47 and Figure 3.48 for NLOS and LOS respectively. It is worth to note that the Rician (LOS) is demonstrating higher volts as compared to the NLOS. The randomness in the variation of the transmitted signal can be modeled with semi empirical or stochastic models.

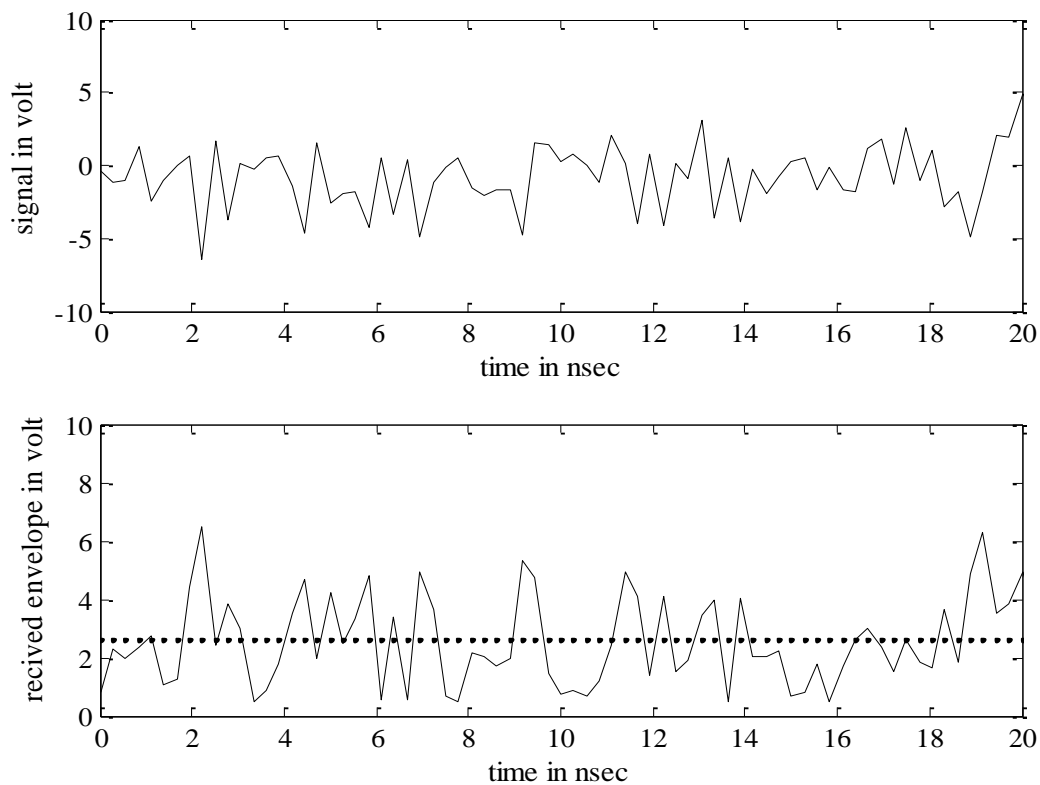


Figure 3. 47 Received envelope (Rayleigh).

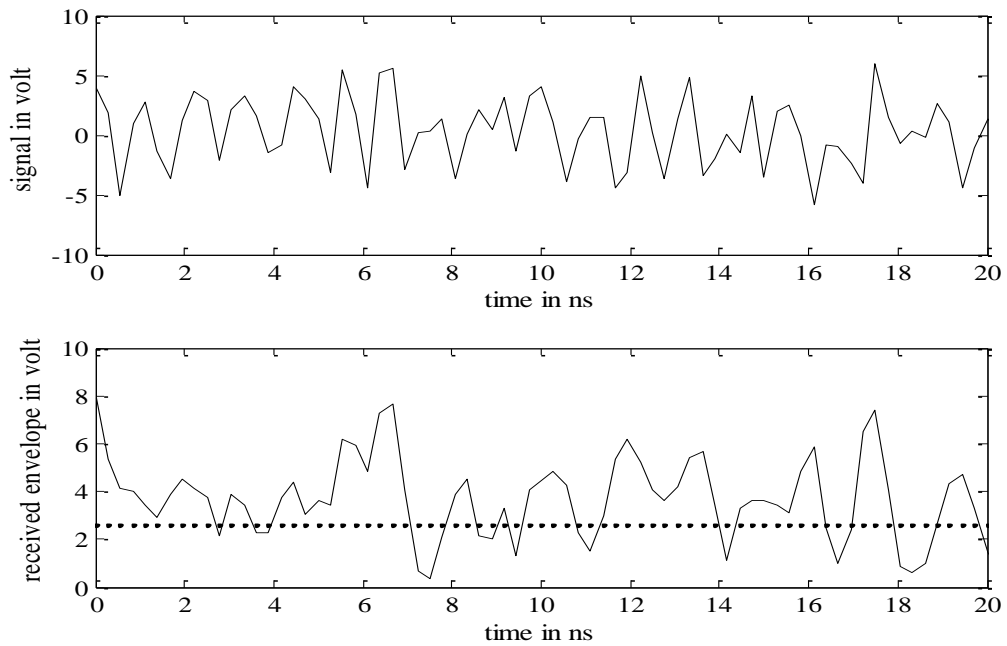


Figure 3. 48 Received envelope (Rician).

3.4.3.3 LTE Physical layer

The LTE Physical layer is modeled using MATLAB/SIMULINK. The Figure 3.49 depicts that the QPSK demonstrates lower bit error rate (BER) as compared to the QAM. In order to achieve the BER of 10^{-1} the QPSK requires 2-4 dB and 16QAM requires 11-12 dB for both the code words. The BER v/s SNR plots are plotted for 2x2 antenna configuration, frequency of 5MHz, EPA 0Hz and 5Hz channel with the Doppler spread in Figure 3.49 and Figure 3.50 respectively. The EVs can receive the information sent by an aggregator at higher data rates and mitigate the problems associated with ISI and Doppler spread.

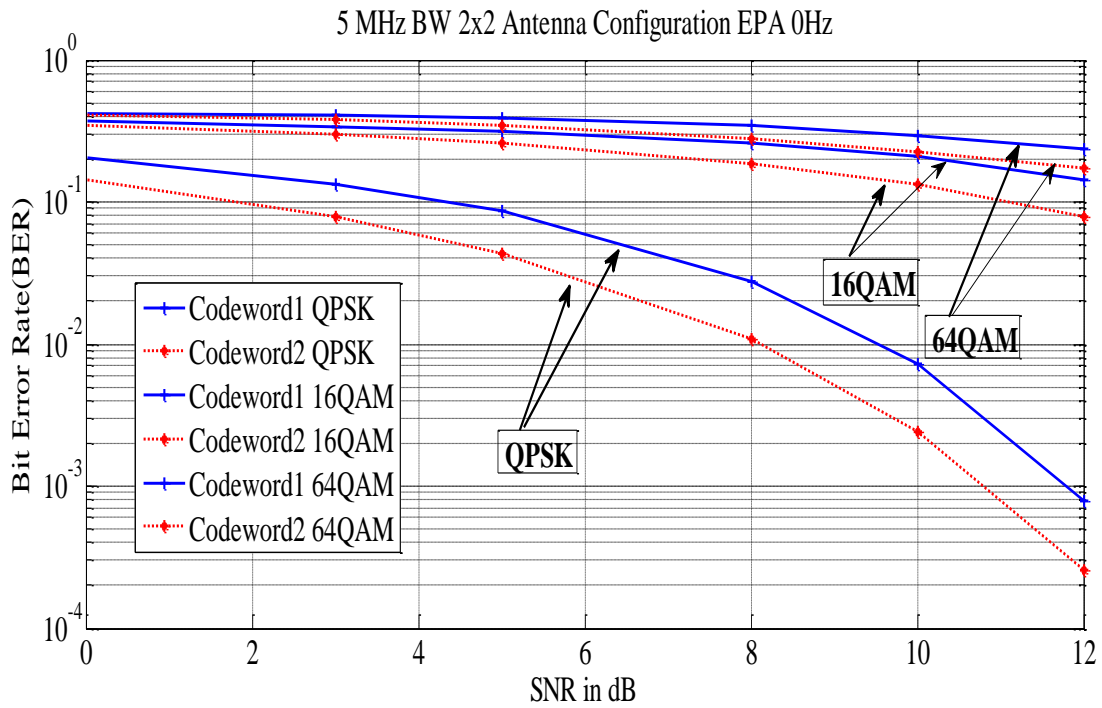


Figure 3. 49 BER v/s SNR for EV to EV Communication Link.

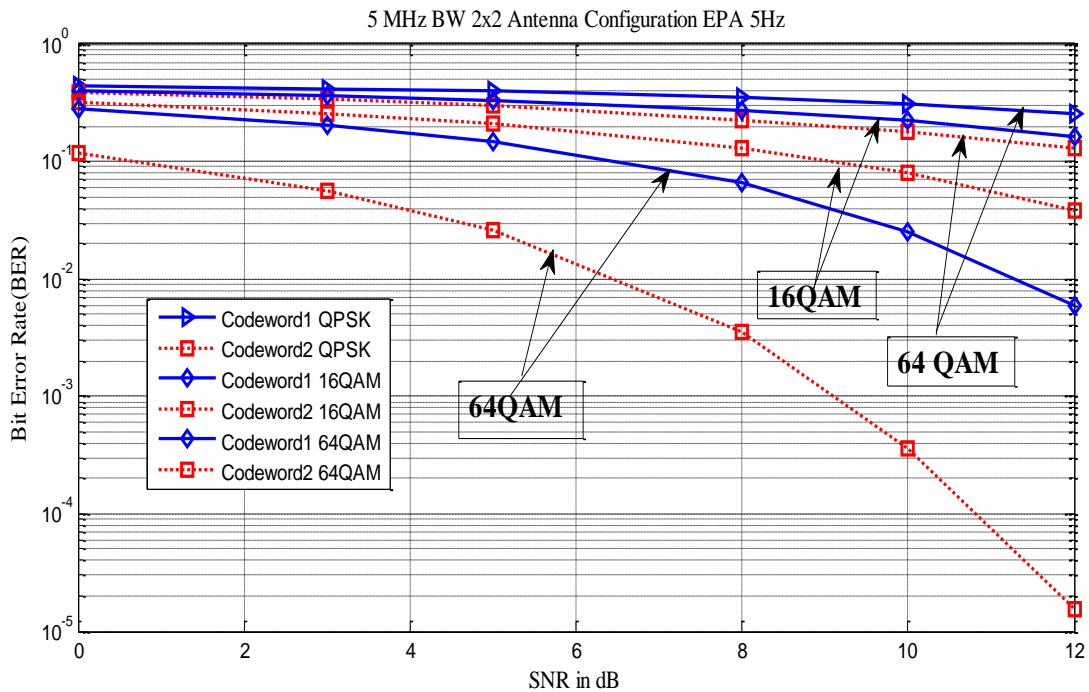


Figure 3. 50 BER v/s SNR for EV to EV Communication Link.

3.5. EV TO SMART METER COMMUNICATION

The communication links between GCC to Aggregator, Aggregator to EV and EV to EV are discussed in sections 3.2 ,3.3 and 3.4 respectively for transferring the grid requirement information to EVs. Once the EVs receive the information, the interested EVs will participate in grid power transactions. The power transaction between EV and the grid is monitored and recorded by Smart Meter and the same is communicated to the EVs. Smart Meter is located at the charging station and acts as a communication interface between EV and the grid for proper and accurate functioning of V2G. As the development of wireless communication infrastructure for EV to Smart Meter is required, the Wi-Fi and WiMAX protocols are proposed for the same in this chapter.

3.5.1 Indoor Wireless Communication Channels

The indoor wireless channels have different fading characteristics compared to the mobile case. The transmitter and receiver in this case are stationary and people move in between and influence the channel. In case of outdoor mobile systems the user is moving through an environment [Kamil and Michal 2013]. For the indoor environment, the effect of fading can be described using Doppler spectrum:

$$S(f) = \frac{1}{1 + A \left(\frac{f}{f_d} \right)^2} \quad (3.29)$$

where A defines $0.1 S(f)$ at frequency f_d .

$$(S(f)) \Big|_{f=f_d} = 0.1, \text{ so,} \quad A = 9 \quad (3.30)$$

The Doppler spread f_d is defined as

$$f_d = \frac{v_o}{\lambda} \quad (3.31)$$

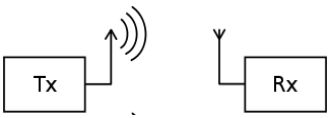
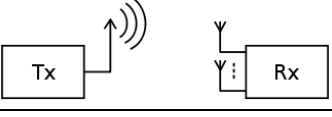
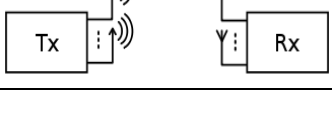
where v_o is environmental speed (based on measurements) and λ is wavelength and is given by:

$$\lambda = \frac{c}{f_c} \quad (3.32)$$

where c represents light speed, f_c carrier frequency, f_{\max} maximum frequency component of Doppler spectrum and it limits the range of frequencies(upper bound). Usually, $f_{\max} = 5 f_d$.

The channel models are developed for wireless local area network (WLAN). The bandwidths up to 100MHz at frequencies of 2 and 5GHz are considered. There are set of six profiles A to F and cover flat fading, residential, small office, typical office, large office/ large space (indoor/outdoor) scenarios. The path loss model and shadowing are available for each channel model. The multiple input multiple output (MIMO) multipath fading channel also exists and describes the multipath delay profile and Doppler spectrum [Schumacher et al. 2002].

Table 3. 8 Types of Antenna

Antenna types		
SISO	One antenna at transmitter and receiver side.	
SIMO	One antenna at transmitter side and multiple antennas at receiver side.	
MISO	Multiple antennas at transmitter side and one antenna at receiver side.	
MIMO	Multiple antenna at transmitter and receiver side respectively.	

The MIMO technique uses multiple antennas both at the transmitter and receiver to improve the performance of the communication. It addresses the issue of multipath, exploits space dimension and improves system capacity, range and reliability. The data throughput is increased without additional bandwidth and increased transmitted power. The fading is reduced and spectral efficiency is increased. The Table 3.8 depict the different types of antenna schemes viz. SISO/SIMO/MISO/MIMO.

The MIMO channel matrix H for each tap at particular instance of time can be separated into a fixed (LOS) matrix and a Rayleigh (NLOS) matrix. The 4X4 MIMO is example is considered

$$\begin{aligned}
 H &= \sqrt{P} \left(\sqrt{\frac{K}{K+1}} H_F + \sqrt{\frac{1}{K+1}} H_v \right) \\
 &= \sqrt{P} \left(\sqrt{\frac{K}{K+1}} \begin{bmatrix} e^{j\phi_{11}} & e^{j\phi_{12}} & e^{j\phi_{13}} & e^{j\phi_{14}} \\ e^{j\phi_{21}} & e^{j\phi_{22}} & e^{j\phi_{23}} & e^{j\phi_{24}} \\ e^{j\phi_{31}} & e^{j\phi_{32}} & e^{j\phi_{33}} & e^{j\phi_{34}} \\ e^{j\phi_{41}} & e^{j\phi_{42}} & e^{j\phi_{43}} & e^{j\phi_{44}} \end{bmatrix} + \sqrt{\frac{1}{K+1}} \begin{bmatrix} X_{11} & X_{12} & X_{13} & X_{14} \\ X_{21} & X_{22} & X_{23} & X_{24} \\ X_{31} & X_{32} & X_{33} & X_{34} \\ X_{41} & X_{42} & X_{43} & X_{44} \end{bmatrix} \right)
 \end{aligned} \tag{3.33}$$

where X_{ij} (i^{th} receiving antenna and j^{th} transmitting antenna), K is Ricean factor and P is tap power.

3.5.2 EV to Smart Meter Communication

3.5.2.1 WI-FI protocol for EV to Smart Meter Communication

The Wi-Fi protocol is proposed for Smart Meter to EV communication in V2G as shown in Figure 3.51. The block diagram of physical layer of Wi-Fi protocol (SISO) is shown in Figure 3.52.



Figure 3. 51 EV to Smart Meter Communication in Charging Station.

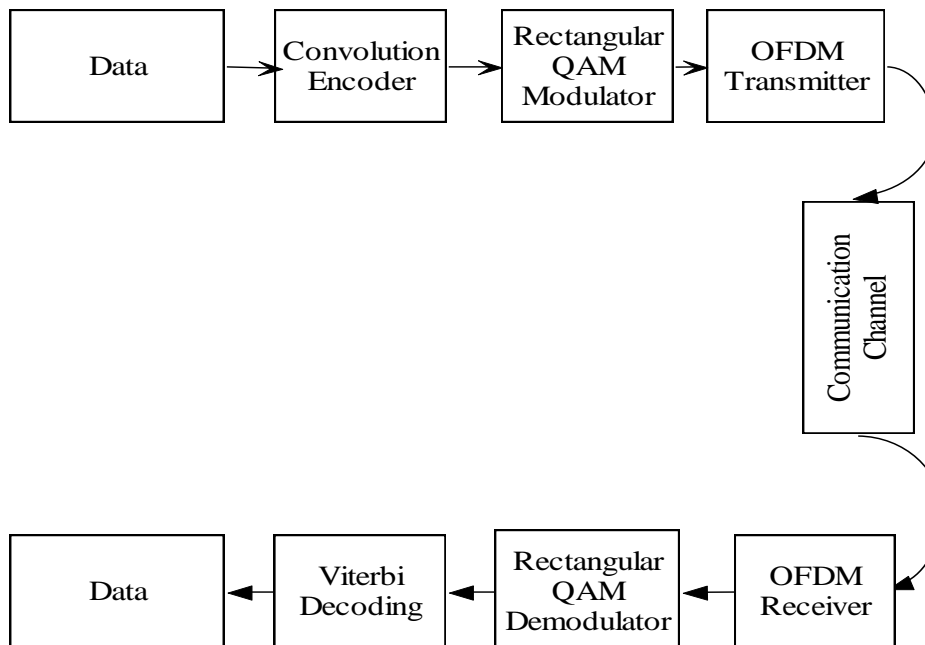


Figure 3. 52 Block diagram of Wi-Fi (SISO) physical layer.

3.5.2.2 WiMAX protocol for EV to Smart Meter Communication

The WiMAX standard defines the ideal profiles using 256-FFT OFDM Physical layer specification and supports up to 50km coverage area and data flow up to 70Mbps. In practice, the coverage area is 5-7 Km and 7Mbps. An OFDM has three subcarriers i) data subcarriers, ii) pilot subcarrier and iii) null subcarriers. The physical layer of WiMAX is discussed in section 3.2.

3.5.3 RESULTS AND DISCUSSION

3.5.3.1 Indoor Wireless Fading Channels

The indoor wireless channel models B and C are considered for simulation as they are specific to residential and small office scenarios. The EVs are usually parked in the basement of the office building or residential apartment. The indoor environment is assumed for EV parking and charging to facilitate the V2G operation. Each model comprises of clusters and they are assigned to set of spatial properties: i) mean angle of arrival (AoA) ii) mean angle of departure (AoD), iii) angular spread (AS) at transmitter and receiver. The parameters have same values for all the tap delays for a given cluster and they determine the transmit and correlation matrices for each tap delay. The parameters for channel model are taken from the standard reference. The 2X2 MIMO (2 transmit antenna and 2 receive antenna) is considered for simulation.

The Doppler effect is different from other typical mobile cellular models and can be chosen for the fading characteristics (indoor wireless channel model). The Doppler spectrum is estimated from the complex path gains for Tx1-Rx1 link of the first path. The Figure 3.53 and Figure 3.54 depict that the obtained Doppler spectrum fits the theoretical values. For each transmit-receive link, the fading envelope waveforms are shown in Figure 3.55, Figure 3.56, Figure 3.57 and Figure 3.58 respectively for the channel model B which is developed for the residential environment [Mathworks

2012]. The results demonstrate that the signal get faded at different intervals and for different combination.

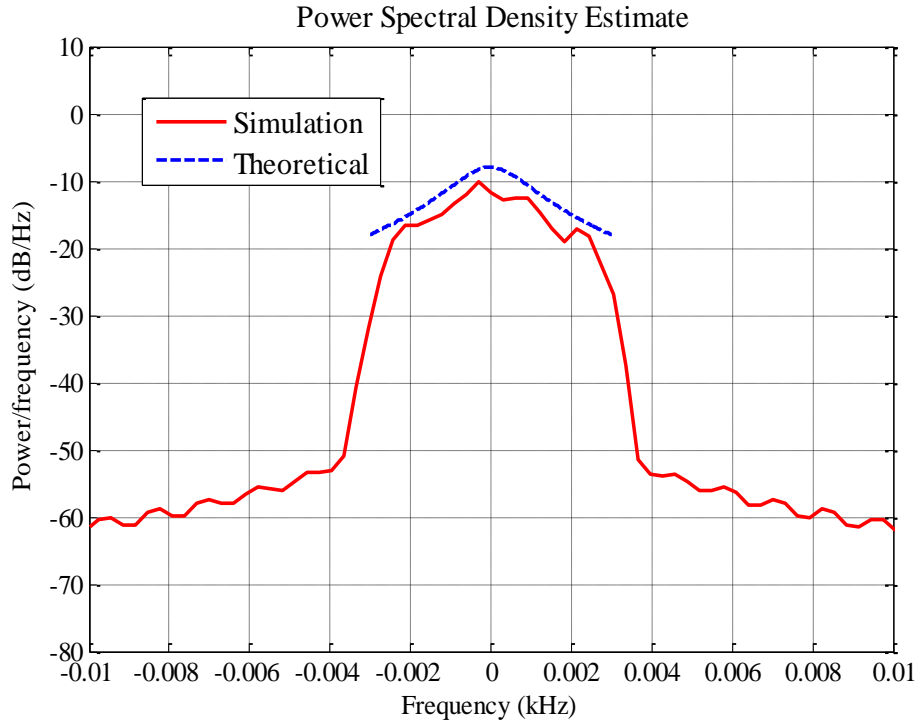


Figure 3. 53 Doppler spectrum estimate.

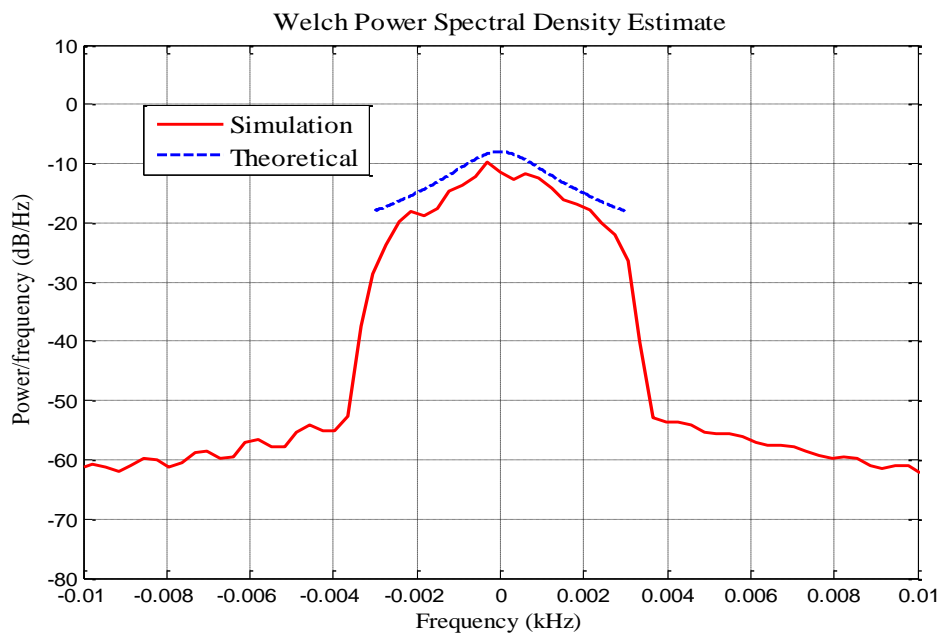


Figure 3. 54 Doppler spectrum estimate.

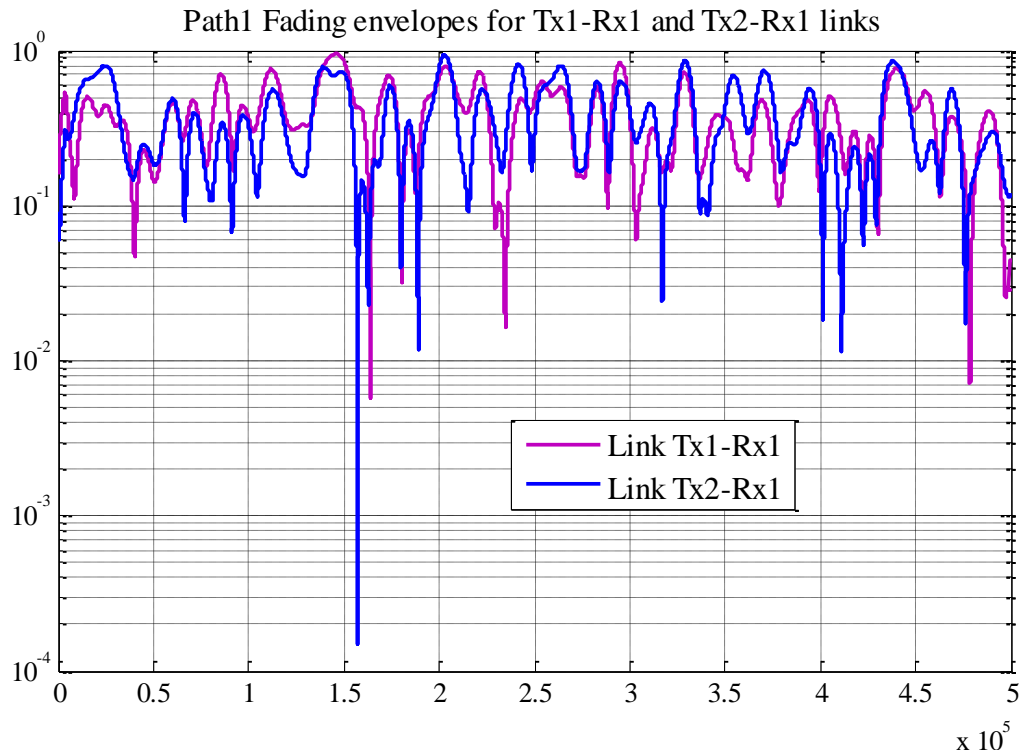


Figure 3. 55 Path1 Fading Envelopes for Tx1-Rx1 and Tx2-Rx2 links.

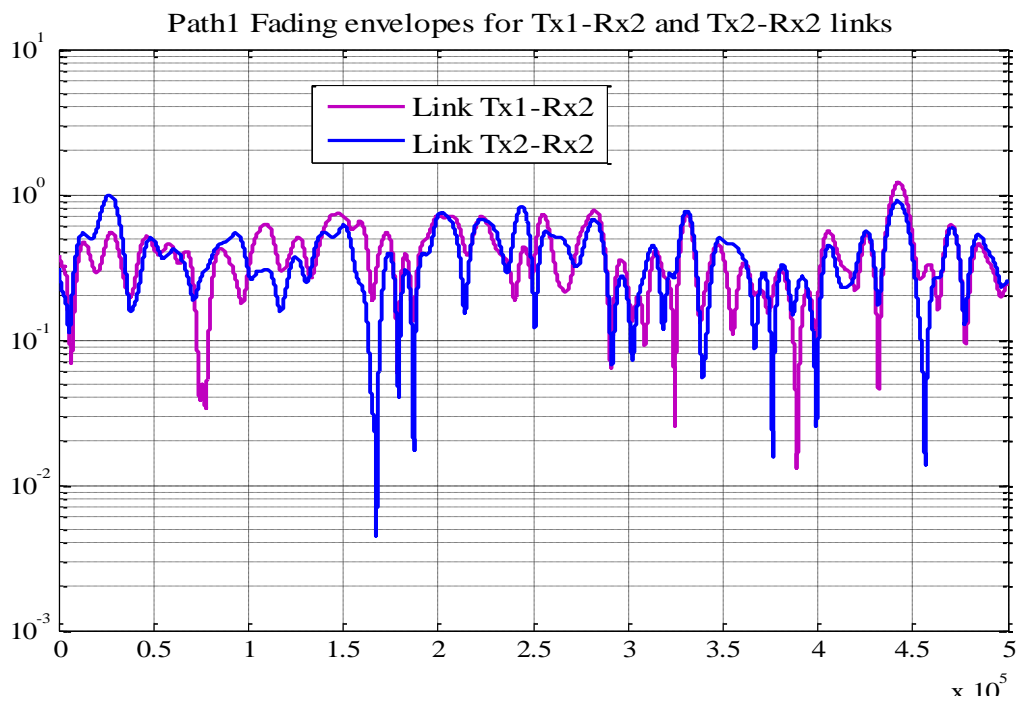


Figure 3. 56 Path1 Fading Envelopes for Tx1-Rx2 and Tx2-Rx2 links.

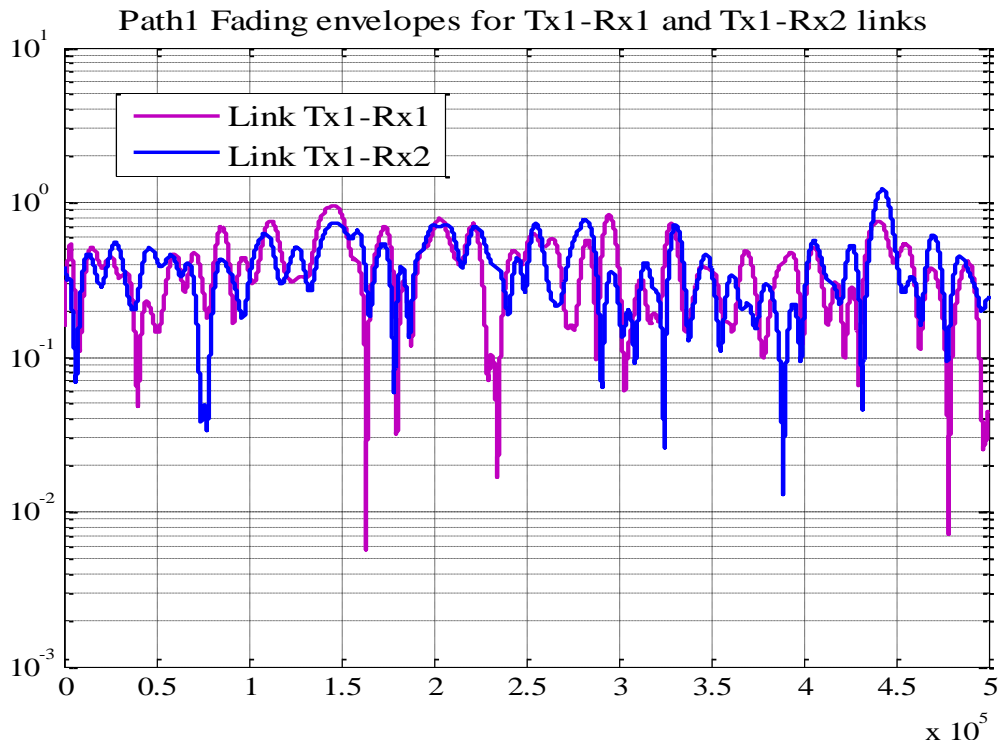


Figure 3. 57 Path1 Fading Envelopes for Tx1-Rx1 and Tx1-Rx2 links.

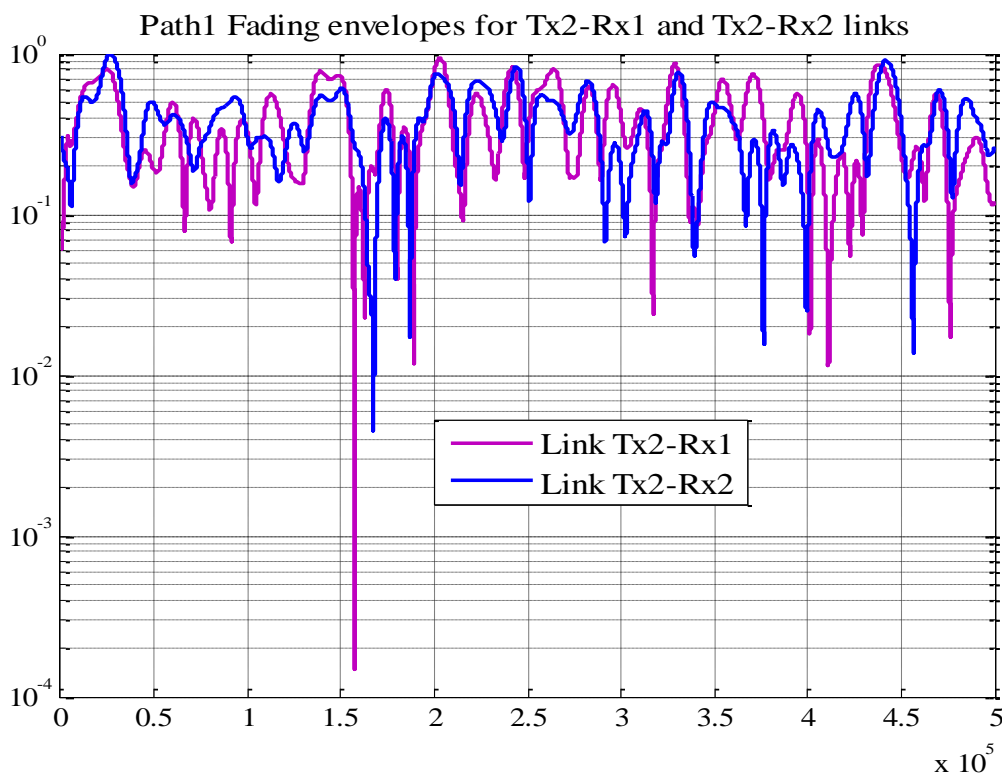


Figure 3. 58 Path1 Fading Envelopes for Tx2-Rx1 and Tx2-Rx2 links.

The Figure 3.59 and 3.60 depict that the obtained Doppler spectrum fits the theoretical values.

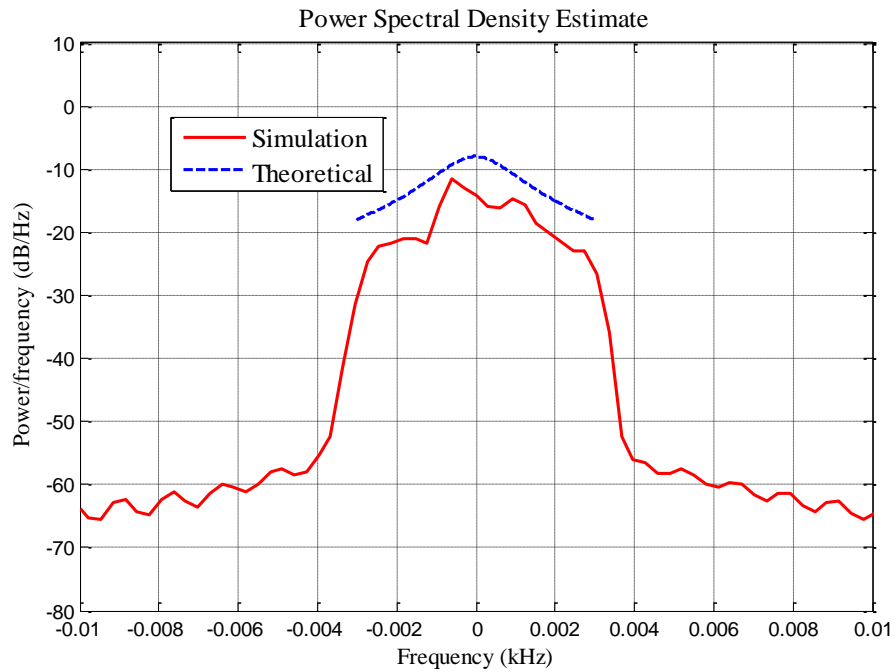


Figure 3. 59 Doppler spectrum estimate.

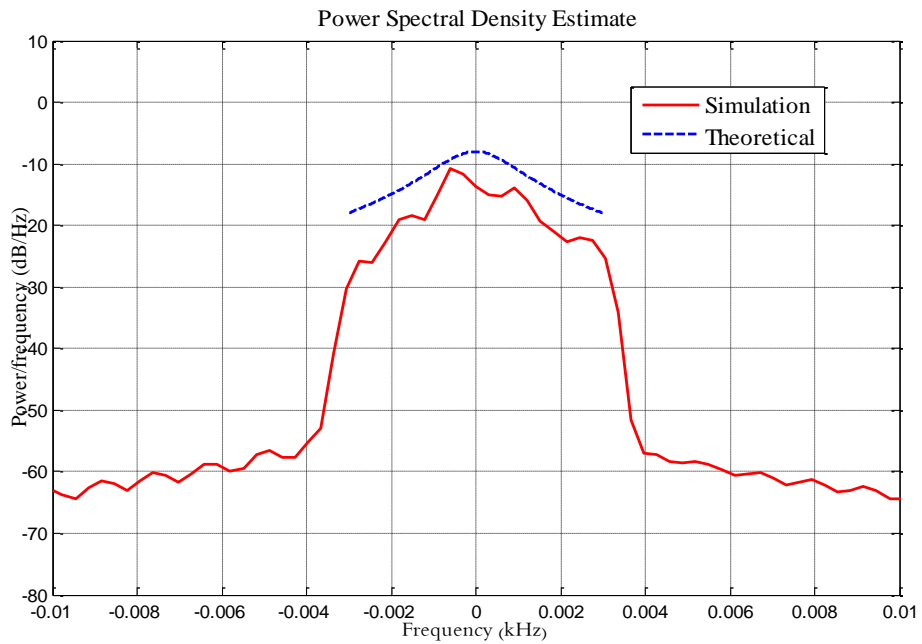


Figure 3. 60 Doppler spectrum estimate.

The fading envelope waveforms for each transmit-receive link are shown in Figure 3.61, 3.62, 3.63 and 3.64 respectively for the channel model C which is developed for the residential / office building environment.

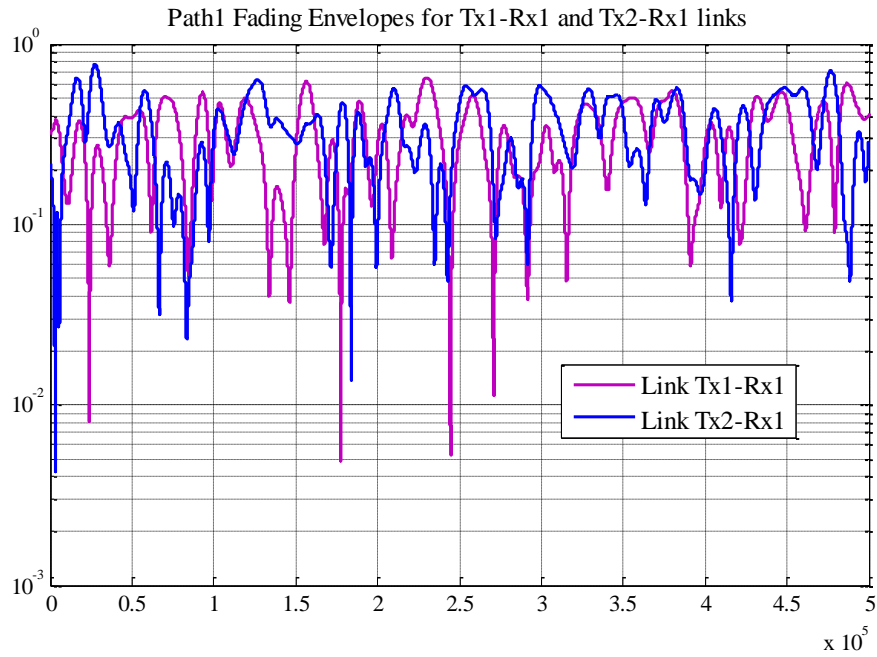


Figure 3. 61 Path1 Fading Envelopes for Tx1-Rx1 and Tx2-Rx1 links.

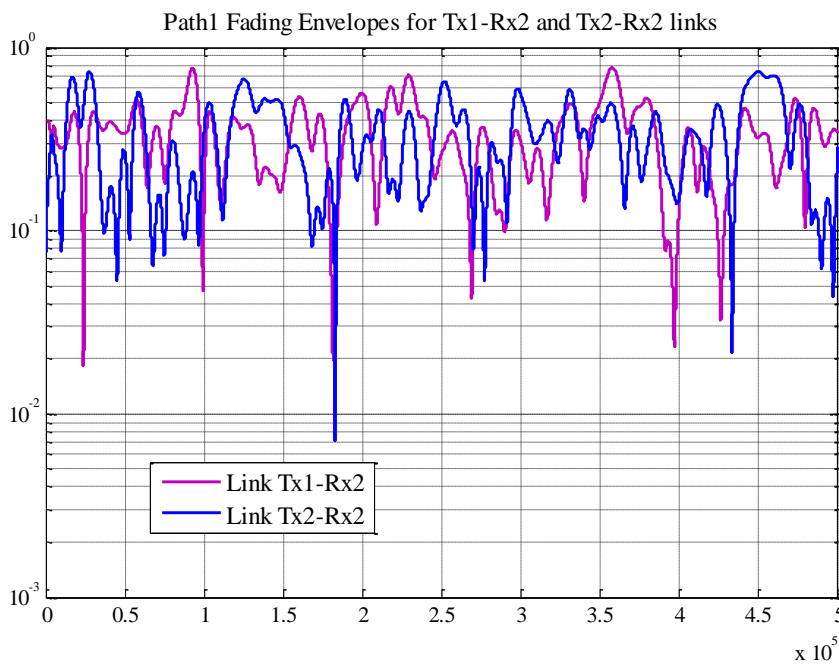


Figure 3. 62 Path1 Fading Envelopes for Tx1-Rx2 and Tx2-Rx2 links.

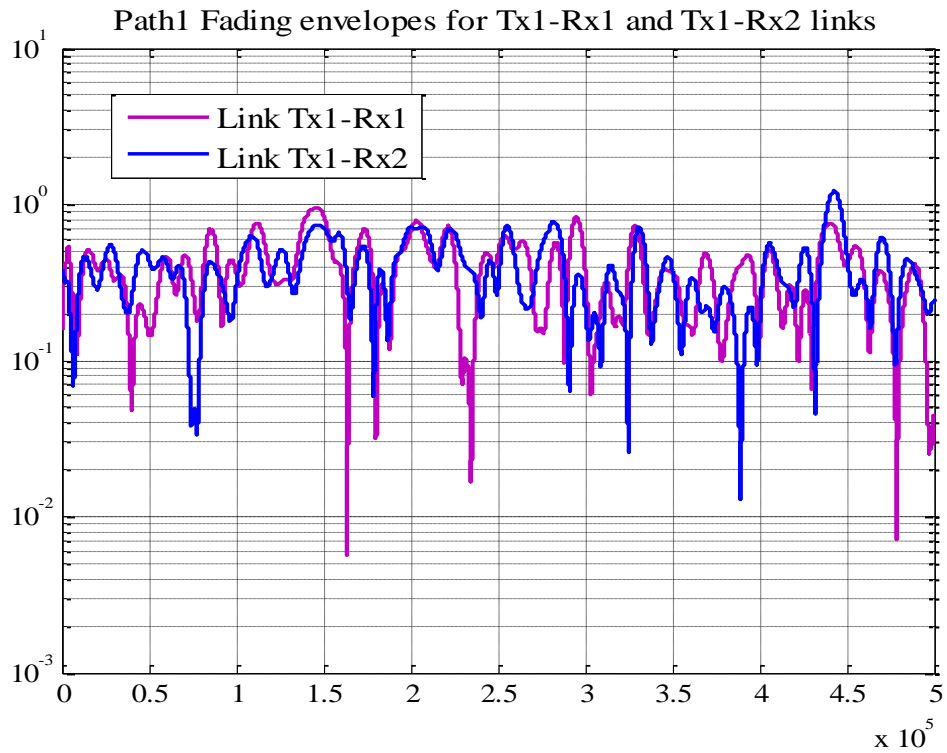


Figure 3. 63 Path1 Fading Envelopes for Tx1-Rx1 and Tx1-Rx2 links.

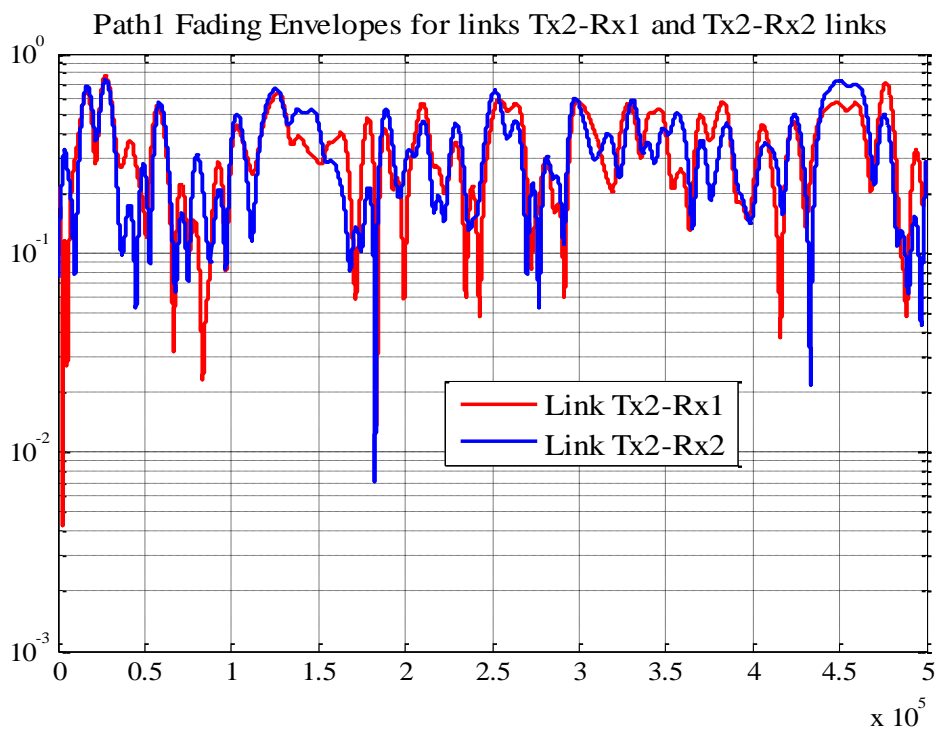


Figure 3. 64 Fading Envelopes for the links Tx2-Rx1 and Tx2-Rx2 for path 1.

3.5.3.2 Wi-Fi Protocol for EV to Smart Meter Communication

The simulation parameters for WiFi (SISO) are shown in Table 3.9 and is simulated for $F_s=20\text{MHz}$, $N=64$, $L=16$, center frequency $F_C=5.0\text{ GHz}$, $v=50$, Doppler frequency $F_D=v*F_C$, delay $\tau=[0, 0.1, 0.4]*1e-6$, path gain $P=[0, -2, -4]$.

The BER v/s SNR plot is shown in Figure 3.65 and portrait that to achieve BER of 10^{-1} :16 QAM requires 26dB, 64 QAM requires 32dB and 64 QAM with coding rate $\frac{1}{2}$ requires 20dB.

Table 3. 9 Parameters for 802.11

Parameters	WiFi Protocol
Bit rate Mbits/sec	6, 9, 12, 18, 24, 36, 48, 54
Modulation code	16-QAM, 64-QAM
Code rate	1/2
Number of Subcarriers	52
Symbol duration in micro sec	4
Guard time in micro sec	0.8
FFT period in micro sec	3.2
Preamble duration in micro sec	16
Subcarrier spacing MHz	0.3125

The BER v/s SNR graph is plotted and is shown in Figure 3.66. To achieve the BER of 10^{-2} : both QPSK $\frac{1}{2}$ and 64 QAM $\frac{2}{3}$ requires 15dB, QPSK $\frac{3}{4}$ requires 8dB, 16QAM $\frac{1}{2}$ requires 10dB and 16 QAM $\frac{3}{4}$ requires 12dB. 16QAM $\frac{1}{2}$ is better as compared to other coding schemes.

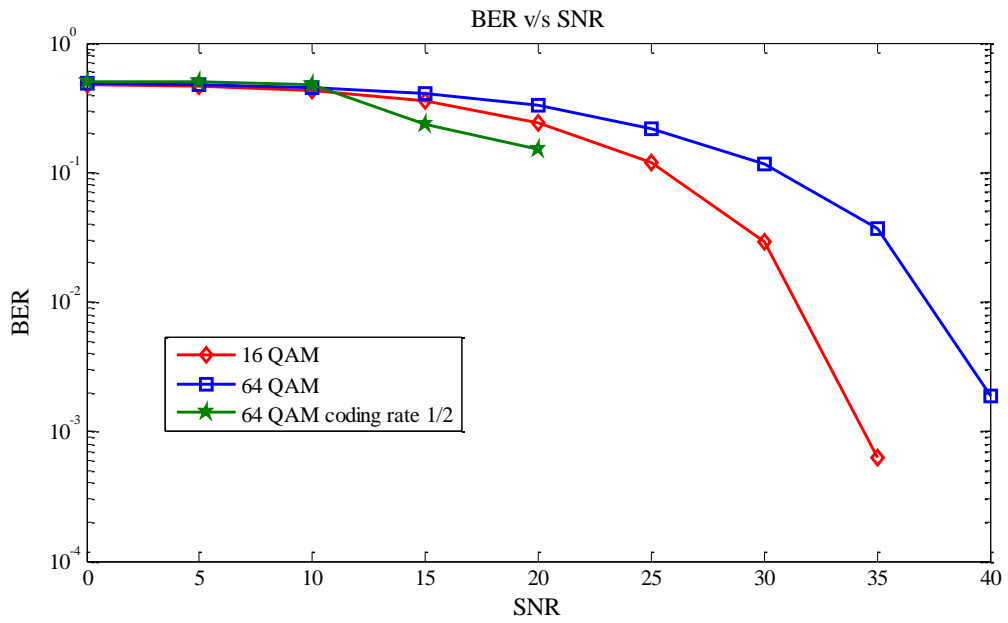


Figure 3.65 BER v/s SNR for EV to Smart Meter Communication link.

3.5.3.3 WiMAX Protocol for EV to Smart Meter Communication

The physical layer WiMAX is modeled and simulated in MATLAB/SIMULINK.

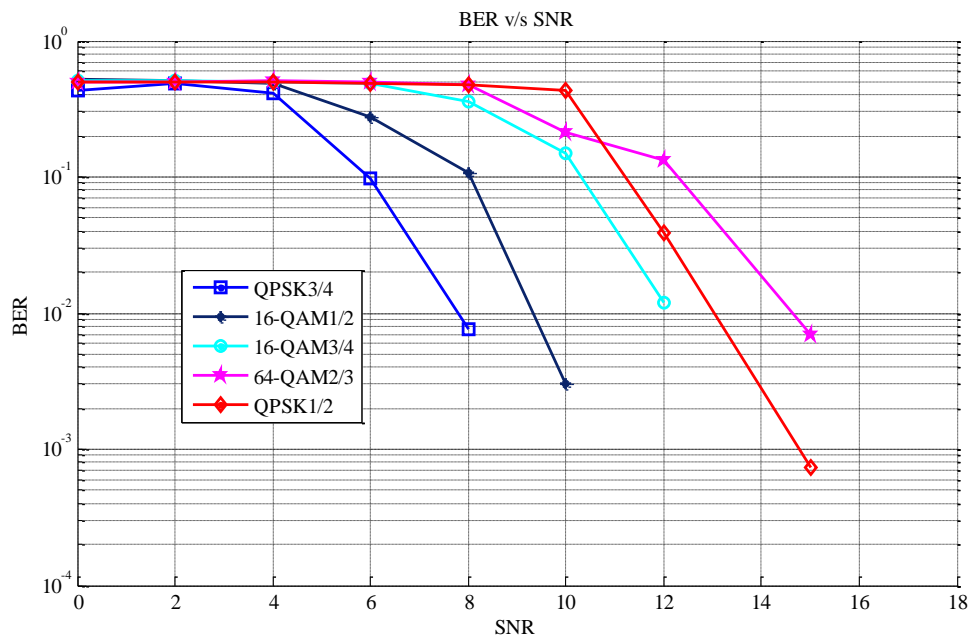


Figure 3.66 BER v/s SNR for EV to Smart Meter Communication link.

3.6 CONCLUSION

The wireless communication link is established between GCC to Aggregator, Aggregator to EV, EV to EV and EV to Smart Meter using applicable communication protocols in V2G operation. The downlink physical layer of fixed WiMAX, mobile WiMAX, LTE and WiFi are modeled and simulated using MATLAB/SIMULINK. The performance of each protocol is investigated using BER v/s SNR curves.

The channel models (path loss models) for the fixed WiMAX, mobile WiMAX and LTE protocols are analyzed and compared. The channel models B and C which are suitable for indoor environment in WiFi protocol are considered for EV to Smart Meter communication. Based on the scenario (i.e urban, suburban, indoor/outdoor) the suitable path loss models are suggested for V2G communication.

The main contributions of this chapter are study and application of wireless communication protocols for V2G Communication in Smart Grid environment.

CHAPTER 4

STOCHASTIC MODELING OF EV PARKING LOT OCCUPANCY AND QUEUING

The information about the grid requirements is communicated to EVs using wireless communication protocols. In order to meet the grid requirements, EVs have to transact power with the Grid and due to this the interfacing EVs through charging slot emerges.

EVs can be charged/discharged using dedicated EV home sockets. As the EVs are parked for 90-95% of the time in the parking lots (parking station, residential apartments and office buildings) they are deprived from using home sockets. Due to this the need arises for charging slots in Parking lots. EVs connected to the grid through the charging slot are shown in Figure 4.1.

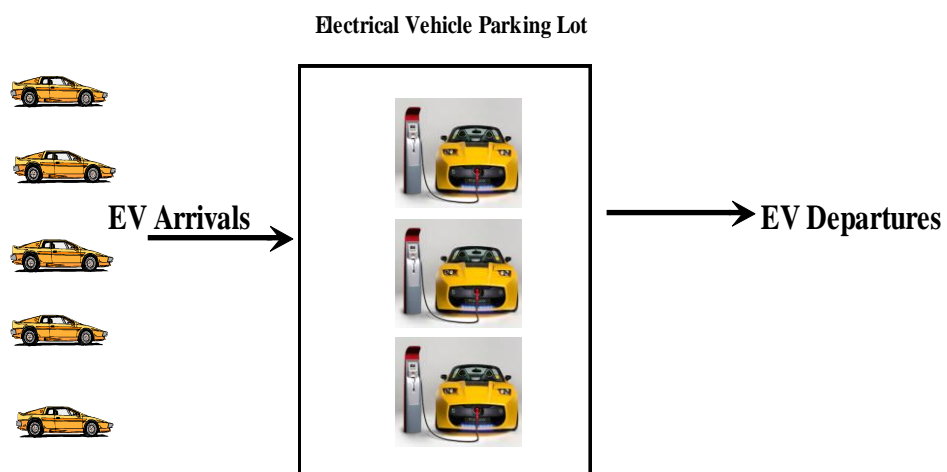


Figure 4. 1 EV arrivals and departures in the EVPL.

As the arrival of EVs in parking lot is time varying and random in nature, facilitating the EVs for grid integration becomes a stochastic problem. This problem can be resolved by developing the stochastic models for EVPL occupancy and Queuing. The timely communication about the resources (availability of charging slot and parking lot) for EV integration is important to avoid waiting time and improve the efficiency.

The study on EVPL occupancy will help us to determine the number of EVs to be accommodated for charging or discharging at that point of time in particular parking lot. The queuing will help us to note the number of EVs in queue and system, EVs waiting time in queue and availability of charging slots.

Markov chain based queuing model (M/M/m) for EVs connected to the charging slots and Stochastic model based on Markov chain for EVPL occupancy are presented in this chapter.

4.1 STOCHASTIC MODELING OF EVPL OCCUPANCY

A Stochastic model based on Markov chain is developed for EVPL occupancy. Let X_n be the number of EVs in the system at time n , then $X_n \in S := \{0, 1, 2, 3, \dots, L-1, L\}$ where, n is the time slot enough to transmit one EV, L is the size of the parking slot in number of EVs. The EVs arrive at the parking lot with a probability a in time slot n . The EV that arrives at time slot n is available to be forwarded in the next time slot $n+1$. The charging slot of the parking lot is involved in charging the other EV and allocates b for forwarding the EVs. As a consequence, the parking lot is able to forward EV with probability b in a given slot. With the probability of $(1-b)$, the charging slot is performing task. The arrivals and departures are independent of each other [Jeonghoon 2010]. The proposed Markov Model for EVPL occupancy is shown in Figure 4.2.

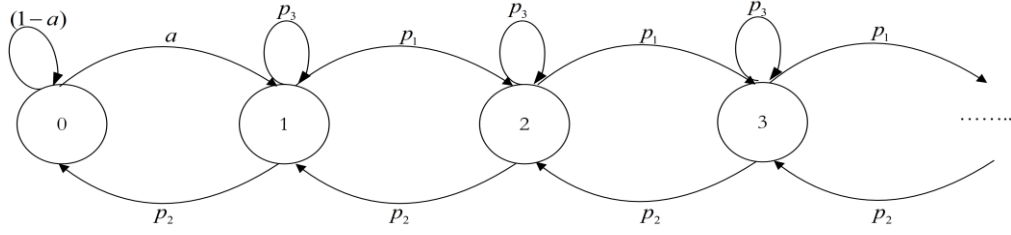


Figure 4. 2 Markov Model for Electrical Vehicle Parking Lot Occupancy.

4.1.1 Transition Probabilities:

The state transition occurs when an EV arrives or departs. When an EV arrives at time n , the parking lot occupancy X_n either stays in the same state or moves to the next state based on the departure: $X_{n+1} = X_n$; if there is a departure in the same time slot and $X_{n+1} = X_{n+1}$; otherwise. Similarly, $X_n = X_n$; if there is no arrival in time slot n and $X_{n-1} = X_n$; otherwise.

$$p_{i,j} = \begin{cases} p_1 = a(1-b), & j = i+1, i = 1, 2, \dots; \\ p_2 = (1-a)b, & j = i-1, i = 1, 2, \dots; \\ p_3 = ab + (1-a)(1-b), & j = i, i = 1, 2, \dots; \\ a, & i = 0, j = 1; \\ (1-a), & i = 0, j = 0; \\ 0, & \text{otherwise} \end{cases} \quad (4.1)$$

The transition probability $p_{0,1}$ from state 0 to 1 is a because there can be no departure when the charging slot is empty. The following are the assumptions [Dhaou et al.2013] made while developing model:

- 1) Off-Board integrators which comply with IEEE 1547 standards for charging or discharging.
- 2) The total time taken is considered as waiting time in queue plus the service time.
- 3) The discrete time birth and death process is considered.

The balance equations are given by

$\Pi = \Pi P$ and $\sum_i \pi_i = 1$. The balance equations are computed using :

$$\pi_0 \cdot a = \pi_1 \cdot p_2; \quad \pi_1 = \pi_0 \cdot a + \pi_1 \cdot p_3 + \pi_2 \cdot p_2; \quad \pi_n = \pi_{n-1} \cdot p_1 + \pi_n \cdot p_3 + \pi_{n+1} \cdot p_2 \text{ for } n \geq 2; \quad (4.2)$$

Summing the first $n+1$ balance equations, we find that

$\pi_n \cdot p_1 = \pi_{n+1} \cdot p_2$ for $n \geq 1$. These equations are called the local balance equations.

The steady state distribution is given as $P_n = \frac{a}{p_2} \left(\frac{p_1}{p_2} \right)^{n-1} \cdot P_0$; where,

$$P_0 = \left(1 + \frac{a}{p_2} \cdot \frac{p_2}{p_2 - p_1} \right)^{-1} \quad (4.3)$$

From the steady state distribution the average backlog $E[X]$ can be computed as

$$E[X] = \sum_n n \cdot P_n \quad (4.4)$$

4.2 QUEUING MODEL OF V2G

The Let $X(t)$ be a random variable depending on a continuous parameter $t \geq 0$ and represents the system state at time 't' considering set of nonnegative integers $\{0,1,2,3,\dots\}$. The collection of random variable $\{X(t), t \geq 0\}$ is a stochastic process [Athanasios 1984; Gerd 1997]. This collection is said to be a Markov process if the probability distribution of the state at $t + y$ depends only on the state at time t regardless of history prior to arriving at t .

In probability notation, for all $n > 0, i_{n-1}, \dots, i_0, i, j$;

$$\begin{aligned} P_{ij} &= P\{X_{n+1} = j | X_n = i, X_{n-1} = i_{n-1}, \dots, X_0 = i_0\} \\ &= P\{X_{n+1} = j | X_n = i\} \end{aligned} \quad (4.5)$$

where, $\{X_n | n = 0,1,2,\dots\}$ is a discrete –time stochastic process that takes values from the set of nonnegative integers.

The EVs arrive to the aggregator at a rate of ‘ λ ’ EVs per second and we assume that all the EVs have same battery capacity. The functions at the server queue are characterized by a service rate and a queuing discipline. The service rate ‘ μ ’ is expressed as number of EVs leaving the charging slot per unit service time. We consider Poisson input process and an exponentially distributed service process. The ‘ m ’ chargers are considered and EVs arriving to the charging station is shown in Figure 4.3.

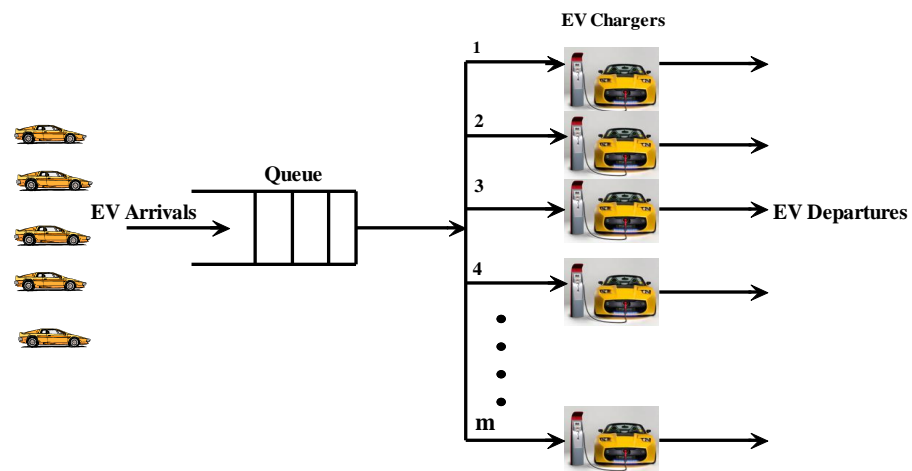


Figure 4. 3 Queuing Model of EVs Connected to the Charging Station.

The queuing theory is used for EV charging model and following assumptions are made [Dhaou et al.2013]:

1. Aggregator has ‘ m ’ charging slots
2. Off-Board integrators are available and comply with IEEE 1547 standards.
3. EV charging or discharging is based on first-come-first-serve basis.
4. The total time taken is considered as waiting time in queue plus the service time.

The state transition diagram for the M/M/m queue is shown in Figure 4.4. The EV entering state n from state $n-1$ is λp_{n-1} and from $n+1$ is μ_{pn+1} . The EV leaves state n and enters state $n-1$ with a flow rate as μp_n and $n+1$ with flow rate λp_n .

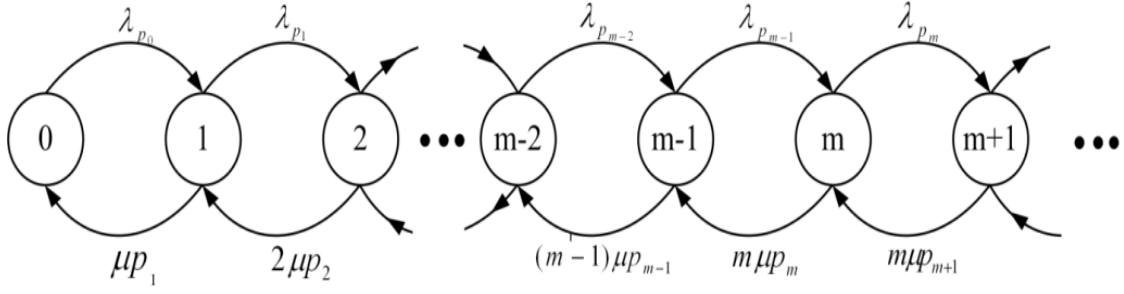


Figure 4.4 State transition diagram for M/M/s queue.

The balance equations are given by $\Pi = \Pi P$ and $\sum_i \pi_i = 1$. In order to obtain the steady state transition probability P_n we separate the solution in two parts as the transition rate is different for $n \geq m$ and $n \leq m$. The detailed balance equation is given by

$$(\lambda + n\mu)\pi_n = \lambda\pi_{n-1} + (n+1)\mu\pi_{n+1} \quad \text{for } n \geq 1 \quad (4.6)$$

or

$$(\rho + n)\pi_n = \rho\pi_{n-1} + (n+1)\pi_{n+1} \quad \text{where, } \rho = \lambda/\mu \quad (4.7)$$

After solving the equation recursively we get

$$\pi_n = \frac{\rho^n}{n!} \pi_0 \quad \text{for } n \leq m \quad (4.8)$$

Similarly for $n \geq m$, we have the balanced equation in the equilibrium

$$(\lambda + m\mu)\pi_n = \lambda\pi_{n-1} + m\mu\pi_{n+1} \quad (4.9)$$

Or

$$(\rho + m)\pi_n = \rho\pi_{n-1} + m\pi_{n+1} \quad (4.10)$$

Once again solving

$$\pi_n = \frac{\rho^n \pi_0}{m! m^{n-m}} \quad \text{for } n \geq m \quad (4.11)$$

The expression for π_0 can be obtained using probability conservation

$$\pi_0 = \left[\sum_{n=0}^{m-1} \frac{\rho^n}{n!} + \sum_{n=m}^{\infty} \frac{\rho^n}{m! m^{n-m}} \right]^{-1} = \left[\sum_{n=0}^{m-1} \frac{\rho^n}{n!} + \frac{\rho^m}{m! (1 - \rho/m)} \right]^{-1} \quad (4.12)$$

where, the relations in equation (8) are used to obtain the above equation

$$\sum_{k=1}^{\infty} x^k = \frac{1}{1-x} \quad \sum_{k=1}^s aq^{k-1} = \frac{a(q^s - 1)}{q-1} \quad (4.13)$$

The queue length is found for the states for which $n \geq m$ since a queue will form if all the m charging slots are busy. By definition

$$\begin{aligned} N_q &= E[N_q] = \sum_{n=m}^{\infty} (n-m)\pi_n \\ &= \sum_{k=0}^{\infty} k\pi_{m+k} \\ &= \sum_{k=0}^{\infty} k \frac{\rho^{k+m}\pi_0}{m!m^k} \\ &= \frac{\rho^m(\rho/m)}{m!(1-\rho/m)^2} \pi_0 \end{aligned} \quad (4.14)$$

By Little's formula we have

$$T_q = \frac{N_q}{\lambda} \quad N = T\lambda \quad (4.15)$$

where,

$$T = T_q + T_s + E[s] = T_q + \frac{1}{\mu} \quad (4.16)$$

since $E[s]=1/\mu$.

The probability that all charging slots are busy, so that an arriving message has to join the queue.

$$P[\text{queueing}] = \sum_{n=m}^{\infty} \pi_n = \sum_{n=m}^{\infty} \pi_0 \frac{\rho^n}{m!m^{n-m}} = \frac{\frac{\rho^m}{m!} \frac{1}{(1-\rho/m)}}{\sum_{n=0}^{m-1} \frac{\rho^n}{n!} + \frac{\rho^m}{m!} \frac{1}{1-\rho/m}} \quad (4.17)$$

4.3 RESULTS AND DISCUSSION

4.3.1 Stochastic modeling of EVPL Occupancy

The results demonstrate that the utilization of the parking lot increases as the probability of EV arrival approaches the value of b as shown in Figure 4.5. The Figure 4.6 depicts the average waiting time delay in hours as the probability of EV arrivals increases. For the probability of EV arrivals to be 0.85 the average delay in hours is 0.07 hours and depends on the EVs being connected to the charging slot. The Figure 4.7 demonstrates the number of backlogs increase as the probability of EV increases. For EV arrival to be 0.9 the average number of EVs waiting is 7 and is obtained using equation 4.4. The Figure 4.8, Figure 4.9 and Figure 4.10 depict the queue size v/s time in hours for 20, 50 and 100 EV arrivals.

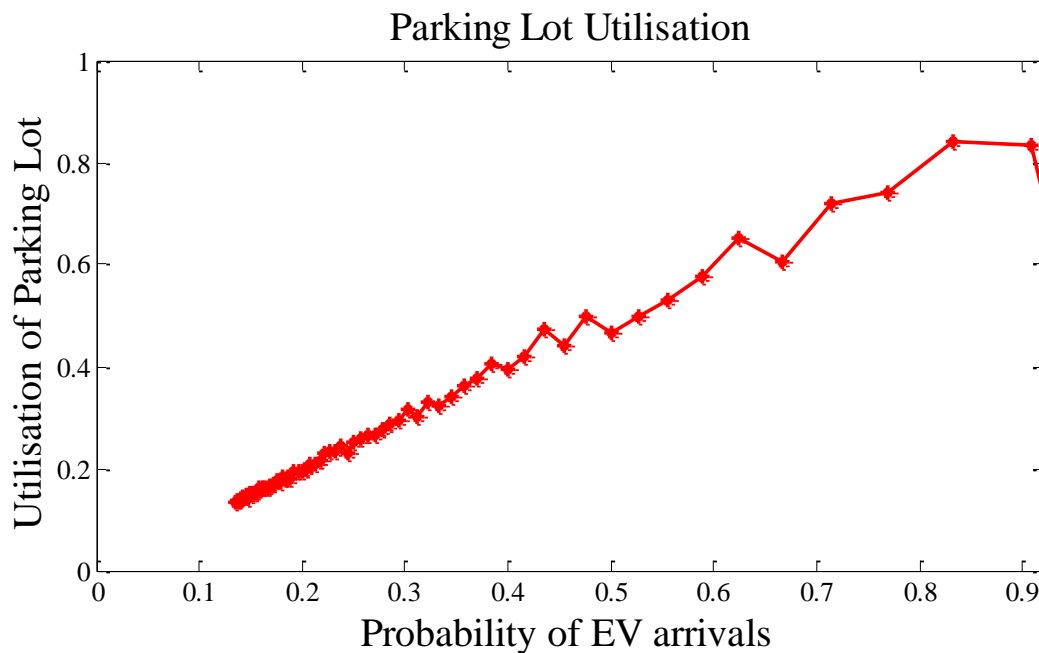


Figure 4. 5 EVPL Utilisation.

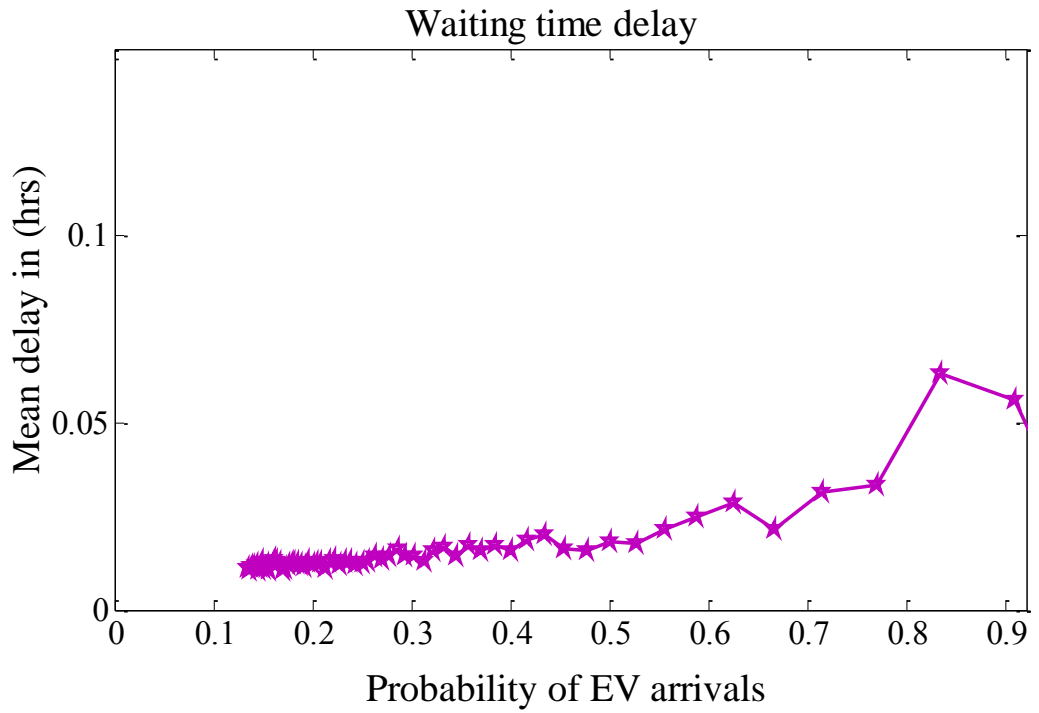


Figure 4. 6 Average waiting time in EVPL.

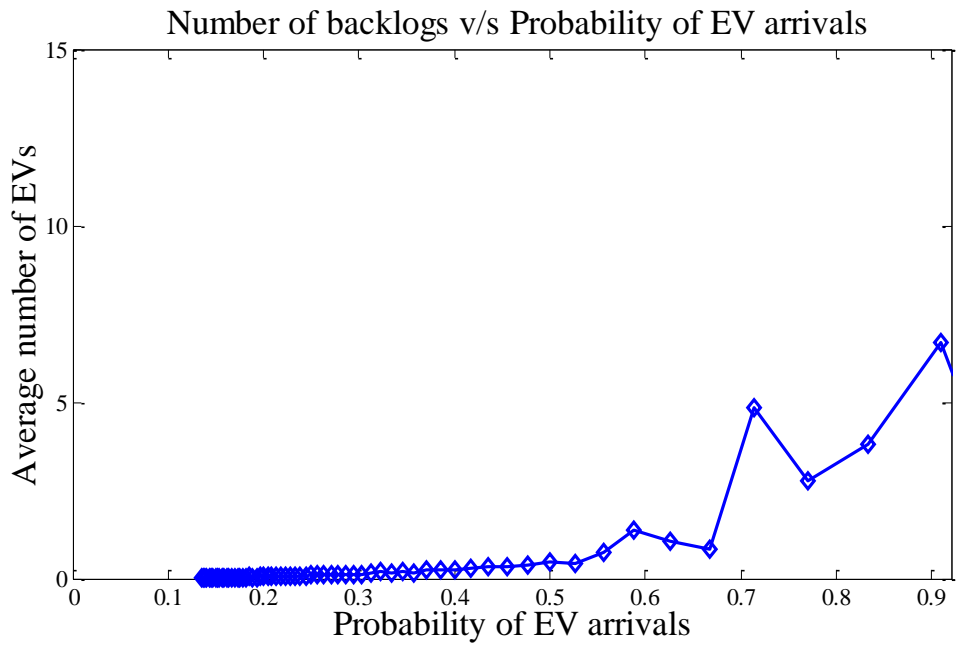


Figure 4. 7 Number of Backlogs v/s Probability of EV arrivals.

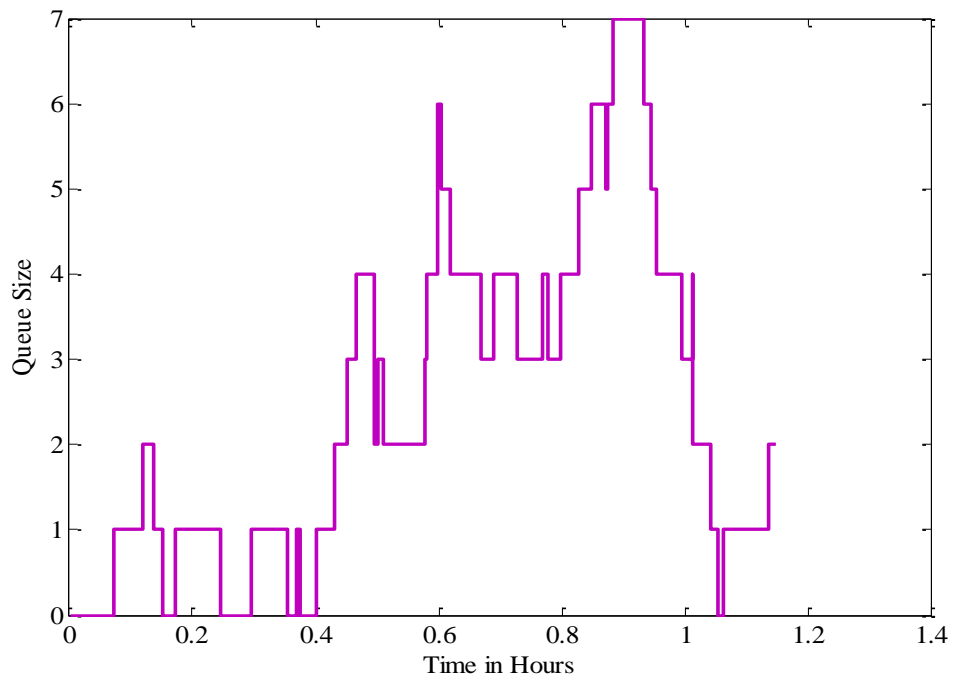


Figure 4. 8 Queue Size v/s Time in Hours for 20 EV arrivals.

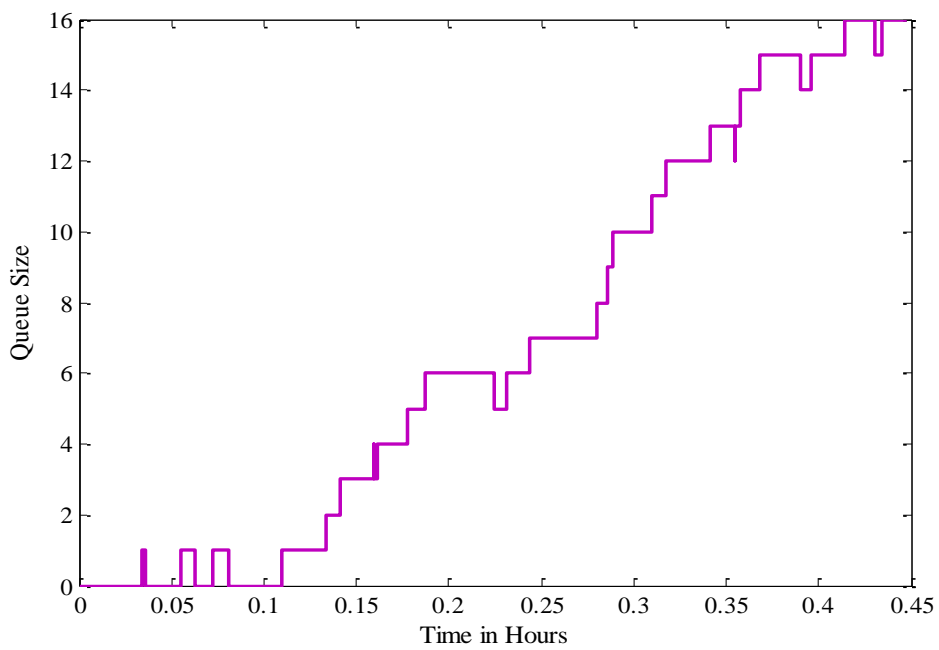


Figure 4. 9 Queue Size v/s Time in Hours for 50 EV arrivals.

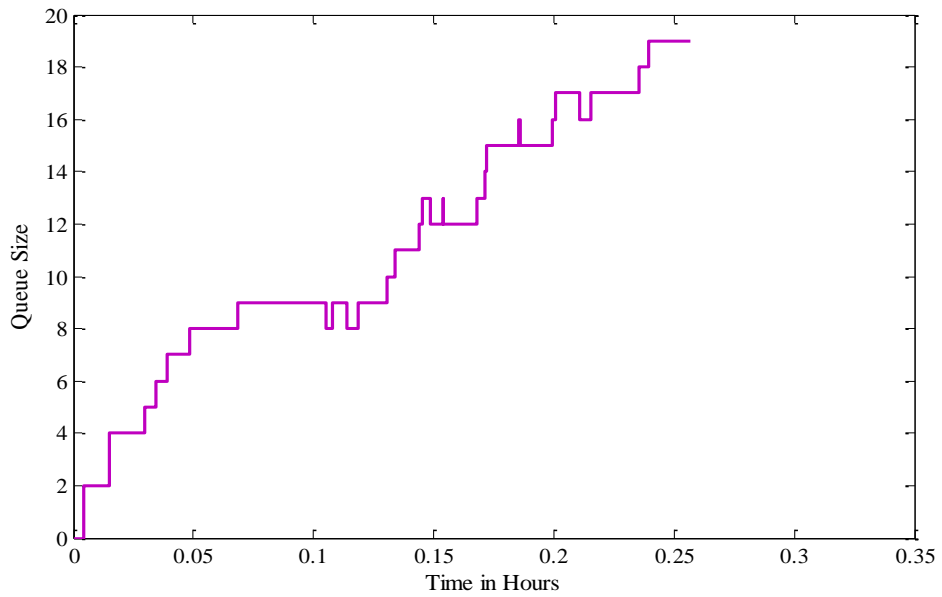


Figure 4. 10 Queue Size v/s Time in Hours for 100 EV arrivals.

4.3.2. Queuing Model Simulation

The PDF in Figure 4.11 illustrates the stochastic process resulting from Poisson arrivals and negative exponential service times for different EV entries.

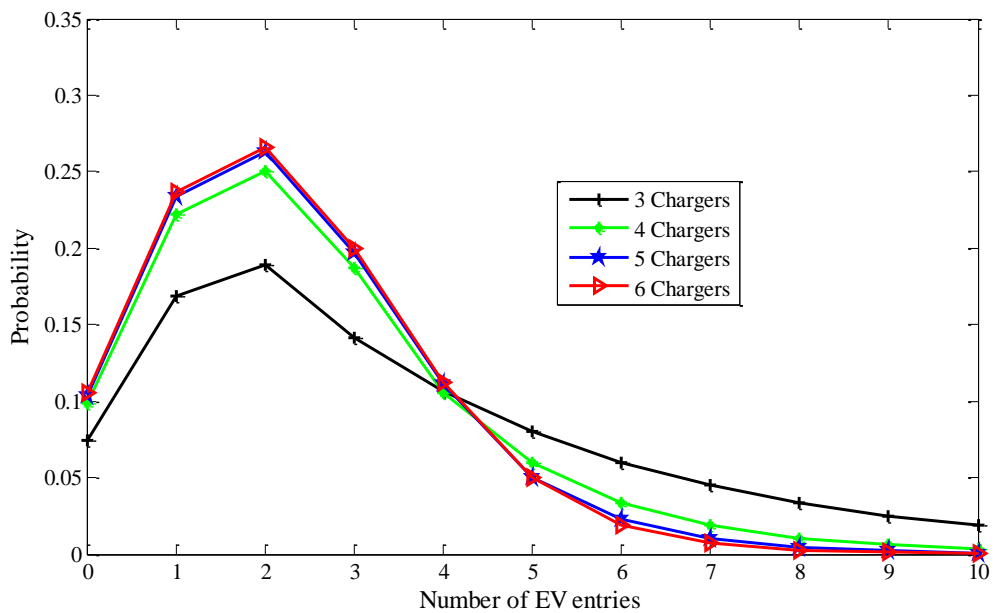


Figure 4. 11 PDF of EVs in System.

We assumed arrival rate $\lambda=3$, service distribution $\mu= 4/3$ for the simulation. The steady state probability is 0.0748, 0.0988, 0.1039, 0.1051 for chargers $S=3, 4, 5, 6$ respectively.

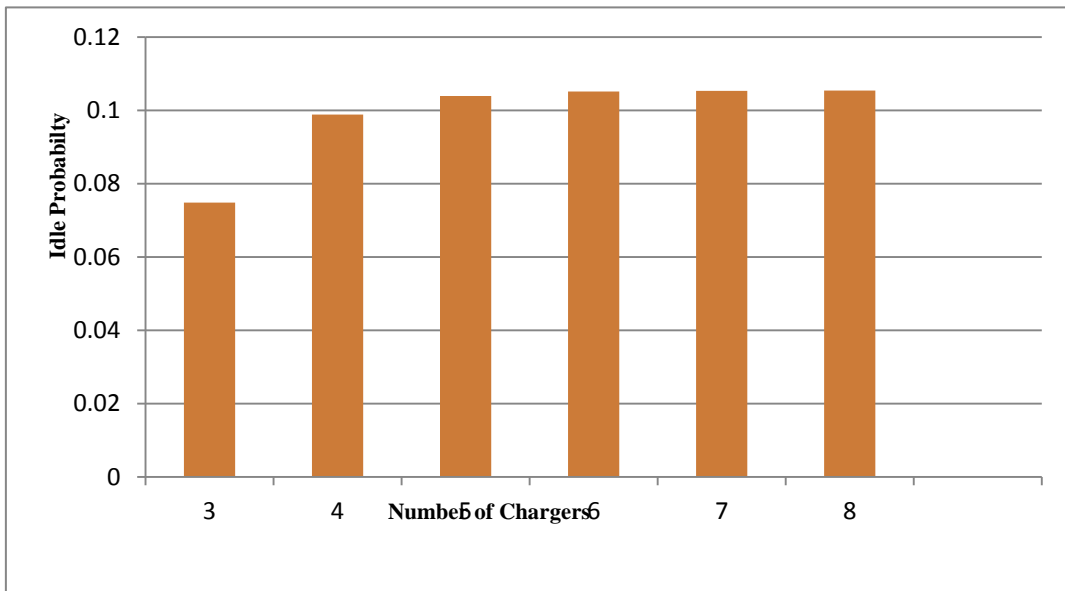


Figure 4. 12 Idle Probability for different Chargers.

The idle Probability varies quickly as the number of chargers increases as shown in Figure 4.12.

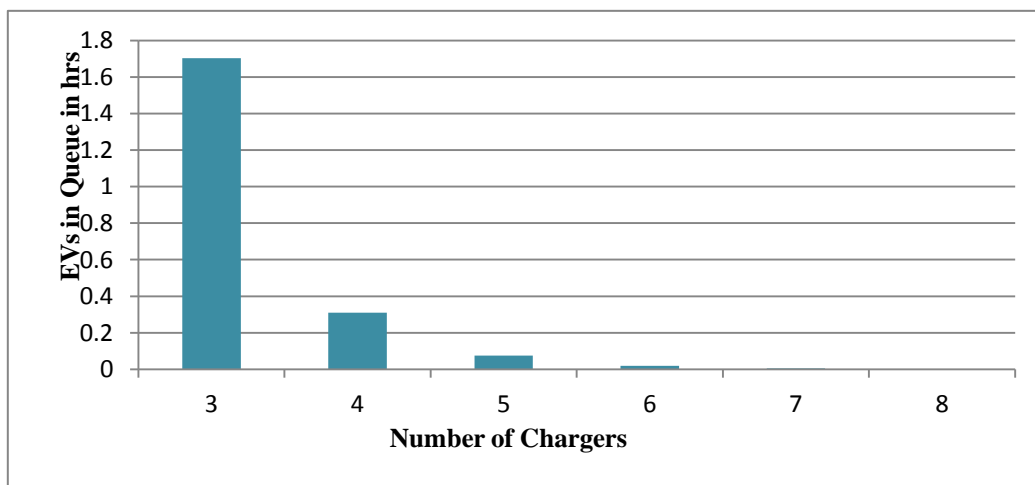


Figure 4. 13 EVs in Queue.

The Figure 4.13 shows that the EVs wait for 1.75 hours for 3 chargers, 0.3 for 4 chargers and as the chargers increase the EVs waiting in queue reduces.

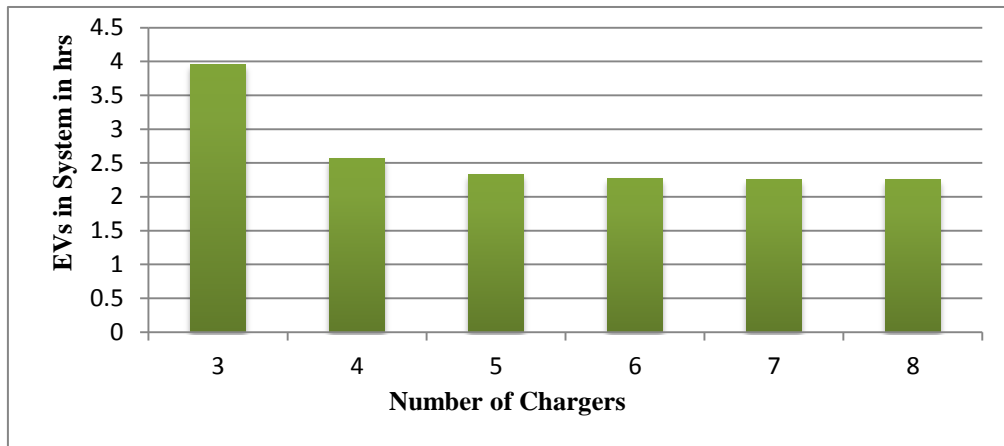


Figure 4. 14 EVs in System.

The EVs in system for the purpose of power transaction is shown in Figure 4.14. The EVs have to be in system for about 4 hours for three chargers, 2.5 hours for four chargers and on an average of 2.4 hours for 5, 6, 7 and 8 chargers. The Figure 4.15 shows the EVs waiting time in queue with constraint.

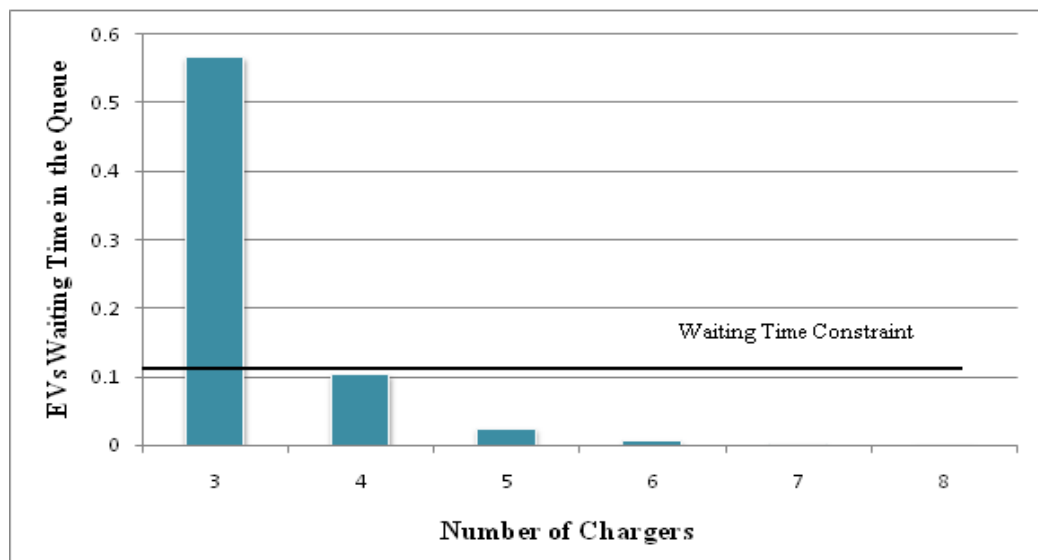


Figure 4. 15 EVs Waiting Time in the Queue.

4.4 CONCLUSION

A Stochastic model based on Markov chain is developed for EVPL occupancy and the simulation is carried out to estimate the charging slots in EVPL and the time required for EV to charge or discharge. Also queuing model is developed for EVs connected to the charging station for power transaction with the grid and simulation results demonstrate the idle probability, EVs waiting in system and EVs waiting in queue in hours. The main contributions of this chapter are development of stochastic model for EVPL occupancy and queuing model for EV charging using Markov's chain.

CHAPTER 5

CONCLUSION AND FUTURE SCOPE

V2G support peak shaving, valley filling and meet the grid requirements and thereby helps in meeting the time varying load demand. In order to support the key requirements of V2G operation like information transfer from Grid to EV and facilitating EVs to participate in power transaction with the grid, a wireless communication infrastructure is developed.

As a first step, V2G integrator for connecting EV to grid and the power flow capabilities of the integrator was developed. The necessary design aspects of the control system required for the development of V2G integrator are discussed. The results demonstrating the suitability of the integrator for bidirectional operation are presented complying with the IEEE 1547 standard.

As a second step, in addition to the V2G integrator, the communication link is established between GCC and EV. As GCC and Aggregator being fixed entities, fixed WiMAX is chosen. The empirical path loss models are analyzed and compared. The SUI model exhibit lower path loss for the Urban and Suburban environments and is found to be moderate. Also, 3GPP LTE protocol downlink physical layer is modeled, simulated and the specific channel models for LTE protocol like EVA, ETU and EPA are considered for BER v/s SNR curves. For Urban environment, ETU model is suitable for GCC to aggregator communication.

Next for Aggregator to EV communication, mobile WiMAX protocol downlink physical layer is modeled, simulated and the performance is investigated using BER v/s SNR curves. The 16 QAM $\frac{1}{2}$ modulation is found to be better for Aggregator to EV communication. Further channel modeling (path loss, shadowing and small scale

fading) is carried out comprehensively for Aggregator to EV communication. IEEE 802.16 model was considered to study the effects of shadowing for three different terrain regions type A, B and C. LOS and NLOS statistical characteristics are plotted using Rayleigh and Rician distribution for small scale fading as EVs are parked in outdoor or basement parking lots.

Sometimes it becomes difficult to maintain communication link between aggregator and all EVs in coverage area due to the effect of multipath. A moving EV or receiver can experience several fades in a very short duration and even EVs might be located in deeply faded region. So, EV to EV communication link is developed to support more number of EVs to participate in power transaction with the grid. The LTE downlink physical layer is modeled, simulated and the performance is investigated using BER v/s SNR curves. WINNER B5f and 3GPP path loss models are found to be suitable for Urban environment whereas, the SUI and WINNER B5f fit for the Suburban environment. The lognormal distribution is considered to describe shadowing and Rayleigh & Rician distributions are considered for small scale fading (NLOS and LOS). In total, EVs receive the information sent by an aggregator at higher data rates and mitigates the problems associated with ISI and Doppler spread.

The interested EV owners take part in power transaction with the grid and for its accountability, EV to Smart Meter wireless link is established using WiFi and WiMAX protocols. The simulation results demonstrate that 64 QAM with coding rate $\frac{1}{2}$ is found to be superior as compared other modulation schemes for WiFi and 16 QAM with coding rate $\frac{1}{2}$ for WiMAX. The indoor wireless channel models B and C (specific to residential and small office scenarios) with Doppler model are considered for small scale fading simulation. The obtained Doppler spectrum fits the theoretical values.

As a last step, a Stochastic model based on Markov chain is developed for EVPL occupancy and the simulation is carried out to estimate the number of charging slots available and time required for EV to charge or discharge. Markov chain based queuing model (M/M/m) is developed for EVs queuing to get charged/discharge and

participate in power transaction with the grid. The simulated results demonstrate the idle probability, EVs waiting in system and EVs waiting in queue.

In nutshell, for in time operation and smooth functioning of V2G in Smart Grid environment, wireless communication link is established between key entities of V2G communication. Also, EVs are mobilized/facilitated to participate in power transaction with the grid using stochastic models. The main contributions of this thesis work are development of wireless infrastructure for V2G communication and stochastic modeling of EVPL occupancy and EV queuing for charging/discharging.

There is a future scope for using Multi Agent based Communication for the Smart EV charging and discharging. Also, Stochastic Modeling of Strategic allocation of EVs in Parking Lot to support V2G Operation in Uncertain Load Demand can be considered.

REFERENCES

3GPP. (2008). "Technical specification group radio access network:E-UTRA and E-UTRAN overall description stage 2".

Abhayawardhana, V. S., Wassel, I. J., Crosby, D., Sellers, M. P., and Brown. M. G. (2005). "Comparison of empirical propagation path loss models for fixed wireless access systems," *61th IEEE Technology Conference*, Stockholm, 73-77.

Andrea, G.(2005) "Wireless Communication", Cambridge University Press, UK

Andrews, J. G., Arunabha, G., and Rias, M. (2007). "Fundamentals of WiMAX: Understanding Broadband Wireless Networking" Prentice Hall.

Bernard, S.(1997)." Digital Communications", Prentice-Hall, 1988.

Brown, J., and Khan, J. Y. (2013)." Key performance aspects of an LTE FDD based Smart Grid communications network", *Journal of Computer Communications*, 36(5), 551–561.

Cheol, P., Eunjo, L ., and Sun, P. (2012). "Link adaptation layer of Home Plug Green PHY for V2G communication interface", *Proceedings of the 18th Asia-Pacific Conference on Communications*, 572-573.

Christophe, G. and George, G. (2009). "A conceptual framework for the vehicle-to-grid (V2G) implementation", *Energy Policy*, (37), 11, 4379-4390.

Chunhua, L., Chau, K.T., Diyun, W., Shuan, G. (2013). "Opportunities and Challenges of Vehicle-to-Home, Vehicle-to-Vehicle, and Vehicle-to-Grid Technologies", *Proceedings of the IEEE*, (101), 11, 2409-2427.

Dallinger, D., Link, J. (2014). “Smart Grid Agent: Plug-in Electric Vehicle”, *IEEE Tran. On Sustain. Energy*, (5), 3, pp.710-717.

Dhaou, S., Soumaya, C., and Lyes, K. (2013). “Queuing Model for EVs Charging at Public Supply Stations ”, *Proceedings of the IEEE Wireless Communications and Mobile Computing Conference (IWCMC)*.

Diyun, W., Chunhua, L., and Shuang, G. (2011). “ Coordinated Control on a vehicle-to-Grid System”, *Proceedings of the International Conference on Electrical Machines and Systems, Beijing, China*.

Esmailian, H., Bioki, M., Rashidinejad, M., and Shojaee, M. (2012). “Techno-economical evaluation of EVS parking lot construction by distribution companies”. *Proceedings of the CIRED 2012 Workshop: Integration of Renewables into the Distribution Grid*.

Ganesh, K.V., Pinaki, M., Keith, C., and Chris, H. (2009). “Real-Time Modeling of Distributed Plug-in Vehicles for V2G Transactions”, *Proc.*, CA, USA, 3937-3941.

Gayatri, S.P., Mohana, S. (2002). “ Simulation of Flat Fading Using MATLAB for Class room Instruction”, *IEEE Trans.on Education*, 45(1), 19-25.

Gerd E. K. (199).”Local Area Networks”, TATA Mc Graw Hill.

Hamid, M., and Kostanic, I. (2013). “Path Loss Models for LTE and LTE-A Relay Stations” *Universal journal of communications and network*, 1, (4), 119-126.

Huei, R. T. (2012). "A Secure and Privacy-Preserving Communication Protocol for V2G Networks", *IEEE Wireless Communications and Networking Conference: Mobile and Wireless Networks*, 2706-2711.

Jim, Z. (2007). "Overview of the 3GPP Long Term Evolution Physical Layer, freescale semiconductors", Tutorial.

Josip, M., Rimac, S., and Bejuk, K. (2007). "Comparison of propagation model accuracy for WiMAX on 3.5GHz," *Proceedings of the 14th IEEE International conference on electronic circuits and systems, Morocco*, 111-114.

Kempton, W and Letendre, S. E. (1997). "Electric vehicles as a new power source for electric utilities," *Transportation Research Part D: Transport and Environment*, (2), 3, 157–175.

Kesler, M., Kisacikoglu, M. C., and Tolbert, L. M. (2014). "Vehicle-to-Grid Reactive Power Operation Using Plug-In Electric Vehicle Bidirectional Offboard Charger," *IEEE Trans. Ind. Electron*, (61), 12, 6778-6784.

Khan, M. A, Husain, I., and Sozer Y. (2012). "A bi-directional DC-DC converter with overlapping input and output voltage ranges and vehicle to grid energy transfer capability," *Proceedings of the IEEE International Electric Vehicle Conference (IEVC)*.

Khan, M. N., and Sabir, G. (2008). "The WiMAX 802.16e Physical Layer Model," *Proceedings of the IET International Conference on Wireless, Mobile and Multimedia Networks*.

Kisacikoglu, M. C., Kesler, M., and Tolbert, L.M. (2015). "Single-Phase On-Board Bidirectional PEV Charger for V2G Reactive Power Operation," *IEEE Trans. on Smart Grid*, (6), 2, 767-775.

Kovacs, A., Marples, D., Schmidt, R., and Morsztyn, R. (2013). "Integrating EVs into the Smart-Grid", *Proceedings of the 13th International Conference on ITS Telecommunications (ITST)*, 413 – 418.

Kyu, D. K., Young, H. J., Jun, G.K., Yong, C. J., and Chung, Y. W. (2012). "Novel high efficiency bidirectional converter using power sharing method for V2G," *Proceedings of the IEEE Vehicle Power and Propulsion Conference (VPPC)*, 9-12.

Letendre, S. E. and Kempton, W. (2002). "The V2G concept: a new model for power?" *Public Utilities Fortnightly*, 16–26.

Lin, S., He, Z., Zang, T., and Qian, Q. (2010). "Impact of Plug-In Hybrid Vehicles on Distribution Systems" Proc., IEEE International Conference on Physics Science and Technology, Hong Kong, China, 1-6.

Luigi, A., and Alessio, M. (2012). "Vanet in Vehicle-to-Grid", University of Cagliari, Italy.

Massimo, C., Dario, F., and Marco, V. (2011). "Bluetooth (B4V2G) for Electrical Vehicle to Smart Grid Connection", *IEEE Intelligent Systems in Embedded Systems*, 13-18.

Mendoza, P. A., Kollmeyer, P. J., and Ludois, D. C. (2013). "V2G integration and experimental demonstration on a lab-scale micro grid," *Proceedings of the IEEE Energy Conversion Congress and Exposition (ECCE)*.

Mohammad, S. (2009). Analysis of Propagation Models for WiMAX at 3.5 GHz, Masters Thesis, Blekinge Institute of Technology, September.

Philip P. B., and Robert, W. d.(2000). “Determining the Impact of Distributed Generation on Power Systems: Part1-Radial Distribution Systems”, *Proceedings of the IEEE Power Engineering Society Summer Meeting*, (3), 1645-1656.

Pinto, J. G., Monteiro, V. , Gonçalves, H., and Afonso, J. L. (2014). “Onboard reconfigurable battery charger for electric vehicles with traction-to-auxiliary mode.” *IEEE Trans. Veh. Technol*, (63), 3, 1004-1116.

Raj, J., Channel Models A Tutorial, (2001).

Raveendranathan, K. C. (2011). “Communication Systems Modeling and Simulation Using MATLAB and SIMULINK” University Press.

Ravindhra, K. (2012). “Long Term Evolution Downlink Physical Layer Simulation in Matlab and Simulink”, *International journal of future computer and communications*, (1), 12, 131-134.

Robert, C. G., Lingfeng, W., and Mansoor, A. (2011). “The impact of plug-in hybrid electric vehicles on distribution networks: A review and outlook”, *Renewable and Sustainable Energy Reviews*, (15), 1, 544-553.

Roberto, C. (2009). “<http://faculty.nps.edu/rcristi/WiMax/2009-08-20-WiMax>”.

Sherali, Z., Ray, H., Yuh, C., Angela, I., and Aamir, H. (2010). “Vehicular ad hoc networks (VANETS): status, results, and challenges,” *Journal of Telecommunication Systems*, (50), 4, 217-241.

Tara, A. Y. (2001). “Understanding LTE and its Performance”, *Springer Science+Business Media*, Heidelberg, Germany.

Teodorescu, R., Blaabjerg, F., Liserre, M, and Loh, P. C. (2006). “Proportional-resonant controllers and filters for grid-connected voltage-source converters.” *IEE Proc., Electr. Power Appl.*, (153), 5, 750-762.

Theodore, S. R. (1999). “Wireless Communications: Principles and Practice”, *Prentice Hall*, PTR.

Thirugnanam, K., Joy, T.P.E.R., Singh, M., and Kumar, P. (2014). "Modeling and Control of Contactless Based Smart Charging Station in V2G Scenario," *IEEE Trans. Smart Grid*, (5), 1, 337-348.

Ustun, T. S., Ozansoy, C. R ., and Zayegh, A. (2013). “Implementing Vehicle-to-Grid (V2G) Technology With IEC 61850-7-420,” *IEEE Trans. Smart Grid*, (4), 2, 1180–1187.

Vinko, E., and Larry, J. G. (1999). “An Empirically Based Path Loss Model for Wireless Channels in Suburban Environments”. *IEEE Trans. Selected areas in communication*, 17(7), 1205–1211.

Wang, Z., and Wang, S. (2013). “Grid Power Peak Shaving and Valley Filling Using Vehicle-to-Grid Systems”, *IEEE Trans. Power Delivery*, 28(3):1822–1829.

Willett, K., and Jasna, T. (2005). “Vehicle-to-grid power fundamentals: Calculating capacity and net revenue”, *Journal of Power Sources*, (144), 1, 268-279.

Wu, D., Liu, C., and Gao, S .(2011)."Coordinated Control on a Vehicle–to-Grid System" *Proc. IEEE International Conference on Electrical Machines and Systems, Beijing, China*, 1-6.

Yilmaz, M., and Krein, P.T. (2013). “Review of the Impact of Vehicle-to-Grid Technologies on Distribution Systems and Utility Interfaces,” *IEEE Trans. Power Electron*, (28), 12, 5673-5689. 2013.

Zountouridou, E. I., Kiokes, G. C., Hatziargyriou, N. K. (2011). “An Evaluation Study of Wireless Access Technologies for V2G Communications”, *Proceedings of the 16th International Conference on Intelligence System Applications to Power Systems, Crete, Greece.*

LIST OF PUBLICATIONS

REFEREED JOURNALS

1. **Santoshkumar.,** and Udaykumar, R.Y. (2015). “*Development of Markov Chain Based Queuing Model and Wireless Infrastructure for EV to Smart Meter Communication in V2G*”, *International Journal of Emerging Electrical Power Systems (IJEEPS)*, (16), 2, 153–163.
2. **Santoshkumar.,** and Udaykumar, R.Y. (2015)” *Development of Wireless Access Support for EV to Smart Meter Communication in Vehicle-to-Grid (V2G)*”, accepted for publication in *International Journal of Renewable Energy Research (IJRER)*, (5), 2, 419-426.
3. **Santoshkumar.,** and Udaykumar, R.Y. (2015). “*Modeling and Comprehensive Analysis of WiMAX Protocol for Grid Control Center to Aggregator Communication in V2G*”, *International Journal of Renewable Energy Research (IJRER)*, (5), 1, 133-138.
4. **Santoshkumar.,** and Udaykumar, R.Y. (2014). “*Modeling and Architectural Frame Work of Off-Board V2G Integrator for Smart Grid*”, *International Journal of Renewable Energy Research (IJRER)*, (4), 4, 826-831.

CONFERENCE PROCEEDINGS

1. **Santoshkumar.,** and Udaykumar, R.Y. (2015). “*Performance Analysis of LTE Protocol for EV to EV Communication in Vehicle-to-Grid (V2G)*” *Proceedings of the 28th Annual IEEE Canadian Conference on Electrical and Computer Engineering (IEEE-CCECE)*, Nova Scotia, Halifax, Canada.

2. **Santoshkumar.,** and Udaykumar, R.Y. (2015). “Performance Analysis of LTE Protocol for EV to EV Communication in Vehicle-to-Grid (V2G)” *Proceedings of the 28th Annual IEEE Canadian Conference on Electrical and Computer Engineering (IEEE-CCECE), Nova Scotia, Halifax, Canada.*
3. **Santoshkumar.,** and Udaykumar, R.Y. (2014). “Performance Investigation of Mobile WiMAX Protocol for Aggregator and Electrical Vehicle Communication in Vehicle-to-Grid (V2G)” *Proceedings of the 27th Annual IEEE Canadian Conference on Electrical and Computer Engineering (IEEE-CCECE), Nova Scotia, Halifax, Canada.*
4. **Santoshkumar.,** and Udaykumar, R.Y. (2014). “Long Term Evolution Protocol for Grid Control Center And Aggregator Communication In V2G for Smart Grid Application” *Proceedings of the IEEE International Conference on Computational Intelligence and Computing Research (IEEE-ICCIC), Madurai, India.*
5. Nagarjuna, K., **Santoshkumar.,** and Udaykumar, R.Y. (2014). “On-Board Vehicle-to-Grid (V2G) integrator for Power Transaction in Smart Grid Environment” *Proceedings of the IEEE International Conference on Computational Intelligence and Computing Research (IEEE-ICCIC), Madurai, India.*
6. **Santoshkumar.,** and Udaykumar, R.Y. (2013). “IEEE 802.16 Protocol for Grid Control Center And Aggregator Communication in V2G for Smart Grid Application” *proceedings of the IEEE International Conference on Computational Intelligence and Computing Research, Madurai,(IEEE-ICCIC), India.*

7. **Santoshkumar.,** and Udaykumar, R.Y. (2015). “Markov chain based stochastic Model of Electric Vehicle Parking Lot Occupancy in Vehicle-to-Grid” *proceedings of the IEEE International Conference on Computational Intelligence and Computing Research, Madurai,(IEEE-ICCIC), India.*

8. **Santoshkumar.,** and Udaykumar, R.Y. (2015). “ Stochastic Model of Electric Vehicle Parking Lot Occupancy in Vehicle-to-Grid (V2G)” *proceedings of the International Conference on Advances in Energy Research (ICAER 2015), IIT Bombay, Mumbai, India.*

CURRICULUM VITAE

Mr. Santoshkumar is a research scholar in the Department of Electrical & Electronics Engineering, National Institute of Technology Karnataka (NITK), Surathkal, Mangalore, INDIA. He obtained Bachelor's degree in Electrical and Electronics Engineering from Karnatak University, Dharwad in the year 1998 with First Class Distinction. He holds Master's degree in Digital Electronics Engineering from Amaravati University, Maharashtra in the year 2003 with First Division. After his Master's degree he served as a Senior Lecturer in the Department of Electrical and Electronics Engineering, BVB College of Engineering and Technology, Hubli from 2003 to 2009. Since July 2009, he is working as an Assistant Professor in Department of Electrical and Electronics Engineering, SDM College of Engineering and Technology, Dharwad. He has 15 years of teaching experience.

He is a *Senior Member IEEE* and has actively involved in research since last 15 years. He has presented several research papers in IEEE flagship International Conferences and published articles and research papers in reputed indexed international journals. He has bagged *three IEEE BEST PAPER AWARDS* in Conferences. His fields of interest are Smart Grid communication, V2G infrastructure development, Stochastic modelling of intermittent renewable energy sources, Power System protection (wide area measurement system) and applications of Signal Processing for power quality issues,

Address:

Mr. Santoshkumar,
Assistant Professor,
Department of Electrical & Electronics Engineering,
SDM College of Engineering and Technology,
Dharwad, Karnataka – 580 002, INDIA.
Phone: +91 9844027103
Email: santoshkumar777@yahoo.com / santoshkumar.s.in@ieee.org.